Development of an automated RNA capture-SELEX for enriching modular RNA light-up sensors

Dissertation

zur

Erlangung des Doktorgrades (Dr. rer. nat.)

der

Mathematisch-Naturwissenschaftlichen Fakultät

der

Rheinischen Friedrich-Wilhelms-Universität Bonn

von

Tjasa Legen

aus

Murska Sobota, Slowenien

Bonn, 2026

Angefertigt mit Genehmigung der Mathematisch-Naturwissenschaftlichen Fakultät der Rheinischen Friedrich-Wilhelms-Universität Bonn

Gutachter/Betreuer:	Prof. Dr. Günter Mayer
Gutachterin:	Jr. Prof. Dr. Elena S. Reckzeh
Tag der Promotion:	02.04.2026
Erscheinungsjahr:	2026

Publications

The following publications are included in this thesis.

1. Legen, Tjasa, and Günter Mayer. "Robotic-Assisted Capture-Systematic Evolution of Ligands by Exponential Enrichment of RNA Aptamers Binding to Small Molecules." ChemBioChem (2025): 2500264. DOI: https://doi.org/10.1002/cbic.202500264
2. Legen, Tjasa, and Günter Mayer. "Modular Approach for Rapid Identification of RNA-Based Sensors." ACS sensors 9.2 (2024): 753-758. DOI: https://doi.org/10.1021/acssensors.3c02060

Additionally, significant contributions have been made to the following publications.

3. Breuers, S., Bryant, L. L., Legen, T., & Mayer, G. "Robotic assisted generation of 2′-deoxy-2′-fluoro-modifed RNA aptamers–High performance enabling strategies in aptamer selection." Methods 161 (2019): 3-9. DOI: https://doi.org/10.1016/j.ymeth.2019.05.022
4. Mayer, G., Legen, T., Patwari, T., & Weber, A. M. "Hunting Cells for Gentle Liberation." Cell Chemical Biology 27.3 (2020): 257-258. DOI: https://doi.org/10.1016/j.chembiol.2020.02.006

Abstract

This thesis examines recent advances in selecting and functionalizing RNA aptamers for molecular sensing applications. Two related studies have been carried out: developing a robotic platform for automated RNA aptamer selection targeting small molecules and creating a modular approach to design fluorogenic RNA sensors. Together, these studies offer a framework that combines standardized aptamer discovery with adaptable sensor design.

The systematic evolution of ligands by exponential enrichment (SELEX) was adapted to a robotic platform, minimizing manual intervention and enhancing reproducibility. Traditional SELEX often involves immobilizing small-molecule targets, which can alter ligand properties. To address this, capture-SELEX was used, in which RNA libraries are immobilized via hybridization to capture-oligodeoxynucleotides (ODNs), and unmodified ligands in solution facilitate the recovery of bound sequences. By optimizing the robotic system, a preferential immobilization strategy for the library was systematically investigated, resulting in more substantial enrichment of binding sequences. The platform completes up to twelve selection cycles in 72 hours and has successfully enriched aptamers for several small molecules, including neomycin B, theophylline, and riboflavin. Interaction analysis using fluorescence polarization and isothermal titration calorimetry confirmed specific binding properties of enriched aptamers, with affinities in the micromolar range. Although the current capture-SELEX protocol used on the robotic system has limitations in the affinity of the enriched aptamers compared to immobilization-based selections, it offers a standardized, high-throughput method for the rapid assessment of the utility of aptamers for small molecules.

In the second part of this work, the capture-SELEX strategy was extended to enable the selection of modular allosteric RNA sensors. RNA libraries were designed to couple ligand-binding aptamers to fluorogenic RNA scaffolds, enabling molecular recognition to be directly translated into fluorescence output. Using this library in capture-SELEX, aptamers that bind thiamine pyrophosphate (TPP) were identified. These aptamers were then fused to Broccoli and its red-shifted variant, Red Broccoli, to develop ligand-responsive sensors. By optimizing the linker and spacer regions, the signal-to-background ratio was improved. The selected sensors demonstrated specificity for TPP and thiamine monophosphate, with minimal response to thiamine or unrelated nucleotides. The modular design facilitated the easy swapping of fluorogenic domains and the adjustment of sensor properties, demonstrating its effectiveness for rapid and efficient development of RNA-based sensors.

Overall, this thesis establishes a scalable framework for RNA aptamer discovery and deployment. By integrating automated selection with modular sensor engineering, the presented approach provides a generalizable strategy for developing RNA-based sensing systems applicable to biosensing, synthetic biology, and molecular diagnostics.

Zusammenfassung

Diese Dissertation untersucht aktuelle Fortschritte bei der Selektion und Funktionalisierung von RNA-Aptameren für molekulare Sensoranwendungen. Hierzu wurden zwei komplementäre Studien durchgeführt: die Entwicklung einer robotischen Plattform zur automatisierten RNA-Aptamer-Selektion gegen kleine Moleküle sowie die Etablierung eines modularen Ansatzes zur Konstruktion fluorogener RNA-Sensoren. Zusammen bilden diese Arbeiten einen integrierten Rahmen, der standardisierte Aptamerentdeckung mit flexibler Sensorgestaltung verbindet.

Die systematische Evolution von Liganden mittels exponentieller Anreicherung (SELEX) wurde auf eine robotische Plattform übertragen, wodurch manuelle Eingriffe reduziert und die Reproduzierbarkeit erhöht wurden. Da die Immobilisierung kleiner Moleküle deren Eigenschaften beeinflussen kann, wurde Capture-SELEX eingesetzt, bei dem RNA-Bibliotheken über Hybridisierung an Oligodesoxynukleotide immobilisiert werden, während unveränderte Liganden in Lösung die Selektion ermöglichen. Durch die systematische Optimierung der Bibliotheksimmobilisierung konnte eine verbesserte Anreicherung anbindenden Sequenzen erzielt werden. Die Plattform ermöglicht bis zu zwölf Selektionszyklen innerhalb von 72 Stunden und führt zur erfolgreichen Anreicherung von Aptamern gegen mehrere kleine Moleküle, darunter Neomycin B, Theophyllin und Riboflavin. Bindungsanalysen mittels Fluoreszenzpolarisation und isothermer Titrationskalorimetrie bestätigten spezifische Wechselwirkungen mit Affinitäten im mikromolaren Bereich.

In der zweiten Studie wurde ein angepasstes Selektionsschema zur Identifizierung von Aptamern entwickelt, die in fluorogene RNA-Sensoren integriert werden können. Hierfür wurden modulare RNA-Bibliotheken mit Andocksequenzen entworfen, die eine allosterische Kopplung zwischen der Zielmolekülbindung und der Fluorophoraktivierung ermöglichen. Mithilfe dieses Ansatzes wurden Aptamere gegen Thiaminpyrophosphat selektiert und mit den fluorogenen RNA-Aptamern Broccoli und Red Broccoli fusioniert. Durch die Optimierung von Linker- und Spacerregionen wurden verbesserte Signal-zu-Hintergrund-Verhältnisse erzielt. Die resultierenden Sensoren wiesen eine hohe Spezifität für Thiaminpyrophosphat und Thiaminmonophosphat auf.

Insgesamt zeigen die Ergebnisse, dass die Kombination aus automatisierter Aptamerselektion und modularer Sensorkonstruktion eine effiziente Strategie zur Entwicklung von RNA-basierten Sensorsystemen darstellt. Die vorgestellten Ansätze ermöglichen eine reproduzierbare Identifizierung neuer Aptamere sowie deren schnelle Umsetzung in funktionale fluorogene Sensoren und bieten damit eine vielseitige Grundlage für Anwendungen in der synthetischen Biologie, Diagnostik und molekularen Analytik.

CONTENT

INTRODUCTION

1. Brief history of aptamers and SELEX

The groundwork for aptamer technology was laid in 1990 with two landmark studies that independently introduced the Systematic Evolution of Ligands by EXponential Enrichment (SELEX) method. In a pioneering article, Tuerk and Gold [1] demonstrated that nucleic acid libraries could be iteratively enriched to yield RNA sequences binding bacteriophage T4 DNA polymerase with high specificity. Their research demonstrated how oligonucleotide libraries could be designed to select sequences that excel in precise molecular recognition, coining the term SELEX. Concurrently, Ellington and Szostak [2] presented the same idea by demonstrating that RNA could be selected to bind small organic dyes with exceptional affinity. This research confirmed the SELEX method as a powerful tool for molecular recognition and introduced the term "aptamer", referring to structured single-stranded nucleic acids that can bind a broad spectrum of targets, ranging from small molecules to complex proteins or even cells.

Aptamers are often described as nucleic acid analogues of antibodies, as both classes of ligands exhibit high specificity and affinity toward molecular targets. While antibody discovery has evolved substantially through *in vitro* techniques such as phage display[3-4], antibody production remains resource-intensive, requiring mammalian expression systems and complex purification procedures.[5] In contrast, aptamers are chemically synthesized, allowing precise control over sequence, modifications, and batch-to-batch reproducibility at lower cost and higher scalability.

These properties have enabled the use of aptamers in applications where antibodies face intrinsic limitations. For instance, the SOMAscan platform employs thousands of modified DNA aptamers for highly multiplexed protein detection in diagnostics[6], demonstrating greater applicability than conventional immunoassays. Likewise, the programmable nature of RNA and DNA aptamers has been exploited to engineer regulatory motifs in gene-editing systems, such as ligand-responsive guide RNAs that modulate CRISPR activity.[7] Although antibodies remain dominant in therapeutic applications, aptamers offer a complementary and versatile alternative, particularly suited for multiplexed diagnostics and synthetic biology.

The iterative SELEX process, which includes binding, separation, amplification, and enrichment, successfully identifies aptamers with affinities ranging from micromolar to picomolar levels (**Figure 1**). Over the past 30 years, numerous variations of the SELEX methodology have been developed to improve specificity, efficiency, and scalability. However, these challenges become particularly pronounced when selecting aptamers against small-molecule targets.

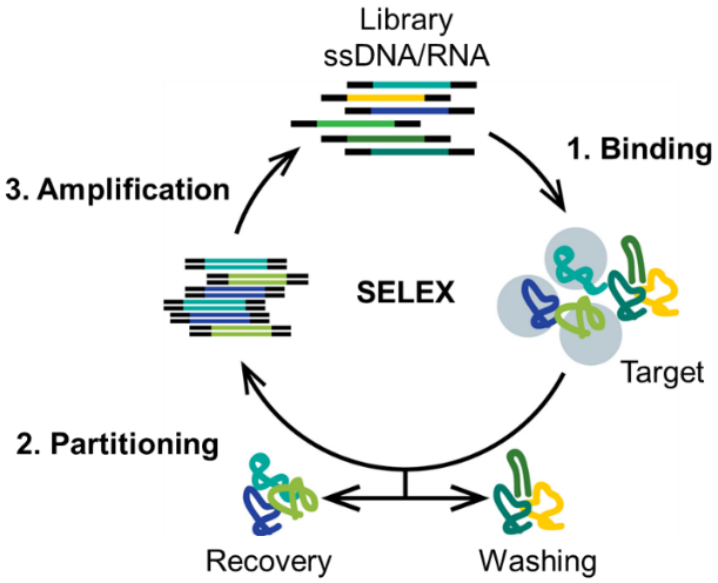

Figure 1. A schematic representation of the main SELEX steps. Main steps in SELEX are: (1) Binding of ssDNA or RNA library to the ligand, (2) washing of unbound or weakly bound sequences and subsequent recovery of binding sequences in the partitioning step, and (3) amplification of recovered sequences in a PCR with the following *in vitro* transcription of RNA in the case of RNA library.

SELEX = Systematic Evolution of Ligands by EXponential Enrichment, ssDNA = single-stranded deoxyribonucleic acid, PCR = polymerase-chain reaction, RNA = ribonucleic acid.

2. SELEX: a versatile tool for aptamer selection

Since its introduction, SELEX has been widely applied to generate DNA and RNA aptamers targeting a broad range of ligands, from small molecules, [8-9] proteins, [10-11] and more complex systems such as cells [12-13]. The choice between DNA and RNA nucleic acids for aptamer development depends on the intended application. Often, RNA or DNA is also modified, either before selection or at the aptamer level, to increase interaction strength or improve the stability of the nucleic acid molecule.[14-15]

RNA aptamers are frequently described as structurally versatile due to their roles in ribozymes and riboswitches.[16-18] However, this structural flexibility does not inherently translate into superior binding affinity, as both RNA and DNA aptamers can achieve nanomolar or picomolar affinities depending on the target and selection conditions. A key advantage of RNA aptamers is their genetic encodability, which enables intracellular expression for applications in gene regulation, sensing, and synthetic biology.

In intracellular settings, RNA aptamers are generally limited to natural nucleotides, restricting the incorporation of chemically diverse base modifications during expression. To overcome stability limitations, RNA aptamers are frequently chemically modified, most commonly at the 2′ position, to enhance nuclease resistance and *in vivo* half-life.[19] In contrast, DNA aptamers can exploit diverse base modifications during *in vitro* selection, as exemplified by slow off-rate modified aptamers (SOMAmers)

[6] and click-SELEX-derived DNA aptamers (clickmers)[14], which expand chemical functionality through hydrophobic or aromatic side chains and often achieve enhanced affinity and specificity, and a higher success rate of aptamer selectability.

2.1 DNA/RNA library design

The SELEX process starts with a carefully designed, chemically synthesized single-stranded DNA (ssDNA) library. The 5' and 3' terminal regions in the library remain fixed, while the central region is randomized. Oligonucleotide libraries containing random segments of 20 to 80 nucleotides (nt) [20] are frequently used in *in vitro* selection experiments, balancing sequence diversity with practical amplification efficiency.

For RNA aptamer selection, the ssDNA library is converted into double-stranded DNA (dsDNA) via limited PCR amplification[20], typically using five to six PCR cycles, to preserve the library's diversity.[20-21] A T7 promoter sequence is introduced through the forward primer, enabling subsequent *in vitro* transcription of RNA from the amplified DNA template (**Figure 2**).

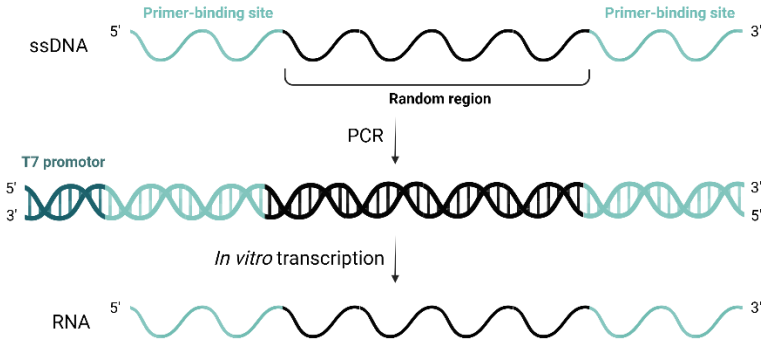

Figure 2. Scheme of RNA library generation from a chemically synthesized ssDNA library.

PCR = polymerase chain reaction, RNA = ribonucleic acid, ssDNA = single-stranded deoxyribonucleic acid.

Primer binding regions are typically designed with balanced GC content (40–60%) to ensure stable annealing to the template and melting temperatures compatible with standard PCR conditions.[22-23] Lastly, avoidance of secondary structures like hairpins or primer-dimers is critical, as these can disrupt efficient template hybridization and amplification. By thoughtfully addressing these factors, primer design can help mitigate artifact formation during the SELEX process.[24]

2.2 Buffer selection

Buffer composition plays a central role in SELEX, as it directly influences aptamer folding, target stability, and binding specificity.[25] Selection buffers are typically chosen to reflect the intended application environment while maintaining target solubility and structural integrity. For small molecules and ions, commonly used buffers include HEPES, Tris-HCl, or PBS.[8, 26-27] Divalent and monovalent cations, particularly Mg^{2+} and K^{+}, are frequently included to stabilize RNA secondary structures and, in

some cases, promote G-quadruplex formation.[28-29] While G-quadruplexes are not universally required for aptamer binding, they are essential for particular fluorogenic light-up aptamers, where π-stacking interactions restrict fluorophore flexibility and enhance fluorescence emission.[30-31]

2.3 Different targets

SELEX has been successfully applied to targets spanning a broad chemical spectrum, including inorganic [32-33] and small organic molecules, [34-35] proteins, [10-11] carbohydrates, [9] antibiotics, [27, 36] and even cells.[12-13] Because of their varying chemical structures and interaction characteristics, different molecules need distinct selection approaches. The most crucial and challenging part of the SELEX process is separating bound from unbound sequences after incubation with the target. While larger molecules like proteins or cells can be separated easily based on size or surface immobilization, smaller molecules pose a greater challenge due to their minimal size differences in nucleic acid libraries and library-ligand complexes and the difficulties involved in labelling of the ligands. Over the past years, various SELEX strategies have been developed, primarily inspired by different molecular properties of targets.

2.4 SELEX variations

Despite being established for over thirty years, SELEX lacks a universal method applicable to all target types and uses. Instead, the SELEX process has been adapted into various forms, each tailored to meet the specific characteristics of the target molecule. Factors like target size, charge, solubility, and cellular location influence the selection of a SELEX approach, including specialized techniques such as cell-SELEX for whole-cell targets[37], capture-SELEX for small molecules[27], and counter-SELEX for improved specificity.[38] These adaptations have broadened the range of aptamer uses, facilitating applications in biosensing, diagnostics, therapeutics, and synthetic biology.

Efforts to refine SELEX have led to the development of various variants, including negative selection, counter-SELEX, bead-based SELEX, and others. The first two aim to enhance the final specificity of enriched aptamers: one by removing sequences that bind nonspecifically to irrelevant molecules or matrix components, thus improving the overall specificity; and the other by introducing structurally related molecules during selection to eliminate cross-reactive sequences. Other SELEX methods focus more on differences in the partitioning process, which are specific to the target type. For example, bead-based SELEX simplifies handling of nucleic acid libraries and targets by immobilizing them on solid supports, making separation easier. Additionally, separation of larger molecules like proteins without labelling can be achieved through size differences, using techniques such as capillary electrophoresis (CE-SELEX), size-exclusion chromatography (SEC-SELEX), nitrocellulose filter binding, or gel shift SELEX (EMSA-SELEX).

Unfortunately, neither the size difference between free nucleic acids and nucleic acid-ligand complexes nor the immobilization of the small-molecule target can be readily employed for small-molecule aptamer

selection. The process of attaching small molecules to solid supports can alter their native conformation or introduce steric hindrance, thereby affecting their binding characteristics. Therefore, efforts have been made to select aptamers for small molecules using immobilization-free SELEX. Townshend, et al. [39] employed the *de novo* rapid *in vitro* evolution of RNA biosensors (DRIVER) methodology, which uses aptamer-coupled ribozyme libraries along with a ribozyme regeneration technique and high-throughput characterization (CleaveSeq). This approach facilitated the multiplexed discovery of biosensors for ligands such as theophylline, acyclovir, noscapine, and several others. Another approach, which does not require ligand immobilization, is graphene oxide-SELEX (GO-SELEX), in which free ssDNA adsorbs to graphene oxide (GO), while ssDNA bound to small molecules is released.[40-42] Finally, a capture-SELEX method was established where the library is immobilized, and the small molecule is free in solution.[27] The bound and unbound sequences are here separated by the release of bound sequences into solution upon target binding.

Despite these methodological advances, no universally applicable SELEX strategy exists, and selection success remains highly target-dependent, particularly for small molecules. RNA aptamers selected to bind specific small-molecule targets can be particularly valuable in applications such as drug delivery, sensing, and gene regulation, in ways similar to their natural counterparts, riboswitches.

3. Riboswitches: natural aptamers and inspiration for aptamer's application

As previously mentioned, part of the naturally occurring RNA has evolved into structural and catalytic polymers used for gene regulation, either by employing catalytic activity during structure formation in ribozymes or by employing structure-switching activity upon molecular recognition in riboswitches.

The later RNA elements found in bacteria, plants, and fungi are located in the untranslated regions (UTRs) of messenger RNAs (mRNAs) and serve as direct sensors for small molecules and metabolites.[43] Riboswitches contain an intrinsic aptamer domain that binds to ligands, triggering structural changes that control gene expression, as shown in **Figure 3**. A well-known example is the thiamine pyrophosphate (TPP) riboswitch, which selectively binds TPP and regulates genes associated with thiamine metabolism.[16, 44] Other riboswitches, among many, respond to metabolites such as adenine,[45] guanine,[46] and fluoride.[47]

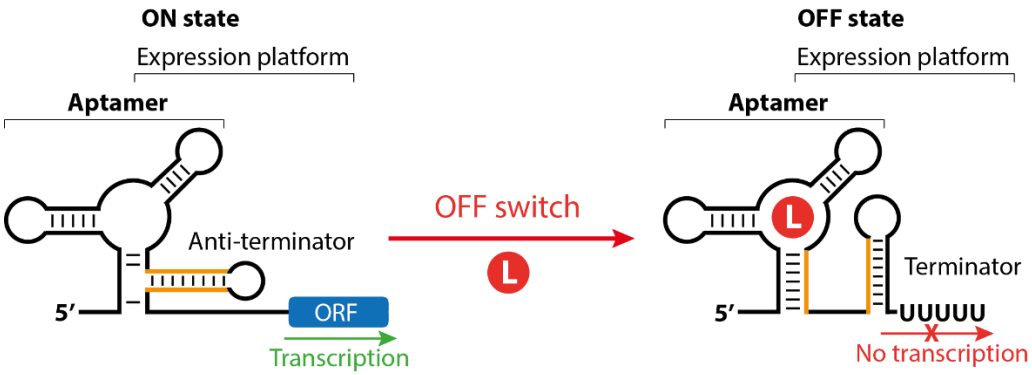

Figure 3. An example of a riboswitch's function and structure, featuring an aptamer and an expression domain. The figure was modified according to Salvail and Breaker [43].

L = ligand, ORF = open reading frame.

Similar to naturally occurring riboswitches, RNA aptamers can be adapted into molecular sensors to develop synthetic RNA sensors. In contrast to SELEX-derived aptamers, riboswitches function effectively within their native biological context, merging molecular recognition with gene regulation. However, the first synthetic RNA sensor was developed before the discovery of riboswitches by joining an ATP aptamer to an existing ribozyme to enable ATP-controlled ribozyme self-cleavage.[48] This study paved the way for the field of allosteric RNA sensors.[49] Furthermore, an important technological advancement was made by the emergence of fluorogenic RNA aptamers. The first aptamer selection for fluorophores was performed with sulforhodamine B and fluorescein to utilize them for double-labelling experiments to detect intracellular transcription localization.[50] Later, a Spinach light-up aptamer was selected, enabling an RNA molecule to activate a fluorophore and provide a direct optical readout of RNA folding and ligand binding.[51] Subsequent work combined riboswitch-derived ligand-sensing aptamer module with fluorogenic RNA scaffolds to generate fully genetically encoded, allosteric fluorescent RNA sensors capable of detecting small molecules in living cells.[31]

While many natural riboswitches are known, they only cover a small range of biologically important ligands and are not easily adaptable to new targets. Moreover, using artificial aptamers poses challenges, as linking a target-specific aptamer to a fluorescent RNA module is complex and often demands extensive optimization to enable effective allosteric signal transmission.[52] Thus, a carefully designed SELEX method can be employed to discover aptamers targeting desired small molecules, which can be integrated into engineered constructs that replicate riboswitch designs.[53-54] This strategy expands the potential use from biosensing to gene regulation, and paves the way for RNA-based therapeutics and diagnostics.

4. Aim: High-throughput selection of RNA aptamers targeting small molecules and their application

The labour-intensive, frequently unsuccessful SELEX method underscores the need for a high-throughput approach for aptamer selection. Previously, a robotic-assisted selection method for RNA aptamers targeting proteins was established, accelerating the isolation of 2'-deoxy-2'-fluoro-modified RNA aptamers for therapeutic use.[55] Unfortunately, a SELEX design for selecting protein targets cannot be easily applied to selecting RNA aptamers targeting small molecules. Accordingly, this thesis aimed to develop an automated selection strategy specifically tailored to small-molecule targets.

RNA aptamers have been shown to perform well in target-controlled molecular gene editing and intracellular sensing.[56-57] As previously emphasized, selecting aptamers that target small molecules can be particularly challenging due to their chemical properties. Because of their small size and limited functional groups for immobilization, this study utilized a capture-SELEX approach. This immobilisation-free selection method has been widely used in several studies to select aptamers for a variety of small-molecule targets.[34-36] Nevertheless, a thorough investigation of different selection conditions and library design has not been previously done. Therefore, this study initially focused on determining optimal conditions for RNA library immobilization and optimizing selection steps suitable for the robotic platform. Furthermore, the suitability and selectability of the automated method were tested for several small-molecule targets.

The second part of the study focused on applying the automated selection method for RNA aptamers to identify novel RNA-based sensors capable of detecting any target of choice. In the design of allosteric RNA sensors, the simple linking of the aptamer and functional parts is not always straightforward;[52, 58] hence, a tailored library design to select allosteric RNA aptamers can improve their structural performance. Thus, the second part of this study introduces a thoughtful design of the RNA library structure, which can be used for *de novo* selection of target-specific allosteric RNA sensors coupled with the existing fluorogenic light-up RNA aptamers. To enable modular use of fluorogenic aptamers that bind to two different fluorophores, emitting light at green or red wavelengths, the library design was tailored to support coupling with both aptamers. Although the selection was performed only for a single target, for which the selected aptamer is not particularly important given the availability of a natural riboswitch, this study provides a foundation and platform for high-throughput selection of allosteric sensors for any target. Furthermore, while the library was designed specifically for coupling to a particular fluorogenic aptamer, a similar design can be easily applied to any fluorogenic aptamer.

5. Capture-SELEX

Capture-SELEX's name was first introduced by Stoltenburg, et al. [27] for the selection of DNA aptamers targeting aminoglycoside antibiotics. However, the underlying principle had already been applied earlier

by Nutiu and Li [32], Morse [59], and Rajendran and Ellington [33], who independently employed library immobilization strategies to select DNA or RNA aptamers against small-molecule targets such as ATP, GTP, tobramycin, and zinc. Since then, capture-SELEX has been widely adopted and further refined for a broad range of low-molecular-weight ligands.

Capture-SELEX is specifically designed for targets that cannot be readily immobilized without disturbing their native structure. Instead of attaching the ligand to a solid support, the nucleic acid library is indirectly immobilized via hybridization to a complementary capture-oligodeoxynucleotide (ODN) coupled to magnetic beads (**Figure 4**). The selection process begins with hybridizing the library to the capture-ODN, followed by the introduction of the target molecule into solution. Subsequently, it is assumed that the target binding induces a conformational change in the aptamer candidates, thereby reducing their hybridization efficiency with the capture sequence and facilitating their release into solution. These eluted sequences, which, among others, show preferential binding to the target but can also be nonspecifically dissociating, are then amplified and reintroduced into subsequent selection cycles to enhance affinity and specificity.

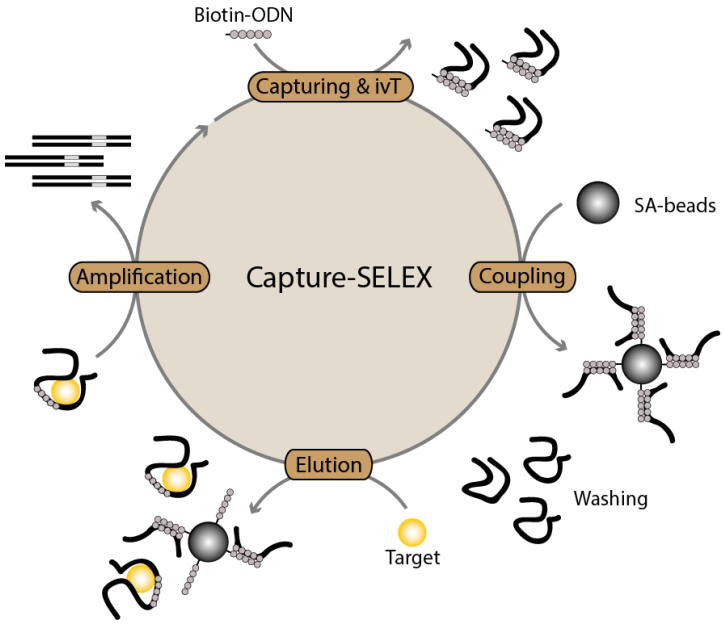

Figure 4. Scheme of the capture-SELEX method. Main steps are 1) capturing of RNA to short ODN during transcription, 2) coupling of RNA-ODN duplexes on magnetic beads and removing weakly bound sequences, 3) elution of binding sequences by addition of a target solution, and 4) reverse transcription and amplification (RT-PCR) of dissociated sequences. ODN = oligodeoxynucleotides, SA = streptavidin.

While this strategy preserves the native chemical properties of the ligand, it introduces additional constraints on selection stringency. Successful enrichment depends on a delicate balance between sufficient hybridization stability to suppress nonspecific dissociation and adequate flexibility to allow target-induced release. Consequently, capture-SELEX often yields aptamers with moderate affinities, typically in the micromolar range.

Table 1: Summary of capture-SELEX publications using small-molecule ligands

N	Library	Target Name	Library	K_d [M]	Reference
1	DNA	ATP, GTP	PBS-N10-DS15-N20-PBS	n.a.	Nutiu and Li [32]
2	DNA	Zinc	DS12-PBS-N50-PBS	15×10^{-6}	Rajendran and Ellington [33]
3	RNA	Tobramycin	DS6-PBS-N60-PBS	$16\text{-}500 \times 10^{-6}$	Morse [59]
4	DNA	Kanamycin A	PBS-N10-DS12-N40-PBS	3.9×10^{-6}	Stoltenburg, et al. [27]
5	DNA	Cortisol	DS7-9-PBS-N40-PBS	16.1×10^{-6}	Martin, et al. [60]
6	DNA	Tobramycin	DS12-PBS-N60-PBS	0.2×10^{-6}	Spiga, et al. [61]
7	DNA	Thioflavin T	DS18-N30-PBS	4.17×10^{-6}	Wang, et al. [62]
8	DNA	Penicillin G	PBS-N10-DS12-N40-PBS	n.a.	Paniel, et al. [63]
9	DNA	Geniposide	DS18-N40-PBS	2×10^{-6}	Zhang, et al. [64]
10	RNA	Rebaudioside A Carminic acid	PBS-N10-DS12-N40-PBS	n.a.	Lauridsen, et al. [65]
11	DNA	Vanillin	PBS-N10-DS12-N40-PBS	0.9×10^{-6}	Kuznetsov, et al. [35]
12	DNA	Furaneol	PBS-N10-DS12-N40-PBS	1.1×10^{-6}	Komarova, et al. [34]
13	DNA	Serotonin Dopamine Glucose S1P	PBS-DS15-N30-36-DSc8-PBS	30×10^{-9} 150×10^{-9} 10×10^{-3} 180×10^{-9}	Nakatsuka, et al. [9]
14	RNA	ATP	PBS-N40-DS13-N10-PBS	n.a.	Boussebayle, et al. [21]
15	RNA	Paromomycin	PBS-N40-DS13-N10-PBS	20×10^{-9}	Boussebayle, et al. [36]
16	DNA	Caffeine	DS18-N30-PBS	$2.2\text{-}14.6 \times 10^{-6}$	Huang and Liu [66]
17	DNA	Salicylic acid	DS18-N30-PBS	26.7×10^{-6}	Gu, et al. [67]
18	DNA	Chloramphenicol	DS18-N30-PBS	9.8×10^{-6}	Zhao, et al. [68]
19	DNA	Flunixin	DS15-N30-DSc8-PBS	250×10^{-9}	Alkhamis and Xiao [38]
20	DNA	Leucine Variconazole	PBS-DS15-N36-DSc8-PBS	170×10^{-9}	Yang, et al. [69]
21	DNA	Kanamycin A	DS18-N30-PBS	320×10^{-9}	Zhao and Liu [70]
22	RNA	Okadaic acid Dinophysistoxin-1 Azaspiracid-1	PBS-N40-DS19	2.139×10^{-6} 3.755×10^{-7} 2.429×10^{-6}	Sun, et al. [71]

Note: If several aptamers have been identified for a single target, only the affinity of the best binding aptamer was reported here.
DS = docking sequence, DSc = docking sequence complement, PBS = primer-binding site, n.a. = not applicable, S1P = sphingosine-1-phosphate.

Table 1 summarizes representative capture-SELEX studies targeting small molecules using DNA or RNA libraries. Despite substantial variation in library architectures, docking-sequence lengths, and selection conditions, the majority of reported dissociation constants fall within the micromolar range. Only a limited number of studies report nanomolar affinities, typically achieved through highly optimized library designs or stringent selection pressures. Some publications that yielded aptamers with nanomolar affinity employed a specially designed library containing a loop with a random region flanked by a stem formed by a DS and its complement (DSc) in the absence of a capture-ODN.[9, 38] Other approaches yielding aptamers binding in nanomolar ranges developed carefully optimized and target-tailored selection protocols, which often incorporate precise control of the initial ligand concentration and systematic counter-selection using structurally related analogs to enhance specificity.[9, 36, 38] In a study by Alkhamis and Xiao [38], it was shown that gradually decreasing the target concentration, especially with a steep gradient, greatly increased the likelihood of selecting high-affinity binders. Additionally, their use of a strict counter-selection process effectively reduced off-target interactions, highlighting the importance of counter-selection in isolating highly specific aptamers using the capture-SELEX platform.

Despite these advances, no systematic investigation has yet evaluated how docking-sequence length and placement influence enrichment efficiency and affinity in capture-SELEX. An automated, operator-independent platform capable of executing multiple selections in parallel would therefore be valuable for optimization and reproducible performance.

5.1 Automated SELEX

Automation has substantially improved the reproducibility and throughput of SELEX workflows. In 1998, Cox, et al. [72] developed an automated RNA selection protocol, utilizing a robotic system to streamline the *in vitro* selection of RNA aptamers, thereby reducing manual intervention and selection time. In their follow-up publications, they employed the protocol to select aptamers targeting the lysozyme and U1A proteins, thereby demonstrating the ability of an aptamer to inhibit protein function and the ability of SELEX to select sequences resembling the sequence of a naturally binding nucleic acid, respectively.[73-74] Building upon this, Eulberg, et al. [75] introduced an automated SELEX process that minimized manual intervention, streamlining the *in vitro* selection of RNA-based aptamers. Further advancements included the development of a semi-automated SELEX method termed "Just in Time-Selection".[76] This approach combined magnetic separation with BEAMing technology to isolate DNA aptamers, significantly accelerating the selection process. In 2019, Breuers, et al. [55] reported a robotic-assisted generation of 2’-deoxy-2’-fluoro-modified RNA aptamers.

Building on these advancements, Zhang, et al. [77] developed an automated capture-SELEX device designed to screen for aptamers targeting β-conglycinin, a soy allergen, leading to the identification of a high-affinity aptamer, β-5, with a dissociation constant (K_d) of 18.24 ± 2.42 nM.

While these systems demonstrated the feasibility of automation, most were optimized for protein targets and cannot be directly translated to small-molecule selection without substantial modification. This gap motivated the development of automated capture-SELEX strategies tailored explicitly to low-molecular-weight ligands.

5.2 Establishment of automated capture-SELEX selecting RNA aptamers (Publication 1) [78]

In this work, a fully automated capture-SELEX platform was developed to enable operator-independent selection of RNA aptamers targeting small molecules.[78] The system was implemented on a Biomek XP liquid-handling workstation and designed to perform all selection steps, including hybridization, washing, elution, reverse transcription, PCR amplification, and *in vitro* transcription, without manual intervention.

The selection strategy was based on the capture-SELEX principle, which previously proved to be an efficient method for aptamer selection targeting small molecules. Previous papers utilized two different ways of library capturing on the magnetic beads via complementary biotinylated ODN, which were named high-density beads (HDB) [27] and low-density beads (LDB) [21] capturing. So far, a systematic comparison between these two approaches has not been carried out; thus, they were evaluated side by side in this study. The binding profile of the enriched library pool revealed a higher elution of sequences by a neomycin B target from LDB selection compared to HDB selection. It was postulated that the LDB selection is superior to the HDB, because it optimizes the density of capture ODNs on the beads, thereby improving target binding and elution efficiency. LDB facilitated the recovery of high-affinity sequences by reducing steric hindrance and nonspecific interactions. Subsequently, the LDB selection was automated to avoid manual intervention throughout all 12 cycles, totalling 72 hours. The initial robot selection targeting neomycin B exhibited a binding profile consistent with the enriched pool, and a similar enrichment profile was observed in next-generation sequencing (NGS) data, aligning with the results from manual LDB selection. The most enriched sequence from the robotic LDB selection, LR1, was also prevalent in the manual LDB selection. LR1 demonstrated an affinity of 3 μM in fluorescence polarization assays and 34.7 ± 1.97 μM in isothermal titration calorimetry (ITC). Although no counter-SELEX was used during the process, the aptamer bound specifically to neomycin B and showed weaker binding to kanamycin, a chemically similar molecule. It did not bind to other tested compounds such as ampicillin, cAMP, arginine, or theophylline. The K_d for LR1 binding to kanamycin was approximately four times higher than its binding to neomycin B, as measured by ITC at 130.0 ± 30.9 μM.

Following validation with neomycin B, the automated platform was applied to 13 additional small-molecule targets. Functional aptamers were successfully identified for four ligands, corresponding to a success rate of approximately 30%. While this rate may appear modest, it is consistent with reported outcomes for small-molecule SELEX and reflects the inherent difficulty of selecting high-affinity binders against chemically simple targets.[79-80] The observed affinity range is also consistent with

expectations for capture-SELEX, where indirect partitioning limits selection stringency compared to immobilization-based protocols. Nevertheless, capture-SELEX offers distinct advantages, including preservation of ligand integrity, standardized workflows, and compatibility with automation.

A fluorescence-based assay was also introduced, offering a quick, quantitative way to evaluate aptamer binding. This method removes the necessity for lengthy radioactive tests and RNA labelling. The assay utilized the displacement of the fluorescently labelled capture-ODN from the complementary RNA in the presence of the binding target. Optimizing the capture-ODN length improved the dynamic range. All RNAs contained the same complementary sequence to the capture-ODN, but different RNA sequences exhibited varying affinities to the same capture-ODNs. By customizing the capture-ODN length for each RNA sequence, assay performance could be enhanced. Additionally, affinity measurements from the fluorescence polarization assay were compared to those from ITC. Although fluorescence polarization consistently yielded lower K_d values than ITC, the measured K_d values were often lower yet within a similar range, as is common since different methods can produce varying binding affinity results.[81]

Overall, the robotic capture-SELEX system transforms a traditionally labour-intensive and operator-dependent process into a standardized, high-throughput selection pipeline. While affinity optimization remains target-dependent, the platform provides a robust foundation for systematic investigation of SELEX parameters and downstream functional deployment.

6. Application of RNA aptamers targeting small molecules

RNA aptamers have been widely applied as molecular recognition elements in biosensing, diagnostics, and gene regulation.[9, 68, 71, 82] Their high specificity and strong binding make them suitable for incorporation into diagnostic tools like electrochemical sensors [9, 83] and fluorescence assays.[58, 84]

In electrochemical aptamer-based sensors (EAB), target-recognizing aptamers are typically immobilized on a gold electrode for signal generation. DNA aptamers that detect natural molecules, such as serotonin, dopamine, glucose, and sphingosine-1-phosphate, were successfully selected and utilized in EAB.[9] Additionally, Nakatsuka, et al. [85] developed high-affinity aptamer-functionalized nanopipette sensors capable of detecting serotonin levels secreted by human neurons, with enough specificity to distinguish neurotransmitters and their metabolites. While highly sensitive, these platforms require specialized instrumentation and are not readily adaptable to intracellular sensing.

6.1 Fluorogenic RNA aptamers as sensor scaffolds

A major breakthrough in RNA-based sensing was the development of fluorogenic light-up RNA aptamers, which activate small-molecule fluorophores upon binding. The first fluorogenic light-up aptamer was reported in 2011 by Paige [51], who developed an RNA aptamer that binds fluorophores similar to those in green fluorescent protein (GFP), called 3,5-difluoro-4-hydroxybenzylidene

imidazolinone (DFHBI). This RNA-fluorophore complex, named Spinach, mimics enhanced GFP and produces bright green fluorescence comparable to fluorescent proteins. In a subsequent study, they demonstrated live-cell imaging of S-adenosylmethionine (SAM) by expressing an RNA-based sensor containing a SAM-binding RNA aptamer derived from a natural riboswitch embedded in the stem loop of Spinach, thereby controlling Spinach aptamer folding by the binding and structure stabilization of SAM aptamer.[31] Additionally, they fused multiple aptamers that bind adenosine, guanine, or guanosine 5′-triphosphate (GTP) to Spinach through a stem sequence acting as a "transducer".[31] Furthermore, Jaffrey's group used fluorescence-activated cell sorting (FACS) of millions of aptamers expressed in *Escherichia coli* to select an improved Broccoli aptamer binding to DFHBI, which is superior in folding when cytosolic magnesium levels are low. Broccoli exhibits strong folding and green fluorescence in cells, and shows increased fluorescence compared to Spinach.[26] Since then, numerous fluorogenic aptamers have been reported binding to a wide range of fluorophores such as Mango,[86] Corn,[87] Pepper,[88] and several others shown in **Figure 5A**. In Li, et al. [57], they developed a new red fluorophore called OBI (3,5-difluoro-4-hydroxybenzylidene-imidazolinone-2-oxime-1-benzoimidazole), which is especially useful for live-cell imaging due to its low red background fluorescence in cells. They then used Red broccoli, which is structurally similar to regular Broccoli and binds to the OBI, displaying bright red fluorescence inside cells. Additionally, they demonstrated that Red broccoli can be fused to a SAM-binding aptamer, creating a sensor that produces red fluorescence in response to SAM levels in mammalian cells treated with OBI. Previous publications described two structural modes of action of RNA based sensors: first, incorporating a ligand-binding aptamer into the stem loop of a fluorogenic RNA aptamer, which regulates the folding of the fluorogenic aptamer through ligand binding (**Figure 5B**);[31, 57] and the second, by interaction of part of a ligand-binding aptamer sequence with part of the fluorogenic aptamer, thereby preventing the fluorogenic aptamer from folding in the absence of the ligand. (**Figure 5C**).[52, 58]

Despite substantial progress, the development of RNA-based fluorescent sensors remains labour-intensive and target-specific. Traditional sensor design requires detailed structural knowledge of both the ligand-binding aptamer and the fluorogenic scaffold, as well as extensive empirical optimization of linker and transducer regions to achieve effective allosteric coupling. Moreover, most existing sensors rely on naturally occurring riboswitches or previously characterized aptamers, limiting their applicability to a narrow set of ligands. Consequently, there is a lack of generalizable strategies for rapidly converting newly selected aptamers into functional RNA sensors. To address this limitation, the automated capture-SELEX platform described in the previous chapter was adapted to enable the direct selection of allosteric RNA sensors. Rather than selecting aptamers solely for binding affinity, the strategy was designed to enrich for sequences structurally compatible with fluorogenic RNA scaffolds and capable of signal transduction.

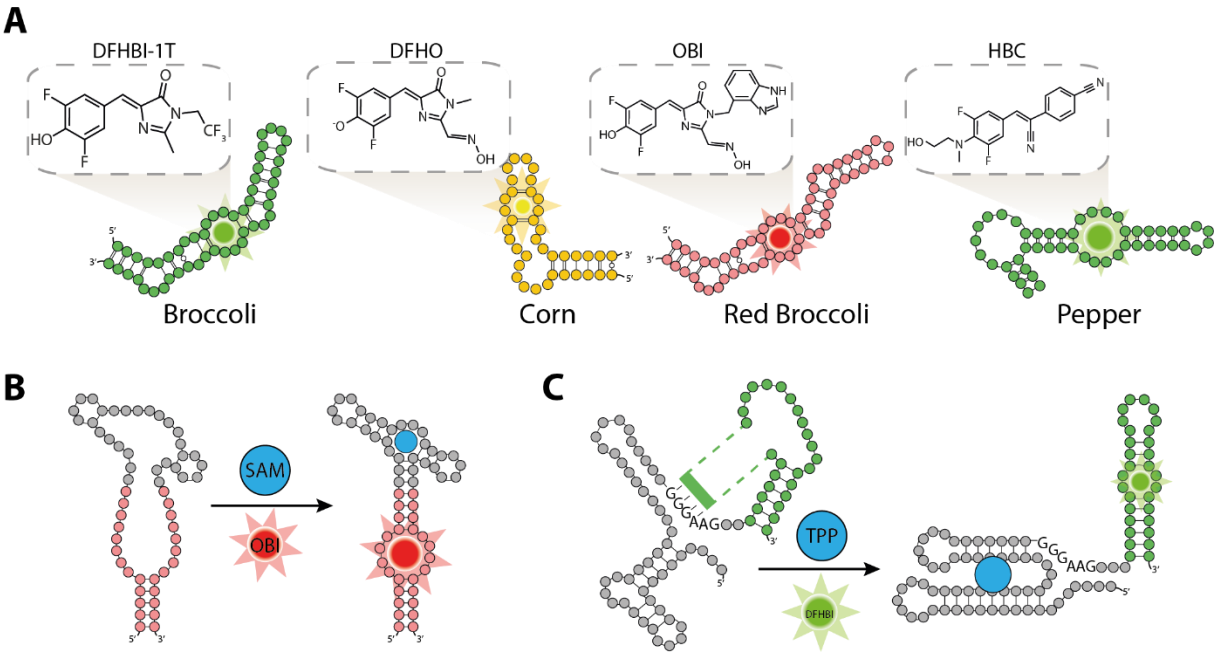

Figure 5. Fluorogenic RNA aptamers and their incorporation into light-up RNA sensors. A) Various fluorogenic RNA aptamers bind to different fluorophores, emitting fluorescence upon binding across a spectrum of colours.[26, 57, 87-88] **B)** SAM-based light-up sensor with integrated Red broccoli fluorogenic aptamer.[57] The SAM riboswitch is incorporated into the stem loop of the Red broccoli sensor. When SAM binds to the SAM riboswitch, it stabilizes the Red broccoli structure, allowing it to bind to the OBI molecule. Modified from Li, et al. [57] **C)** TPP-based light-up sensor with integrated Spinach fluorogenic aptamer.[58] The TPP-riboswitch interacts with the Spinach sequences, preventing the formation of the Spinach structure. When TPP binds to the riboswitch, it undergoes a conformational change, releasing the complementary Spinach sequence. This allows the DFHBI molecule to bind to the folded Spinach structure. Modified from You, et al. [58].

DFHBI = (Z)-4-(3,5-difluoro-4-hydroxybenzylidene)-1,2-dimethyl-1H-imidazol-5(4H)-one, DFHO = (3,5-difluoro-4-hydroxybenzylidene imidazolinone-2-oxime), HBC = (4-((2-hydroxyethyl)(methyl)amino)-benzylidene)-cyanophenylacetonitrile, OBI = 3,5-difluoro-4-hydroxybenzylidene-imidazolinone-2-oxime-1-benzoimidazole, SAM = S-adenosyl-L-methionine, TPP = thiamine pyrophosphate.

6.2 Development of modular allosteric RNA sensors (Publication 2) [89]

In the second publication, this modular strategy was implemented to enable de novo selection of RNA-based fluorescent sensors.[78, 89] The approach leverages the docking sequence used for library immobilization during capture-SELEX as an interaction interface with fluorogenic aptamers such as Broccoli and Red Broccoli. In this design, hybridization between the ligand-binding module and the fluorogenic scaffold prevents fluorescence in the absence of the target, while ligand-induced folding disrupts this interaction, restoring fluorescence.

During the initial phase of the study, the molecular structure of the RNA sensor library was optimized to identify the interaction between the two modules, ensuring a strong enough interaction to prevent Broccoli folding in the absence of the ligand and to facilitate easy displacement of the docking sequence by aptamer folding upon ligand addition. Out of five docking strand lengths complementary to the Broccoli sequence (SE4–SE12), SE8 with 8-nt complementary sequence was identified as the most suitable choice. Shorter sequences (SE4, SE6) showed weak hybridization with Broccoli, leading to higher background fluorescence, while longer sequences (SE10, SE12) hindered signal induction by the addition of complementary ODN. While the SE12 library also showed relatively low background

fluorescence without the ODN and a high turn-on when the ODN was added, the hybridization energy in this case might be stronger than the ligand-aptamer interaction. This was later confirmed when hybridization with a 12-nt docking strand was not sufficiently disrupted by target binding, as shown by fluorescence anisotropy measurements, indicating that SE8 achieves the best balance. Additionally, extending the stem of the Broccoli domain further improved performance.

Furthermore, as a proof of concept, thiamine pyrophosphate (TPP) was selected as the target ligand due to the availability of its natural riboswitch.[16] Capture-SELEX was performed using the optimized SE8 library under the low-density bead (LDB) protocol established in Legen and Mayer [78]. After the Next-generation sequencing (NGS) analysis, the five most abundant sequences (S1−S5) and the sequences with the highest rate of enrichment from rounds 8−12 were examined. Although some of the most enriched sequences showed fairly good binding, no sequence from the latter group demonstrated binding either in the fluorescence polarization assay or when coupled to Broccoli and analysed by fluorescence measurement of DFHBI-1T binding.

S1 and S5 sequences from the five most abundant sequences were chosen for further characterization of binding and improvement of signal increase due to the addition of the ligand. Firstly, the affinities of S1 and S5 for TPP were tested, and it was determined that both aptamers bind with similar affinities, 479 ± 136 and 462 ± 94.8 μM, respectively, which are much lower than the affinity of the natural TPP riboswitch.[16] Nevertheless, the characterization of the aptamers coupled to the Broccoli was continued, and it was proven that the additional spacer sequence length consisting of adenines between the S1 and S5 aptamer and Broccoli aptamer sequences increases the fluorescence signal by ligand addition, especially by the length of the polyA spacer of seven nucleotides. Furthermore, the specificity of the adjusted S1- and S5-sensor was tested using structurally similar molecules, such as thiamine monophosphate, thiamine, guanosine triphosphate, and adenosine triphosphate. While both S1- and S5-sensors show reduced binding to the thiamine monophosphate, binding to the rest of the ligands is minimal or not binding at all. To further demonstrate allosteric activation of the sensor by TPP binding, point mutations were introduced into the regions of S1 and S5 that complement Broccoli. These mutations resulted in a significant loss of sensing ability, even with a single point mutation.

To demonstrate modularity, both aptamers were also coupled to the Red Broccoli scaffold, yielding red-shifted sensors that retained ligand responsiveness. The sensor showed a concentration-dependent increase in red fluorescence across the tested TPP concentration range of 0.5 to 2 mM.

While the selected sensors exhibit modest turn-on ratios and require millimolar ligand concentrations, these limitations mainly reflect the moderate affinities of the selected aptamers. Importantly, the modular selection framework is compatible with further optimization strategies, including more stringent selection pressures, counter-selection schemes, and droplet-based high-throughput screening approaches.[52, 90] Together, these approaches provide a clear pathway toward generating RNA sensors with affinities and dynamic ranges comparable to natural riboswitches.

6.3 Gene regulation using RNA aptamers

Additionally, RNA aptamers have therapeutic applications, including targeted drug delivery and gene regulation.[91-92] Attaching aptamers to drugs or genetic materials enables improved precision and effectiveness in treatments. In synthetic biology, RNA aptamers are components of genetic circuits and regulatory networks. For example, riboswitches, natural RNA elements that regulate gene expression in response to metabolite binding, have inspired the design of synthetic aptamers capable of controlling gene expression.

Numerous reports describe the use of natural riboswitches in artificial gene regulation systems (**Figure 6**). Hedwig, et al. [93] employed a bacterial xanthine I riboswitch aptamer that detects oxypurinol, the active metabolite of the commonly prescribed anti-gout medication allopurinol. They demonstrated that oxypurinol binds to the aptamer like the natural ligand. Using the natural aptamer, they constructed two gene-regulating mechanisms that depend on the presence of oxypurinol: using Hammerhead (HHR) ribozymes to achieve OFF-switches, or regulating the splice-site accessibility of an alternative exon to generate ON-switches. Furthermore, Nomura, et al. [94] showed that the usage of guanine aptamer naturally found in the 5′ UTR of *Bacillus subtilis* [46] and *in vitro* selected theophylline aptamer [95] coupled to the Hepatitis delta virus (HDV) ribozymes works as a natural ON/OFF switch in mammalian cells. Likewise, Strobel, et al. [96] described a fast and broadly applicable method to functionally screen complex riboswitch libraries by coupling guanine and tetracycline aptamers to HDV, HHR and Twister ribozymes as well as U1-snRNP polyadenylation. Using cDNA-amplicon-seq, they identified several combinations of ON- or OFF-switches. Using a similar gene-regulating system based on U1-snRNP polyadenylation Rovira, et al. [97] presented *de novo* selection of highly effective tetracycline-based riboswitches named Systematic Evolution of Riboswitches by Exponential Enrichment (SEREX).

In a different approach, Mou, et al. [56] embedded a tetracycline aptamer selected *in vitro* within the 3’ UTR of an mRNA, located downstream of a microRNA (miRNA) target site. They demonstrated that without tetracycline, gene expression is turned off because the miRNA binds and recruits the RNA-induced silencing complex (RISC). Conversely, when the ligand is present, the aptamer's complementary strand binds with the miRNA target site as a result of structural changes induced by ligand binding. Furthermore, Mol, et al. [98] inserted a tetracycline aptamer in proximity to the 5′ splice site, thereby controlling the intron retention via the binding of tetracycline to the aptamer.

The diverse applications of aptamers in gene regulation, as emphasized above, underscore the need to develop new, rapid, and structurally dynamic aptamer selection methods. Creating *de novo* riboswitches is crucial for expanding RNA-based gene regulators beyond those found naturally. Automating the selection process with a robotic platform as described in Legen and Mayer [78] enables precise, high-throughput discovery of ligand-responsive aptamers under consistent conditions.

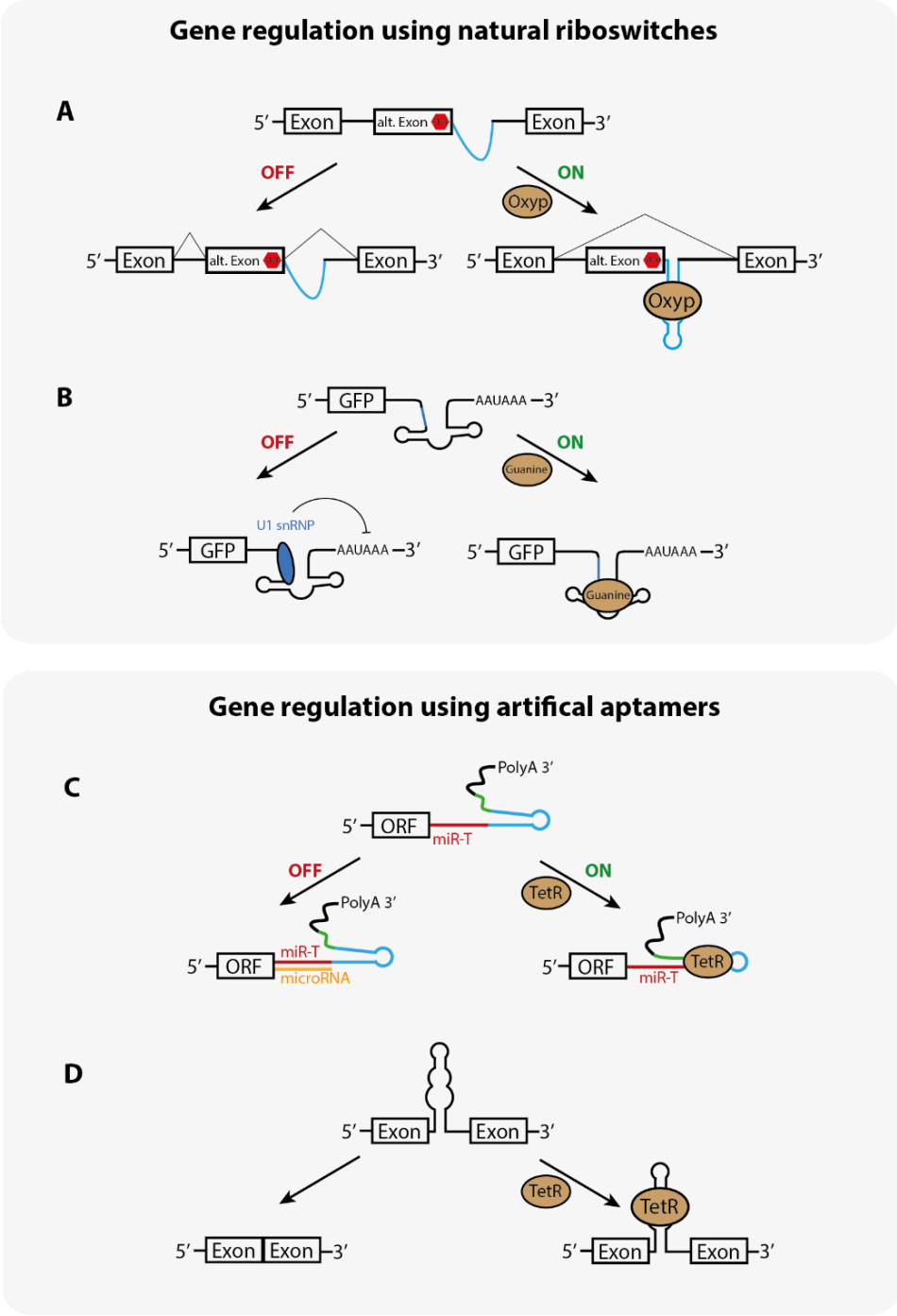

Figure 6. Gene regulation using natural riboswitches and artificially selected aptamers. A) Gene regulation through a natural xanthine riboswitch that recognizes oxypurinol analogs.[93] When oxypurinol is absent, an alternative exon is retained, which contains a stop codon and leads to gene repression. Without oxypurinol, the folding of the xanthine riboswitch located in the intron causes the exon to be skipped, resulting in gene upregulation. Modified from Hedwig, et al. [93] **B)** Gene regulation through a natural guanine riboswitch utilizing a U1 snRNP binding and polyadenylation prevention.[96] In the absence of the guanine, the U1 snRNP binds to the exposed U1 binding site, thereby preventing the polyadenylation and gene expression. In the presence of guanine, the aptamer undergoes a conformational change, disrupting the U1 binding site and thereby allowing the expression of the gene. Modified from Strobel, et al. [96] **C)** Gene regulation involves an artificially selected tetracycline aptamer that interferes with the miR-T site. Without the tetracycline aptamer, the miR-T site is exposed to microRNA binding, leading to gene repression. When tetracycline is present, the aptamer folds in a way that conceals the miR-T site, resulting in increased gene expression. Modified from Mou, et al. [56]. **D)** Intron retention achieved by using the artificially selected tetracycline aptamer embedded within the intron.[98] When tetracycline is added, the aptamer's folding blocks intron splicing. Modified from Mol, et al. [98].

Alt. Exon = alternative exon, GFP = green fluorescence protein, microRNA = micro ribonucleic acid, miR-T = micro ribonucleic acid target side = Open reading frame, OxyP = oxypurinol, TetR = tetracycline, U1 snRNP = U1 small nuclear ribonucleoprotein.

SUMMARY

This thesis presents two innovative methods: robotic-assisted capture-SELEX [78] and the design of modular allosteric RNA sensors.[89] By combining an automated capture-SELEX platform with a modular strategy for constructing allosteric RNA sensors, this work addresses two central bottlenecks in the field: the lack of standardized, high-throughput aptamer selection methods for small molecules and the difficulty of converting newly identified aptamers into functional sensing devices.

In the first publication, a robotic-assisted capture-SELEX platform was developed to streamline the discovery of RNA aptamers that bind small molecules. Traditional SELEX protocols for small molecules often rely on target immobilization, which can alter ligand structure and affect aptamer enrichment. To address these issues, capture-SELEX was used, where nucleic acid libraries are immobilized via a docking sequence hybridized to a complementary oligodeoxynucleotide (ODN) on magnetic beads, while the target remains free in solution. This approach preserves the target's native conformation and enriches sequences that undergo conformational changes upon binding. By implementing this method on a robotic platform, manual intervention was reduced, and it was demonstrated that up to 12 iterative selection cycles could be completed within 72 hours, significantly reducing the time and labour required compared to conventional manual SELEX.

Currently, the platform's efficiency is limited by the number of available positions and its size. Since the 96-well plates must be divided in half due to limited space on the pipetting platform, the maximum number of parallel selections is only four. Therefore, by switching to a larger platform, the Biomek i5, available from the same company (Beckman Coulter), the high-throughput selection could be easily scaled up to eight targets or selection conditions per 96-well plate. On the contrary, the required time depends on the number of selection rounds and the length of individual process steps. In this study, little focus was placed on optimizing and minimizing the time required for individual incubation steps or on reducing the number of selection rounds, since they were not essential to the initial process establishment. However, with further optimizations, the incubation times for capture, coupling, elution, PCR, and IVT reactions can be drastically reduced.

Automating capture-SELEX involved, in the first step, a thorough re-examination of each process step. Instead of including laborious nucleic acid purification between selection rounds, an approach was introduced in which RNA–target complexes were directly transferred into a reverse transcription reaction, including biotinylated reverse primer, and produced RNA-cDNA complexes were isolated from the target solution and moved to the PCR reaction. The amplified DNA was then transcribed *in vitro* in the presence of biotinylated capture-ODNs. This integration removed the target molecule from the solution before transferring it to the PCR reaction. This proved crucial after the initial failed attempts, as evidenced by the truncation of the library during the selection rounds. In the initial failed selections using theophylline and arginine targets, the truncation was hypothesised to occur because the molecular

structure is relatively stable and withstands the thermal stress of repeated PCR cycles, resulting in a target concentration of 90 µM in the IVT reaction.[99-100] Therefore, this failure most likely occurred because the aptamer selection was hindered by the presence of the target in the *in vitro* transcription and capturing step to ODNs. Consequently, the target's presence prevented binding sequences from hybridizing to the capture-ODNs. Conversely, selection with the neomycin B target, following the same initial protocol, was not affected by the truncation, suggesting the molecule's thermal stability is weaker.[101] Although this claim was not extensively investigated, testing with a reduced initial neomycin B concentration (50 µM) during the selection produced the same library truncation observed in the failed initial selection attempts. Similarly, a selection with no target in the selection buffer produced the same truncation. As a possible explanation, it was assumed that in the absence of the target, some sequences still nonspecifically dissociate from the beads, which might then lose parts of the random region, since it is no longer viable for selection, and the shorter length might be favourable in the PCR reaction.

In parallel, comparative experiments between high-density bead (HDB) selection, in which beads were saturated with capture-ODNs before RNA library binding, and low-density bead (LDB) selection, where capture-ODNs and RNA were hybridized in solution before immobilization, were conducted. The LDB approach clearly outperformed HDB, producing stronger and more specific aptamer recovery, whereas HDB most likely suffered from competition from excess unbound ODNs. Using neomycin B as a model ligand, the LDB protocol enriched aptamers with micromolar affinities, as verified by fluorescence polarization and isothermal titration calorimetry. Importantly, aptamers selected under the automated protocol exhibited strong binding to neomycin B and related aminoglycosides such as kanamycin B, but showed negligible cross-reactivity with unrelated small molecules. The method was extended to a broad panel of chemically diverse small molecules, including riboflavin, theophylline, 5-diphospho-myo-inositol pentakisphosphate (5-IP7), and others, demonstrating that the robotic platform is applicable across a wide range of targets.

After successfully establishing and implementing the capture-SELEX on the robotic platform, some limitations were identified. Many enriched aptamers showed affinities in the micromolar range, which is weaker than the nanomolar affinities reported in some studies using immobilized targets in SELEX.[102] Immobilization of the target enables more efficient separation of bound and unbound sequences and, therefore, more stringent selection conditions.

While most recent studies employing the capture-SELEX method yielded affinities similar to those identified in this study (**Table 1**), some studies still enriched aptamers binding in nanomolar ranges. These studies investigated and optimized initial ligand concentrations, applying sharper concentration drops across selection rounds, and using counter-selection to target similar molecules and increase specificity.[9, 38] Another possible improvement could be using longer capture ODNs, which could steer the selection toward sequences with tighter binding affinities by making it harder for the target to cause the RNA to detach. These minor adjustments to the selection protocol may significantly improve the

performance, and the high-throughput systematic testing would enable rapid testing of optimal conditions.

The current success rate of the established robotic platform was 30%, corresponding to the share of targets for which aptamers with determined affinities were successfully enriched. Similarly, previously reported success rates for SELEX targeting various molecules remain relatively low, especially for small molecules.[80] Multiplexed selection studies show that only a small fraction of tested ligands yield functional aptamers or biosensors, reporting in Townshend, et al. [79] a successful identification of RNA biosensors for only 217 targets out of a 5,120-target library. Thus, despite some limitations, the robotic platform helps improve the SELEX methodology, transforming an operator-dependent process into a standardized, high-throughput, and reproducible pipeline.

While the first publication focused on efficiently generating aptamers, the following one highlighted how these aptamers can be easily transformed into functional biosensors without needing knowledge of their structure. RNA-based fluorescent sensors are valuable tools for the real-time detection of small molecules in living systems; however, designing these sensors typically requires detailed structural knowledge of both the aptamer and the fluorogenic RNA reporter. Additionally, the labour-intensive process of linking aptamers to reporters often yields constructs that are difficult to adapt or modify. This challenge was addressed by developing a modular, allosteric strategy in which aptamers are linked to fluorogenic RNAs, such as Broccoli or Red Broccoli, via docking sequences and flexible linkers. This design enables the target metabolite to induce conformational changes that release the fluorogenic domain, allowing it to fold and activate fluorescence. Previously, a similar strategy has been employed by You, et al. [58] and Geraci, et al. [52], where they utilized either a natural riboswitch targeting thiamine pyrophosphate (TPP) or a selected aptamer targeting fructose 1,6-bisphosphate, respectively, linked to the spinach or baby spinach fluorogenic aptamer. They utilized the complementary interaction between two modules to activate or deactivate the fluorescence signal by ligand addition. To enhance the functionality of the hybrid, You, et al. [58] optimized the transducer sequence of the spinach complementary part to TPP riboswitch and linker sequence connecting both modules, to achieve the highest turn-on values for the TPP RNA-based sensor. Furthermore, Geraci, et al. [52] randomized the linker and end part of the ligand-binding aptamer structure to select functional sensors via droplet sorting that could allosterically operate in the presence of the fructose 1,6-bisphosphate target. This study builds on a similar idea by completely randomizing the selection library, enabling *de novo* aptamer selection for any small-molecule target. The established capture-SELEX platform would allow simultaneous use of the docking sequence for library immobilization to interact with a fluorogenic aptamer.[78]

As a proof of concept, five libraries (SE4–SE12) with varying degrees of complementarity to Broccoli were designed. The complementary sequence of the Broccoli was chosen from the same region of the Red broccoli sequence to facilitate easy switching between the two fluorogenic aptamers later. SE8 library was selected as the most effective one. This test aimed to find the optimal balance between the

hybridization energies of the ligand-binding aptamer and the fluorogenic aptamer. The goal was to ensure that the energy was strong enough to prevent Broccoli from folding in the absence of the ligand, but not so strong as to allow the ligand-binding aptamer to be displaced when the target molecule was present. Since these libraries lacked binding properties, a capture ODN was used for testing. A capture-SELEX was then carried out using thiamine pyrophosphate (TPP), and the enriched aptamers were analysed by next-generation sequencing. TPP-targeting RNA aptamers were manually enriched using the previously established procedure on the robot (publication 1).[78]

Specific aptamers (notably S1 and S5) were identified from these libraries and demonstrated the ability to bind TPP and activate fluorescence when linked to Broccoli via optimized linkers. By fine-tuning the linker composition, including the addition of adenosine-rich spacers, the sensor's dynamic range was significantly improved. The specificity test demonstrated that the sensors responded strongly to TPP and thiamine monophosphate, with minimal activation by thiamine or unrelated nucleotides, such as GDP and ATP. This design was modular, allowing easy replacement of Broccoli with Red Broccoli to create red-shifted sensor variants without compromising functionality. This confirmed that this strategy is versatile and not limited to a single fluorogenic domain, but rather represents a general approach to building light-up RNA sensors.

Although significant progress was made, challenges remain and highlight areas needing further work. The binding affinities of aptamers selected by capture-SELEX, although sufficient for proof-of-concept sensors, need to be improved to match or surpass those of natural riboswitches. This may involve refining selection pressures, incorporating counterselections, or using droplet microfluidic platforms that enable sorting individual aptamers with higher affinities, thereby increasing the affinity of selected aptamers and the success rate of selections targeting different ligands. Following new findings from systematically investigated SELEX conditions and target-tailored structural libraries in several studies[38, 69], these limitations could be overcome, especially with the help of a high-throughput and operator-independent platform. Alkhamis and Xiao [38] presented a well-designed selection process that focuses on investigating specific target concentrations and utilizes multiple similar analogs for counter-selection. Their findings suggest that starting with lower target concentrations and then sharply reducing them during selection can yield aptamers with stronger affinities. They also employed a thoughtful counter-selection strategy, emphasizing its significance. Furthermore, Yang, et al. [69] created a method for guiding aptamer selection by examining how specific chemical functional groups in small-molecule targets influence binding. They then applied this knowledge to design modified SELEX strategies that effectively produced aptamers for challenging targets, including leucine and voriconazole, which had previously been resistant to selection. Improvements to the already selected aptamers could also be achieved through the degeneration of the aptamer sequences to incorporate additional variability, along with repeated and more stringent selection processes to fine-tune the structure of the existing aptamer.[103-104] Additionally, a further characterization and truncation of the aptamer sequence might

improve the aptamer's binding affinity.[105-106] Last but not least, droplet sorting proved to be an efficient method for RNA-sensor selection, as it allows the selection of the best-performing sensors based on their functionality.[52, 90]

While only a proof-of-principle selection for one target was demonstrated using only Broccoli and Red Broccoli as the signalling modules, this method could be applied to any ligand molecule coupled with any fluorogenic aptamer. The performance of sensors can be improved by investigating alternative fluorogenic RNAs and linker structures and testing them in cellular environments. Furthermore, computational methods, such as machine learning-based prediction of aptamer folding and target recognition, could accelerate both selection and sensor design.[107-108] Similar significant progress has been made in the protein field, including the *de novo* design of protein structures, enzymes, logic gates, and molecular switches.[109-111] Addressing these developments, future work could produce aptamers and sensors with affinities and dynamic ranges comparable to natural biological systems.

Furthermore, a crucial next step in validating the functionality of the established TPP sensor is to demonstrate intracellular expression and confirm that it can detect variations in TPP levels within cells. Although this was not presented in this study, several other publications show successful employment of such sensors within cells and their reversible sensing ability. In this pioneering publication, Paige, et al. [31] successfully showcased imaging of the dynamic changes and cell-to-cell variation in the intracellular levels of adenosine 5′-diphosphate (ADP) and S-adenosylmethionine (SAM) in *Escherichia coli*. Furthermore, You, et al. [58] presented a TPP sensor and its intracellular application to track TPP levels, which were manipulated by the addition of adenosine, an inhibitor of *de novo* TPP biosynthesis. On the other hand, RNA sensors have also been employed to image RNA polymerase III transcription [87] and to detect endogenous mRNA within eukaryotic cells.[112] Since the RNA's half-life within cells is relatively short, Litke and Jaffrey [113] have presented an additional approach to tackle this problem. Their work describes a Tornado system that can circularize aptamers within cells by employing Twister ribozymes encoded within the transcripts that autocatalytically cleave and produce the same 5′ hydroxyl and 2′,3′-cyclic phosphate ends. This approach significantly increased the aptamer's concentration within cells, consequently improving both the fluorescence signal and the half-life of RNAs within eukaryotic cells. They also presented the F30 three-way junction scaffold, which, for example, incorporates a fluorogenic aptamer into one stem, while the remaining two stems hold the ligand-binding aptamer and the ligated stem from Tornado. This approach, utilizing the Tornado and F30 scaffold, is a valuable tool for further developing sensors that can be generated using this modular system and robotic platform to design intracellular sensing devices. As an additional step in this study, the functionality of the selected S1 and S5 TPP sensors was tested within the F30 scaffold for future application, either with or without the adenosine-rich linker between the Broccoli and TPP-aptamer. Incorporation of the S5 sensor with an adjusted PolyA linker resulted in a TPP-dependent increase in fluorescence signal,

confirming that the structure of the S5 sensor remains viable within the F30 scaffold and can be used for intracellular applications (not presented in the publication).

Together, these two studies form a connected and complementary framework for the future of RNA aptamer technology. The robotic-assisted capture-SELEX platform tackles the challenge of generating aptamers quickly, reproducibly, and with minimal manual effort, ensuring a reliable supply of candidate binders against a wide range of small molecules. The modular RNA sensor approach enables turning these binders into functional biosensors without requiring in-depth structural knowledge or significant re-engineering. By linking automated discovery with modular deployment, the two studies enable a continuous pipeline from selection to application.

Advances presented in these studies can have several implications. In diagnostics, RNA sensors could be used to detect metabolites or disease biomarkers, enabling early diagnosis and tailored treatment plans.[114-115] Additionally, they can be employed for assay development of *in vitro* transcription efficiency investigation or intracellular mRNA trafficking.[112] In synthetic biology, aptamer-based sensors could be incorporated into gene circuits to control expression based on metabolite levels through several mechanisms, such as U1 splicing, alternative exon skipping, or miRNA-mediated gene expression regulation. Environmental monitoring also provides an opportunity for sensors to identify pollutants or toxins with high precision and sensitivity.[116] Therapeutic applications are also promising, as sensors could be developed to track drug levels in patients and adjust dosing in real-time.[9, 83] Additionally, aptamers were successfully utilized in the targeted delivery of mRNA-based therapeutics.[91]

In conclusion, this thesis establishes a scalable and adaptable pipeline for RNA aptamer discovery and deployment. By integrating automated selection with modular sensor engineering, the work provides a generalizable strategy for transforming molecular recognition into functional RNA devices. This framework lays the groundwork for future applications in biosensing, synthetic biology, and RNA-based diagnostics, where standardized discovery and rapid aptamer functionalization are essential.

REFERENCES

[1] C. Tuerk, L. Gold. "Systematic evolution of ligands by exponential enrichment: RNA ligands to bacteriophage T4 DNA polymerase" *science* **1990**, *249*, 505-510.

[2] A. D. Ellington, J. W. Szostak. "In vitro selection of RNA molecules that bind specific ligands" *nature* **1990**, *346*, 818-822.

[3] G. P. Smith. "Filamentous fusion phage: novel expression vectors that display cloned antigens on the virion surface" *Science* **1985**, *228*, 1315-1317.

[4] L. S. Jespers, A. Roberts, S. M. Mahler, G. Winter, H. R. Hoogenboom. "Guiding the selection of human antibodies from phage display repertoires to a single epitope of an antigen" *Bio/technology* **1994**, *12*, 899-903.

[5] M. Baker. "Blame it on the antibodies" *Nature* **2015**, *521*, 274.

[6] L. Gold, D. Ayers, J. Bertino, C. Bock, A. Bock, E. Brody, J. Carter, V. Cunningham, A. Dalby, B. Eaton. "Aptamer-based multiplexed proteomic technology for biomarker discovery" *Nature Precedings* **2010**, 1-1.

[7] C. Renzl, A. Kakoti, G. Mayer. "Aptamer-Mediated Reversible Transactivation of Gene Expression by Light" *Angewandte Chemie International Edition* **2020**, *59*, 22414-22418.

[8] M. Rosenthal, F. Pfeiffer, G. Mayer. "A Receptor-Guided Design Strategy for Ligand Identification" *Angewandte Chemie International Edition* **2019**, *58*, 10752-10755.

[9] N. Nakatsuka, K.-A. Yang, J. M. Abendroth, K. M. Cheung, X. Xu, H. Yang, C. Zhao, B. Zhu, Y. S. Rim, Y. Yang. "Aptamer–field-effect transistors overcome Debye length limitations for small-molecule sensing" *Science* **2018**, *362*, 319-324.

[10] A. Schmitz, A. Weber, M. Bayin, S. Breuers, V. Fieberg, M. Famulok, G. Mayer. "A SARS-CoV-2 spike binding DNA Aptamer that inhibits Pseudovirus infection by an RBD-independent mechanism" *Angewandte Chemie International Edition* **2021**, *60*, 10279-10285.

[11] A. M. Weber, J. Kaiser, T. Ziegler, S. Pilsl, C. Renzl, L. Sixt, G. Pietruschka, S. Moniot, A. Kakoti, M. Juraschitz. "A blue light receptor that mediates RNA binding and translational regulation" *Nature chemical biology* **2019**, *15*, 1085-1092.

[12] N. Kacherovsky, I. I. Cardle, E. L. Cheng, J. L. Yu, M. L. Baldwin, S. J. Salipante, M. C. Jensen, S. H. Pun. "Traceless aptamer-mediated isolation of CD8+ T cells for chimeric antigen receptor T-cell therapy" *Nature biomedical engineering* **2019**, *3*, 783-795.

[13] M. S. L. Raddatz, A. Dolf, E. Endl, P. Knolle, M. Famulok, G. Mayer. "Enrichment of cell-targeting and population-specific aptamers by fluorescence-activated cell sorting" *Angewandte Chemie International Edition* **2008**, *47*, 5190-5193.

[14] F. Tolle, G. M. Brändle, D. Matzner, G. Mayer. "A versatile approach towards nucleobase-modified aptamers" *Angewandte Chemie International Edition* **2015**, *54*, 10971-10974.

[15] H. Kähkölä, M. Herath, P. Virta, T. Lönnberg. "Post-SELEX modification of quinine aptamers through neoacetalization" *Organic & Biomolecular Chemistry* **2025**, *23*, 1714-1722.

[16] W. Winkler, A. Nahvi, R. R. Breaker. "Thiamine derivatives bind messenger RNAs directly to regulate bacterial gene expression" *Nature* **2002**, *419*, 952-956.

[17] K. Kruger, P. J. Grabowski, A. J. Zaug, J. Sands, D. E. Gottschling, T. R. Cech. "Self-splicing RNA: autoexcision and autocyclization of the ribosomal RNA intervening sequence of Tetrahymena" *cell* **1982**, *31*, 147-157.

[18] A. Roth, R. R. Breaker. "The structural and functional diversity of metabolite-binding riboswitches" *Annual review of biochemistry* **2009**, *78*, 305-334.

[19] S. Ni, H. Yao, L. Wang, J. Lu, F. Jiang, A. Lu, G. Zhang. "Chemical modifications of nucleic acid aptamers for therapeutic purposes" *International journal of molecular sciences* **2017**, *18*, 1683.

[20] R. Stoltenburg, C. Reinemann, B. Strehlitz. "SELEX—A (r) evolutionary method to generate high-affinity nucleic acid ligands" *Biomolecular engineering* **2007**, *24*, 381-403.

[21] A. Boussebayle, F. Groher, B. Suess. "RNA-based Capture-SELEX for the selection of small molecule-binding aptamers" *Methods* **2019**, *161*, 10-15.

[22] W. Rychlik. "Selection of primers for polymerase chain reaction" *Molecular biotechnology* **1995**, *3*, 129-134.

[23] M. Simsek, H. Adnan. "Effect of single mismatches at 3′–end of primers on polymerase chain reaction" *Journal for scientific research. Medical sciences/Sultan Qaboos University* **2000**, *2*, 11.
[24] F. Tolle, J. Wilke, J. Wengel, G. Mayer. "By-product formation in repetitive PCR amplification of DNA libraries during SELEX" *PloS one* **2014**, *9*, e114693.
[25] N. Komarova, A. Kuznetsov. "Inside the black box: what makes SELEX better?" *Molecules* **2019**, *24*, 3598.
[26] G. S. Filonov, J. D. Moon, N. Svensen, S. R. Jaffrey. "Broccoli: rapid selection of an RNA mimic of green fluorescent protein by fluorescence-based selection and directed evolution" *J Am Chem Soc* **2014**, *136*, 16299-16308.
[27] R. Stoltenburg, N. Nikolaus, B. Strehlitz. "Capture-SELEX: selection of DNA aptamers for aminoglycoside antibiotics" *Journal of analytical methods in chemistry* **2012**, *2012*.
[28] A. Pyle. "Metal ions in the structure and function of RNA" *JBIC Journal of Biological Inorganic Chemistry* **2002**, *7*, 679-690.
[29] M. C. Dell'Oca, R. Quadri, G. M. Bernini, L. Menin, L. Grasso, D. Rondelli, O. Yazici, S. Sertic, F. Marini, A. Pellicioli. "Spotlight on G-quadruplexes: from structure and modulation to physiological and pathological roles" *International Journal of Molecular Sciences* **2024**, *25*, 3162.
[30] R. Micura, C. Höbartner. "Fundamental studies of functional nucleic acids: aptamers, riboswitches, ribozymes and DNAzymes" *Chemical Society Reviews* **2020**, *49*, 7331-7353.
[31] J. S. Paige, T. Nguyen-Duc, W. Song, S. R. Jaffrey. "Fluorescence imaging of cellular metabolites with RNA" *Science* **2012**, *335*, 1194.
[32] R. Nutiu, Y. Li. "In vitro selection of structure-switching signaling aptamers" *Angewandte Chemie International Edition* **2005**, *44*, 1061-1065.
[33] M. Rajendran, A. D. Ellington. "Selection of fluorescent aptamer beacons that light up in the presence of zinc" *Analytical and bioanalytical chemistry* **2008**, *390*, 1067-1075.
[34] N. Komarova, M. Andrianova, S. Glukhov, A. Kuznetsov. "Selection, characterization, and application of ssDNA aptamer against furaneol" *Molecules* **2018**, *23*, 3159.
[35] A. Kuznetsov, N. Komarova, M. Andrianova, V. Grudtsov, E. Kuznetsov. "Aptamer based vanillin sensor using an ion-sensitive field-effect transistor" *Microchimica Acta* **2018**, *185*, 1-10.
[36] A. Boussebayle, D. Torka, S. Ollivaud, J. Braun, C. Bofill-Bosch, M. Dombrowski, F. Groher, K. Hamacher, B. Suess. "Next-level riboswitch development—implementation of Capture-SELEX facilitates identification of a new synthetic riboswitch" *Nucleic acids research* **2019**, *47*, 4883-4895.
[37] A. Shaukat, A. Chrouda, S. Sadaf, F. Alhamlan, S. Eissa, M. Zourob. "Cell-SELEX for aptamer discovery and its utilization in constructing electrochemical biosensor for rapid and highly sensitive detection of Legionella pneumophila serogroup 1" *Scientific Reports* **2024**, *14*, 14132.
[38] O. Alkhamis, Y. Xiao. "Systematic study of in vitro selection stringency reveals how to enrich high-affinity aptamers" *Journal of the American Chemical Society* **2022**, *145*, 194-206.
[39] B. Townshend, J. S. Xiang, G. Manzanarez, E. J. Hayden, C. D. Smolke. "A multiplexed, automated evolution pipeline enables scalable discovery and characterization of biosensors" *Nature communications* **2021**, *12*, 1437.
[40] H. Gu, N. Duan, S. Wu, L. Hao, Y. Xia, X. Ma, Z. Wang. "Graphene oxide-assisted non-immobilized SELEX of okdaic acid aptamer and the analytical application of aptasensor" *Scientific reports* **2016**, *6*, 21665.
[41] V.-T. Nguyen, Y. S. Kwon, J. H. Kim, M. B. Gu. "Multiple GO-SELEX for efficient screening of flexible aptamers" *Chemical Communications* **2014**, *50*, 10513-10516.
[42] J. Guan, K. He, S. Gunasekaran. "Selection of ssDNA aptamer using GO-SELEX and development of DNA nanostructure-based electrochemical aptasensor for penicillin" *Biosensors and Bioelectronics: X* **2022**, *12*, 100220.
[43] H. Salvail, R. R. Breaker. "Riboswitches" *Current Biology* **2023**, *33*, R343-R348.
[44] A. S. Mironov, I. Gusarov, R. Rafikov, L. E. Lopez, K. Shatalin, R. A. Kreneva, D. A. Perumov, E. Nudler. "Sensing small molecules by nascent RNA: a mechanism to control transcription in bacteria" *cell* **2002**, *111*, 747-756.

[45] M. Mandal, R. R. Breaker. "Adenine riboswitches and gene activation by disruption of a transcription terminator" *Nature structural & molecular biology* **2004**, *11*, 29-35.
[46] M. Mandal, B. Boese, J. E. Barrick, W. C. Winkler, R. R. Breaker. "Riboswitches control fundamental biochemical pathways in Bacillus subtilis and other bacteria" *cell* **2003**, *113*, 577-586.
[47] J. L. Baker, N. Sudarsan, Z. Weinberg, A. Roth, R. B. Stockbridge, R. R. Breaker. "Widespread genetic switches and toxicity resistance proteins for fluoride" *Science* **2012**, *335*, 233-235.
[48] J. Tang, R. R. Breaker. "Rational design of allosteric ribozymes" *Chemistry & biology* **1997**, *4*, 453-459.
[49] R. R. Breaker. "Engineered allosteric ribozymes as biosensor components" *Current opinion in biotechnology* **2002**, *13*, 31-39.
[50] L. A. Holeman, S. L. Robinson, J. W. Szostak, C. Wilson. "Isolation and characterization of fluorophore-binding RNA aptamers" *Folding and Design* **1998**, *3*, 423-431.
[51] J. S. Paige. "RNA mimics of green fluorescent protein" *Science* **2011**.
[52] I. Geraci, A. Autour, G. Pietruschka, A. Shiian, M. Borisova, C. Mayer, M. Ryckelynck, G. n. Mayer. "Fluorogenic RNA-Based Biosensor to Sense the Glycolytic Flux in Mammalian Cells" *ACS Chemical Biology* **2022**, *17*, 1164-1173.
[53] T. S. Bayer, C. D. Smolke. "Programmable ligand-controlled riboregulators of eukaryotic gene expression" *Nature biotechnology* **2005**, *23*, 337-343.
[54] B. Suess, S. Hanson, C. Berens, B. Fink, R. Schroeder, W. Hillen. "Conditional gene expression by controlling translation with tetracycline-binding aptamers" *Nucleic acids research* **2003**, *31*, 1853-1858.
[55] S. Breuers, L. L. Bryant, T. Legen, G. Mayer. "Robotic assisted generation of 2'-deoxy-2'-fluoro-modifed RNA aptamers - High performance enabling strategies in aptamer selection" *Methods* **2019**, *161*, 3-9.
[56] H. Mou, G. Zhong, M. R. Gardner, H. Wang, Y.-W. Wang, D. Cheng, M. Farzan. "Conditional regulation of gene expression by ligand-induced occlusion of a microRNA target sequence" *Molecular Therapy* **2018**, *26*, 1277-1286.
[57] X. Li, L. Mo, J. L. Litke, S. K. Dey, S. R. Suter, S. R. Jaffrey. "Imaging intracellular S-adenosyl methionine dynamics in live mammalian cells with a genetically encoded red fluorescent RNA-based sensor" *Journal of the American Chemical Society* **2020**, *142*, 14117-14124.
[58] M. You, J. L. Litke, S. R. Jaffrey. "Imaging metabolite dynamics in living cells using a Spinach-based riboswitch" *Proceedings of the National Academy of Sciences* **2015**, *112*, E2756-E2765.
[59] D. P. Morse. "Direct selection of RNA beacon aptamers" *Biochemical and Biophysical Research Communications* **2007**, *359*, 94-101.
[60] J. A. Martin, J. L. Chávez, Y. Chushak, R. R. Chapleau, J. Hagen, N. Kelley-Loughnane. "Tunable stringency aptamer selection and gold nanoparticle assay for detection of cortisol" *Analytical and bioanalytical chemistry* **2014**, *406*, 4637-4647.
[61] F. M. Spiga, P. Maietta, C. Guiducci. "More DNA–aptamers for small drugs: A capture–SELEX coupled with surface plasmon resonance and high-throughput sequencing" *ACS combinatorial science* **2015**, *17*, 326-333.
[62] H. Wang, J. Wang, L. Xu, Y. Zhang, Y. Chen, H. Chen, R. Pei. "Selection and characterization of thioflavin T aptamers for the development of light-up probes" *Analytical Methods* **2016**, *8*, 8461-8465.
[63] N. Paniel, G. Istamboulié, A. Triki, C. Lozano, L. Barthelmebs, T. Noguer. "Selection of DNA aptamers against penicillin G using Capture-SELEX for the development of an impedimetric sensor" *Talanta* **2017**, *162*, 232-240.
[64] A. Zhang, D. Chang, Z. Zhang, F. Li, W. Li, X. Wang, Y. Li, Q. Hua. "In vitro selection of DNA aptamers that binds geniposide" *Molecules* **2017**, *22*, 383.
[65] L. H. Lauridsen, H. B. Doessing, K. S. Long, A. T. Nielsen. "A capture-SELEX strategy for multiplexed selection of RNA aptamers against small molecules" *Synthetic Metabolic Pathways: Methods and Protocols* **2018**, 291-306.

[66] P.-J. J. Huang, J. Liu. "Selection of aptamers for sensing caffeine and discrimination of its three single demethylated analogues" *Analytical Chemistry* **2022**, *94*, 3142-3149.
[67] L. Gu, H. Zhang, Y. Ding, Y. Zhang, D. Wang, J. Liu. "Capture-SELEX for a short aptamer for label-free detection of salicylic acid" *Smart Molecules* **2023**, *1*, e20230007.
[68] Y. Zhao, A. Z. Li, J. Liu. "Capture-SELEX for Chloramphenicol Binding Aptamers for Labeled and Label-Free Fluorescence Sensing" *Environment & Health* **2023**, *1*, 102-109.
[69] K. Yang, N. M. Mitchell, S. Banerjee, Z. Cheng, S. Taylor, A. M. Kostic, I. Wong, S. Sajjath, Y. Zhang, J. Stevens. "A functional group–guided approach to aptamers for small molecules" *Science* **2023**, *380*, 942-948.
[70] Y. Zhao, J. Liu. "pH-Directed Capture-SELEX for Nanomolar Affinity Aptamers for Kanamycin Detection" *Analysis & Sensing* **2024**, e202400099.
[71] W. Sun, J. Yang, Y. Yang, X. Li, R. Jiang, J. Li, F. Cao, M. Sun, L. Wang. "Optimization of Rna Capture-Selex and Aptamer Characterization for Multiple Marine Toxins" *Available at SSRN 5148182*.
[72] J. C. Cox, P. Rudolph, A. D. Ellington. "Automated RNA selection" *Biotechnology progress* **1998**, *14*, 845-850.
[73] J. C. Cox, A. D. Ellington. "Automated selection of anti-protein aptamers" *Bioorganic & medicinal chemistry* **2001**, *9*, 2525-2531.
[74] J. C. Cox, A. Hayhurst, J. Hesselberth, T. S. Bayer, G. Georgiou, A. D. Ellington. "Automated selection of aptamers against protein targets translated in vitro: from gene to aptamer" *Nucleic acids research* **2002**, *30*, e108-e108.
[75] D. Eulberg, K. Buchner, C. Maasch, S. Klussmann. "Development of an automated in vitro selection protocol to obtain RNA-based aptamers: identification of a biostable substance P antagonist" *Nucleic acids research* **2005**, *33*, e45-e45.
[76] T. Hünniger, H. Wessels, C. Fischer, A. Paschke-Kratzin, M. Fischer. "Just in time-selection: A rapid semiautomated SELEX of DNA aptamers using magnetic separation and BEAMing" *Analytical chemistry* **2014**, *86*, 10940-10947.
[77] Y. Zhang, S. Zhang, Z. Ning, X. Lin, N. Duan, Z. Wang, S. Wu. "Development of an Automated Capture-SELEX Device for Efficient Screening of β-Conglycinin Aptamer" *Journal of Agricultural and Food Chemistry* **2024**, *72*, 28148-28156.
[78] T. Legen, G. Mayer. "Robotic-Assisted Capture-Systematic Evolution of Ligands by Exponential Enrichment of RNA Aptamers Binding to Small Molecules" *ChemBioChem* **2025**, 2500264.
[79] B. Townshend, M. Kaplan, C. D. Smolke. "Highly multiplexed selection of RNA aptamers against a small molecule library" *Plos one* **2022**, *17*, e0273381.
[80] S. J. Reinholt, A. Ozer, J. T. Lis, H. G. Craighead. "Highly multiplexed RNA aptamer selection using a microplate-based microcolumn device" *Scientific Reports* **2016**, *6*, 29771.
[81] F. Bottari, E. Daems, A.-M. de Vries, P. Van Wielendaele, S. Trashin, R. Blust, F. Sobott, A. Madder, J. C. Martins, K. De Wael. "Do aptamers always bind? The need for a multifaceted analytical approach when demonstrating binding affinity between aptamer and low molecular weight compounds" *Journal of the American Chemical Society* **2020**, *142*, 19622-19630.
[82] B. R. Baker, R. Y. Lai, M. S. Wood, E. H. Doctor, A. J. Heeger, K. W. Plaxco. "An electronic, aptamer-based small-molecule sensor for the rapid, label-free detection of cocaine in adulterated samples and biological fluids" *Journal of the American Chemical Society* **2006**, *128*, 3138-3139.
[83] A. M. Downs, K. W. Plaxco. "Real-time, in vivo molecular monitoring using electrochemical aptamer based sensors: opportunities and challenges" *ACS sensors* **2022**, *7*, 2823-2832.
[84] M. You, J. L. Litke, R. Wu, S. R. Jaffrey. "Detection of low-abundance metabolites in live cells using an RNA integrator" *Cell chemical biology* **2019**, *26*, 471-481. e473.
[85] N. Nakatsuka, A. Faillétaz, D. Eggemann, C. Forró, J. Voros, D. Momotenko. "Aptamer conformational change enables serotonin biosensing with nanopipettes" *Analytical Chemistry* **2021**, *93*, 4033-4041.
[86] E. V. Dolgosheina, S. C. Jeng, S. S. S. Panchapakesan, R. Cojocaru, P. S. Chen, P. D. Wilson, N. Hawkins, P. A. Wiggins, P. J. Unrau. "RNA mango aptamer-fluorophore: a bright, high-affinity complex for RNA labeling and tracking" *ACS chemical biology* **2014**, *9*, 2412-2420.

[87] W. Song, G. S. Filonov, H. Kim, M. Hirsch, X. Li, J. D. Moon, S. R. Jaffrey. "Imaging RNA polymerase III transcription using a photostable RNA–fluorophore complex" *Nature chemical biology* **2017**, *13*, 1187-1194.
[88] X. Chen, D. Zhang, N. Su, B. Bao, X. Xie, F. Zuo, L. Yang, H. Wang, L. Jiang, Q. Lin. "Visualizing RNA dynamics in live cells with bright and stable fluorescent RNAs" *Nature Biotechnology* **2019**, *37*, 1287-1293.
[89] T. Legen, G. n. Mayer. "Modular Approach for Rapid Identification of RNA-Based Sensors" *ACS sensors* **2024**, *9*, 753-758.
[90] J.-C. Baret, O. J. Miller, V. Taly, M. Ryckelynck, A. El-Harrak, L. Frenz, C. Rick, M. L. Samuels, J. B. Hutchison, J. J. Agresti. "Fluorescence-activated droplet sorting (FADS): efficient microfluidic cell sorting based on enzymatic activity" *Lab on a Chip* **2009**, *9*, 1850-1858.
[91] J. S. Lee, M. Kim, H. Jin, M. Kwak, E. Cho, K.-S. Kim, D.-E. Kim. "DNA aptamer-conjugated lipid nanoparticle for targeted PTEN mRNA delivery to prostate cancer cells" *International journal of pharmaceutics* **2024**, *662*, 124519.
[92] G. Zhu, G. Niu, X. Chen. "Aptamer–drug conjugates" *Bioconjugate chemistry* **2015**, *26*, 2186-2197.
[93] V. Hedwig, M. Spöring, J. Ottlinger, S. Köse, H. Nar, G. Schnapp, D. Gottschling, H. Klein, G. Aspnes, M. Klugmann. "Engineering oxypurinol-responsive riboswitches based on bacterial xanthine aptamers for gene expression control in mammalian cell culture" *Nucleic Acids Research* **2025**, *53*, gkae1189.
[94] Y. Nomura, L. Zhou, A. Miu, Y. Yokobayashi. "Controlling mammalian gene expression by allosteric hepatitis delta virus ribozymes" *ACS synthetic biology* **2013**, *2*, 684-689.
[95] R. D. Jenison, S. C. Gill, A. Pardi, B. Polisky. "High-resolution molecular discrimination by RNA" *Science* **1994**, *263*, 1425-1429.
[96] B. Strobel, M. Spöring, H. Klein, D. Blazevic, W. Rust, S. Sayols, J. S. Hartig, S. Kreuz. "High-throughput identification of synthetic riboswitches by barcode-free amplicon-sequencing in human cells" *Nature Communications* **2020**, *11*, 714.
[97] E. Rovira, B. Moreno, N. Razquin, L. Blázquez, R. Hernández-Alcoceba, P. Fortes, F. Pastor. "Engineering U1-Based Tetracycline-Inducible Riboswitches to Control Gene Expression in Mammals" *ACS nano* **2023**, *17*, 23331-23346.
[98] A. A. Mol, F. Groher, B. Schreiber, C. Rühmkorff, B. Suess. "Robust gene expression control in human cells with a novel universal TetR aptamer splicing module" *Nucleic Acids Research* **2019**, *47*, e132-e132.
[99] P. Szterner, B. Legendre, M. Sghaier. "Thermodynamic properties of polymorphic forms of theophylline. Part I: DSC, TG, X-ray study" *Journal of thermal analysis and calorimetry* **2010**, *99*, 325-335.
[100] I. M. Weiss, C. Muth, R. Drumm, H. O. Kirchner. "Thermal decomposition of the amino acids glycine, cysteine, aspartic acid, asparagine, glutamic acid, glutamine, arginine and histidine" *BMC biophysics* **2018**, *11*, 1-15.
[101] N. Hodges, J. Singh. "ENHANCEMENT OF NEOMYCIN STABILITY USING PROPYLENE-GLYCOL AND SODIUM METABISULFITE" *Journal of Pharmacy and Pharmacology* **1978**, *30*, 737-739.
[102] M. G. Wallis, U. von Ahsen, R. Schroeder, M. Famulok. "A novel RNA motif for neomycin recognition" *Chemistry & biology* **1995**, *2*, 543-552.
[103] J. Canoura, H. Yu, O. Alkhamis, D. Roncancio, R. Farhana, Y. Xiao. "Accelerating post-SELEX aptamer engineering using exonuclease digestion" *Journal of the American Chemical Society* **2020**, *143*, 805-816.
[104] S. Lennarz, T. C. Alich, T. Kelly, M. Blind, H. Beck, G. Mayer. "Selective Aptamer-Based Control of Intraneuronal Signaling" *Angewandte Chemie International Edition* **2015**, *54*, 5369-5373.
[105] A. Dhiman, A. Anand, A. Malhotra, E. Khan, V. Santra, A. Kumar, T. K. Sharma. "Rational truncation of aptamer for cross-species application to detect krait envenomation" *Scientific reports* **2018**, *8*, 17795.

[106] J. Macdonald, P. Houghton, D. Xiang, W. Duan, S. Shigdar. "Truncation and mutation of a transferrin receptor aptamer enhances binding affinity" *Nucleic acid therapeutics* **2016**, *26*, 348-354.
[107] J. D. Yesselman, D. Eiler, E. D. Carlson, M. R. Gotrik, A. E. d'Aquino, A. N. Ooms, W. Kladwang, P. D. Carlson, X. Shi, D. A. Costantino. "Computational design of three-dimensional RNA structure and function" *Nature nanotechnology* **2019**, *14*, 866-873.
[108] M. J. Wu, J. O. Andreasson, W. Kladwang, W. Greenleaf, R. Das. "Automated design of diverse stand-alone riboswitches" *ACS synthetic biology* **2019**, *8*, 1838-1846.
[109] Z. Chen, R. D. Kibler, A. Hunt, F. Busch, J. Pearl, M. Jia, Z. L. VanAernum, B. I. Wicky, G. Dods, H. Liao. "De novo design of protein logic gates" *Science* **2020**, *368*, 78-84.
[110] J. B. Siegel, A. Zanghellini, H. M. Lovick, G. Kiss, A. R. Lambert, J. L. St. Clair, J. L. Gallaher, D. Hilvert, M. H. Gelb, B. L. Stoddard. "Computational design of an enzyme catalyst for a stereoselective bimolecular Diels-Alder reaction" *Science* **2010**, *329*, 309-313.
[111] E. Marcos, B. Basanta, T. M. Chidyausiku, Y. Tang, G. Oberdorfer, G. Liu, G. Swapna, R. Guan, D.-A. Silva, J. Dou. "Principles for designing proteins with cavities formed by curved β sheets" *Science* **2017**, *355*, 201-206.
[112] Q. Wang, F. Xiao, H. Su, H. Liu, J. Xu, H. Tang, S. Qin, Z. Fang, Z. Lu, J. Wu. "Inert Pepper aptamer-mediated endogenous mRNA recognition and imaging in living cells" *Nucleic Acids Research* **2022**, *50*, e84-e84.
[113] J. L. Litke, S. R. Jaffrey. "Highly efficient expression of circular RNA aptamers in cells using autocatalytic transcripts" *Nature biotechnology* **2019**, *37*, 667-675.
[114] F. Shafiei, K. McAuliffe, Y. Bagheri, Z. Sun, Q. Yu, R. Wu, M. You. "based fluorogenic RNA aptamer sensors for label-free detection of small molecules" *Analytical Methods* **2020**, *12*, 2674-2681.
[115] W. Zhou, P.-J. J. Huang, J. Ding, J. Liu. "Aptamer-based biosensors for biomedical diagnostics" *Analyst* **2014**, *139*, 2627-2640.
[116] E. C. Reynoso, P. S. Sfragano, M. González-Perea, I. Palchetti, E. Torres. "Aptasensors for the Detection of Environmental Contaminants of High Concern in Water Bodies: A Systematic Review" *Chemosensors* **2024**, *12*, 59.

ABBREVIATIONS

Table 2. List of abbreviations.

Abbreviation	Meaning
ADP	Adenosine diphosphate
ATP	Adenosine triphosphate
BEAMing	Beads, Emulsion, Amplification, Magnetics
bio-RV primer	Biotinylated reverse primer
cAMP	Cyclic adenosine monophosphate
cDNA	Complementary DNA
cDNA-amplicon-seq	Sequencing of cDNA amplicons
CE-SELEX	Capillary electrophoresis-SELEX
CleaveSeq	High-throughput cleavage-based characterization assay used with DRIVER
DNA	Deoxyribonucleic acid
dNTP	Deoxynucleoside triphosphate
DFHO	3,5-difluoro-4-hydroxybenzylidene imidazolinone-2-oxime
DFHBI	3,5-difluoro-4-hydroxybenzylidene imidazolinone
DFHBI-1T	(Z)-4-(3,5-difluoro-4-hydroxybenzylidene)-2-methyl-1-(2,2,2-trifluoroethyl)-1Himidazol-5(4H)-one)
DS	Docking sequence
DSc	Docking sequence complement
DRIVER	De novo Rapid In Vitro Evolution of RNA biosensors
E. coli	Escherichia coli
EAB	Electrochemical aptamer-based
EMSA-SELEX	Electrophoretic mobility shift assay-SELEX
EtBr	Ethidium bromide
FACS	Fluorescence-activated cell sorting
FP	Fluorescence polarization
FW	Forward primer
G/C (content)	Guanosine/cytidine content of an oligonucleotide (GC%)
GFP	Green fluorescent protein
GO	Graphene oxide
GO-SELEX	Graphene oxide-assisted SELEX
GTP	Guanosine triphosphate
HDB	High-density beads
HEPES	4-(2-Hydroxyethyl)-1-piperazineethanesulfonic acid
HDV	Hepatitis delta virus
HHR	Hammerhead ribozyme
ITC	Isothermal titration calorimetry
IVT	*In vitro* transcription
K^+	Potassium ion
LDB	Low-density beads
Mg^{2+}	Magnesium ion

Abbreviation	Meaning
miRNA	MicroRNA
mRNA	Messenger RNA
n.a.	Not applicable
N	Randomized nucleotides of indicated length in a library
NGS	Next-generation sequencing
NTC	No-template control
nt	Nucleotides
OBI	3,5-difluoro-4-hydroxybenzylidene-imidazolinone-2-oxime-1-benzoimidazole
ODN	Oligodeoxynucleotide
ORF	Open reading frame
PBS	Phosphate-buffered saline
PBS (library)	Primer-binding site
PCR	Polymerase chain reaction
RNA	Ribonucleic acid
RISC	RNA-induced silencing complex
rpm	Revolutions per minute
SA	Streptavidin
SAM	S-adenosyl-L-methionine
SEC-SELEX	Size-exclusion chromatography-SELEX
SELEX	Systematic Evolution of Ligands by EXponential Enrichment
SEREX	Systematic Evolution of Riboswitches by EXponential enrichment
S1P	Sphingosine-1-phosphate
ssDNA	Single-stranded DNA
T7 promoter	Promoter recognized by T7 RNA polymerase
Tm	Melting temperature
TPP	Thiamine pyrophosphate
TP	Thiamine monophosphate
Tris-HCl	Tris(hydroxymethyl)aminomethane hydrochloride
U1-snRNP	U1 small nuclear ribonucleoprotein
UTR	Untranslated region
dsDNA	Double-stranded DNA
RV	Reverse primer
5-IP7	5-diphospho-myo-inositol pentakisphosphate

APPENDIX A

Robotic-Assisted Capture-Systematic Evolution of Ligands by Exponential Enrichment of RNA Aptamers Binding to Small Molecules

Tjasa Legen[1,2] and Günter Mayer[1,2]

Received: March 27, 2025
Published online: July 9, 2025

DOI: https://doi.org/10.1002/cbic.202500264

Own contributions

- Design and planning of experiments
- Execution of experiments
- Evaluation of experimental results
- Drafting of the manuscript

[1] Life and Medical Sciences Institute (LIMES), University of Bonn, 53121, Germany
[2] Center of Aptamer Research and Development (CARD), University of Bonn, 53121, Germany

ChemBioChem

Research Article
doi.org/10.1002/cbic.202500264

Chemistry Europe
European Chemical Societies Publishing

www.chembiochem.org

Robotic-Assisted Capture-Systematic Evolution of Ligands by Exponential Enrichment of RNA Aptamers Binding to Small Molecules

Tjasa Legen and Günter Mayer*

Due to their small size, stability, and cost-effectiveness compared to antibodies, aptamers developed by systematic evolution of ligands by exponential enrichment (SELEX) are promising candidates for the detection of small molecules. In SELEX, a small target molecule is usually covalently immobilized on a surface to separate bound from unbound nucleic acid sequences. However, this immobilization alters the molecule, that is, additional chemical entities are added and the electron distribution is altered, compromising the enrichment properties. To overcome this problem, a capture SELEX method has been successfully developed in which the RNA or DNA libraries are bound to a surface via a complementary oligodeoxynucleotide, and the soluble ligand is used to capture nucleic acids that bind to it from that surface. Herein, the development of an automated version of the capture SELEX method for the identification of RNA aptamers that bind small molecules is described. This method is fully automated and performs up to 12 iterative selection cycles without manual interference in 72 h. The approach is therefore suitable as rapid route to aptamers and enables resource-efficient test selections to assess "aptamerogenicity" of a target.

1. Introduction

Systematic evolution of ligands by exponential enrichment (SELEX) was introduced as an in vitro technique designed to enrich binding molecules from an oligonucleotide library of $\approx 10^{15}$ different sequences. Although the method was introduced as early as 1990,[1,2] standardized procedures for selecting aptamers that target a wider range of molecules are lacking. Instead, there are different versions of the procedure, which mainly depend on the used target molecule, the separation methodology, or buffer compositions.[3] Besides these in vitro variations, in vivo selection methods were developed that make use of mouse models to target tissue.[4,5] In this regard, a plethora of variants of the selection procedure have been established, that are effective in selecting aptamers that bind to different target molecules. However, these methods are hardly comparable in their results, as they were often revised from experiment to experiment and the conditions within a single SELEX experiment were adapted. Therefore, streamlining the SELEX process is an important task that would allow the results to be compared and, if done quickly, the targeting accuracy of a molecule with aptamers to be determined rapidly. To achieve this, we established automated and standardized selection procedures of aptamers binding to proteins.[6,7] We focused on targeting small molecules and to avoid problems associated with target immobilization on solid supports, we choose the capture SELEX method.[8] The main steps of capture SELEX are immobilization of RNA libraries to magnetic beads using a complementary oligodeoxynucleotide (ODN), the elimination of weakly bound sequences, the recovery of binding sequences by the addition of the small target molecule, followed by the amplification and in vitro transcription of the enriched sequences. For efficient automatization, each step had to be specifically tailored and optimized for a robotic platform. We describe the development of an automated SELEX procedure and its application for the selection of aptamers that target several small molecules. We evaluated different strategies for selecting aptamers using the test target neomycin B and used the most effective strategy to select aptamers for various small molecules. The developed process is fast and enables the high-throughput identification of RNA aptamers that bind to small molecules.

T. Legen, G. Mayer
Life and Medical Sciences Institute (LIMES)
University of Bonn
53121, Germany
E-mail: gmayer@uni-bonn.de

T. Legen, G. Mayer
Center of Aptamer Research and Development (CARD)
University of Bonn
53121, Germany

Supporting information for this article is available on the WWW under https://doi.org/10.1002/cbic.202500264

2. Results

2.1. Optimization and Adaptation of Capture SELEX for Use on the Robotic Platform

In capture SELEX, the RNA library is immobilized on a matrix by hybridization to a complementary oligodeoxynucleotide (capture-ODN) with a docking sequence embedded in the RNA library (**Figure 1**A). Sequences that bind to a target molecule and undergo conformational changes can no longer hybridize to

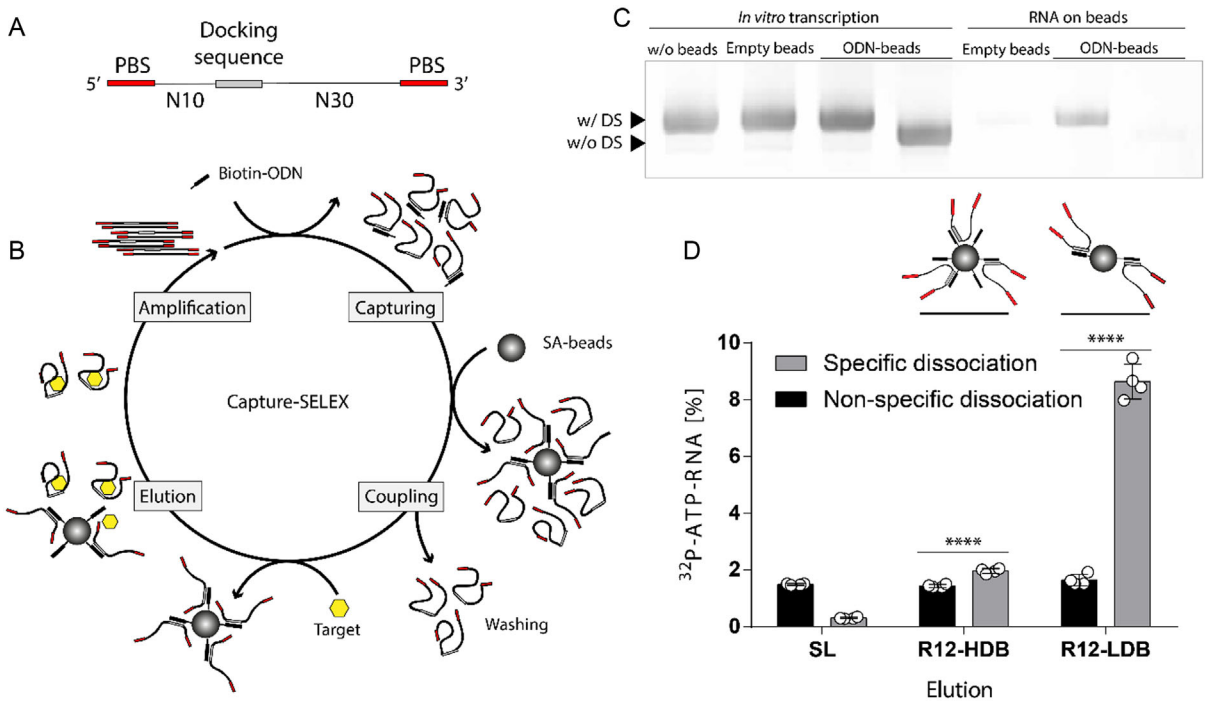

Figure 1. Capture SELEX optimization for automated selection of RNA aptamers targeting small molecules. A) Scheme of RNA library flanked by PBS and a constant 12-nt DS positioned between N10- and N30-long random region. B) Scheme of RNA capture SELEX. Main steps are 1) capturing of RNA to short oligodeoxynucleotides (ODN) during transcription, 2) coupling of RNA-ODN duplexes on magnetic beads and removing of weakly bound sequences, 3) elution of binding sequences by addition of a target solution, and 4) reverse transcription and amplification (RT-PCR) of dissociated sequences. SA: streptavidin. C) RNA library with or without DS was either transcribed in the absence of beads, presence of empty beads, or presence of ODN-beads complexes complementary to the DS. RNA captured onto the beads was eluted by 8 M Urea and it is depicted with RNA on beads on the gel. RNA can be transcribed and captured to the ODN-beads, with almost no unspecific interaction. D) Radioactive binding studies with the round 12 library (R12) of neomycin B selection using HDB selection or LDB selection compared to the SL. Captured RNA was either eluted with the selection buffer (nonspecific dissociation) or with 1 mM of neomycin B (specific dissociation). Scheme of the difference of HDB versus LDB is shown above the bars. The selection with LDB shows much greater and specific binding. Error bars show standard deviation ($n = 2$). Unpaired t-test $p < 0.0001$.

the capture-ODN and are therefore recovered, amplified by reverse transcription (RT)-polymerase chain reaction (PCR), and used in subsequent selection cycle after transcription into RNA (Figure 1B). We began the implementing capture SELEX in an automated process by using libraries generated from primer binding sites previously used in automation[6,9,10] and docking sequences used in capture SELEX studies (Figure 1A).[8] In our design, the docking sequence is flanked by a 10 nt upstream and a 30 nt downstream random region (Figure 1A).

We have set up our robotic platform to eliminate the need for manual handling during the enrichment procedure. This eliminates the nucleic acid purification steps that are usually carried out in manual capture SELEX experiments. To implement this concept, we transferred the RNA-target complexes obtained during the SELEX process directly into the RT-PCR reaction. After amplification, an aliquot of the unpurified PCR products was used as a template for transcription in vitro.[6] To optimize the process, we added magnetic streptavidin beads modified with capture-ODNs to the transcription mix. As the RNA is transcribed, it binds to the capture-ODNs on the beads. We analyzed whether the addition of beads without or coupled with capture-ODNs affected the transcription efficiency, but no noticeable difference in RNA yield was observed in the presence or absence of the beads (Figure 1C). This effect was also independent of the presence of a docking sequence (DS) in the RNA library (Figure 1C). After removal of the reaction solution, we thoroughly washed the beads to eliminate nonspecifically bound RNA. Subsequently, the captured RNA was recovered from the beads with 8 M urea, and the RNA obtained was compared using denaturing polyacrylamide gel electrophoresis (PAGE) (Figure 1C). Our results showed that the RNA binds specifically to the capture-ODNs on the beads and that only small amounts of RNA bind to streptavidin beads without capture-ODN as well as only small amounts of RNA without a docking sequence bind to capture-ODN-beads (Figure 1C).

2.2. Manual Capture SELEX with High- and Low-Density Capture-ODN Beads

We first tested two different capture SELEX approaches, which differ in the way the RNA library is captured on the beads. In the first approach, the beads were saturated with capture-ODNs before the RNA library was immobilized.[8] In the second approach, the RNA library and capture ODNs were incubated in solution in equal amounts and then immobilized on the beads.[11] The main difference between these two methods is that in the first approach, more residual free ODNs remain coupled on the beads because the spherical shape of the beads prevents complete hybridization with RNA. In the second approach, the amount of capture-ODNs on the beads that are not bound to RNA is low. We named the two methods "high-density beads

(HDB) selection" and "low-density beads (LDB) selection" and performed twelve selection cycles with neomycin B as target molecule, since it is known to be suitable for capture-SELEX.[12] After 12 selection cycles, we evaluated the binding of the enriched libraries using Cherenkov measurement and ^{32}P-labeled RNA. The specific recovery of bound sequences by adding neomycin B [1 mM] was observed and compared with the values of the starting library. In addition, we analyzed the nonspecific sequence recovery using a buffer without neomycin B (Figure 1D). Remarkably, the nonspecific sequence dissociation remained consistent across all three libraries (Figure 1D). However, specific recovery increased slightly for the HDB-enriched and strongly for the LDB-enriched RNA library. The enriched libraries also showed an increase in capture properties regardless of the method used (Figure S1, Supporting Information).

2.3. Robotic Capture-SELEX

Due to its more pronounced enrichment, we chose the LDB variant for implementation on the robotic platform to select RNA aptamers binding to small molecules. The first automated capture SELEX was performed using neomycin B. Analysis of the PCR products from each selection cycle showed a constant amplification behavior without significant occurrence of by-products (Figure S2, Supporting Information). All selections followed the same stringent conditions, as described in Table 1, Supporting Information. Interaction analysis of the enriched library shows enhanced binding to neomycin B (**Figure 2**A). We performed next-generation sequencing (NGS) of both manual (Figure 1D) and the robotic capture SELEX. The number of unique sequences in the LDB selections showed a similar trend, whether performed manually or automated. The HDB-variant evolved more slowly and to a lesser extent (Figure 2B). The nucleotide distribution of the RNA from the 12th selection cycles shows the accumulation of different patterns, but is less pronounced in the manual LDB selection (Figure S3, Supporting Information). Among the 20 most abundant sequences in all three selections, only one sequence appeared in all three selections, while two sequences were shared by the LDB variants (Figure S3A, Supporting Information). Motif analysis across all three SELEX experiments revealed two motifs specific to the HDB strategy only and three motifs found

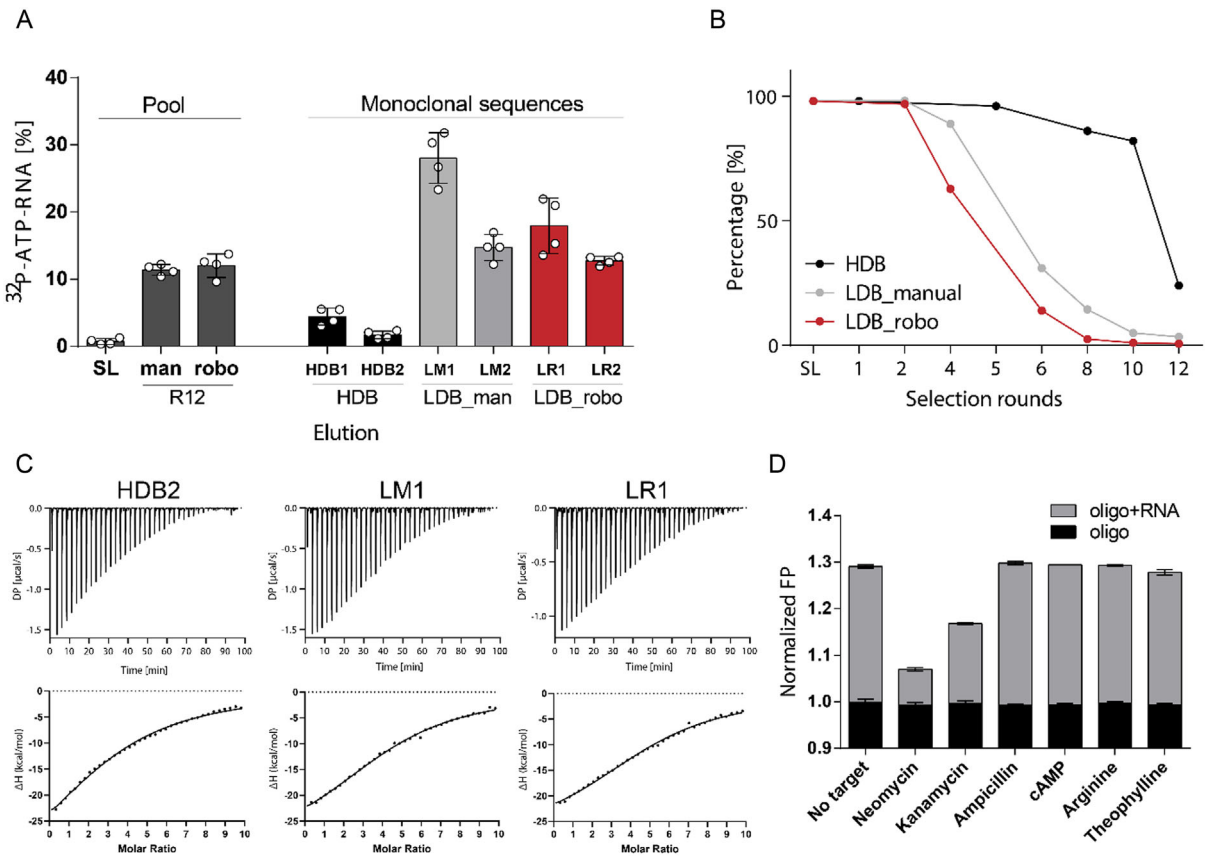

Figure 2. NGS analysis and comparison of different selection strategies for neomycin B. A) Radioactive binding studies of monoclonal sequences enriched through different capture-selection strategies compared to round 12 of manual and robotic selection. The first two most enriched sequences were chosen in each selection strategy. Applied target concentration was 1 mM. Error bars show standard deviation (n = 2). B) Graph of unique sequences in different selection rounds. The sequences are enriched later in the selection with HDBs as in the selection with LDBs. The enrichment rate of sequences in manual versus robotic (robo) selection is almost equal. C) Affinity of aptamers HDB1, LM1, and LR1 toward neomycin B target measured by ITC. K_d of HDB2, LM1, and LR1 aptamers is 55.9 ± 3.57 μM, 38.0 ± 2.10 μM, and 34.7 ± 1.97 μM, respectively. 1 mM of neomycin B was titrated to 20 μM of the respective aptamer. D) Specificity of the LR1 aptamer measured by FP. The aptamer binds to neomycin B and kanamycin B, but not to other targets: ampicillin, cAMP, theophylline, and L-arginine. Target concentration is 100 μM. The concentration of capture-ODN and aptamer LR1 was 100 nM and 500 nM, respectively. Error bars show standard deviation ($n = 3$).

common to all strategies, underlining the reproducibility of performance (Figure S4B,C, Supporting Information).[13]

Next, we evaluated the binding properties of the most enriched sequences from all three SELEX experiments (Figure S4D, Supporting Information). We selected the two most enriched sequences from each selection and, by this test, covered all motifs and sequences found in all three selections or both LDB selections (Figure S4, Supporting Information). Although the two most enriched sequences in HDB selection, HDB1 and HDB2, had a high frequency (10.4% and 10.0%, respectively), they displayed low binding intensities according to Cherenkov measurements (Figure 2A, Figure S4, Supporting Information). In contrast, the most enriched sequences from the manual LDB (LM1 and LM2; 9.8% and 7.9%, respectively) and the robot-assisted LDB (LR1 and LR2; 33.7% and 26.9%, respectively) showed a stronger binding (Figure 2A, Figure S4, Supporting Information).

The interaction of the sequences with neomycin B and the approximate kinetics of binding were further analyzed by using a fluorescence polarization assay, as previously described in Legen and Mayer.[14] The assay utilizes the hybridization of fluorescently labeled short ODNs to the RNA docking sequence, which increases the polarization. Conversely, RNA bound to the ligand when present in solution, results in decreased polarization. After initial assay optimization, the binding of various enriched RNA libraries to neomycin B, that is, starting library (SL), and the enriched libraries from HDB, LDB manual, and LDB robotic selections, and an improved LDB selection later discussed in section. Automated capture selection for different ligands was tested using 100 μM of the neomycin B target in the solution. Figure S5A, Supporting Information showed a decrease in fluorescence polarization for the RNA libraries from the selections performed with LDB as opposed to HDB, consistent with the results from Cherenkov measurements (Figure 1D and Figure 2A). In addition, binding of monoclonal sequences selected for neomycin B was examined. Aptamers LM1, LM2, LR1, and LR2 showed strong binding to the target, while HDB1 and HDB2 showed weak or no binding, respectively (Figure S5B, Supporting Information), consistent with the results from the radioactive binding assay (Figure 2A).

To increase the sensitivity of the assay for low-affinity binding aptamers and to increase the dynamic range, the stability of the ODN-RNA duplexes was adjusted. ODNs of different lengths from 8 to 12 nucleotides or an ODN with a point mutation were used. The annealing efficiency of different ODN lengths was observed, with all ODNs annealing efficiently to the LM1 aptamer except the 8-nt ODN (Figure S5C, Supporting Information). Subsequently, the dynamic range of different ODN lengths that annealed efficiently to the LM1 aptamer was examined, with the 9-nt ODN showing the highest fluorescence polarization change between free RNA and RNA with the target (Figure S5D, Supporting Information).

Finally, we used shortened, fluorescently labeled ODNs to titrate different concentrations of neomycin B to aptamers HDB1, LM1, and LR1 (Figure S6A, Supporting Information), and determined the approximate affinity to be 10 μM, 4 μM and 3 μM, respectively. Furthermore, we designed a scrambled sequence of LM1 aptamer (ScrLM1) to show that the aptamers' binding is sequence-specific. In fact, as shown in Figure S6B, Supporting Information, we observed no detectable decrease in fluorescence polarization when neomycin B was added to the capture ODN and ScrLM1 hybrid. Next, we utilized isothermal titration calorimetry (ITC) to confirm and more accurately determine the dissociation constants (K_d). Due to the elevated differential power (DP) values observed during the titration of neomycin B in buffer (Figure S6C, Supporting Information), we subtracted the heat generated by ligand titration in buffer from the heat generated by the titration of the ligand to the respective aptamers (Figure 2C). This time, we examined the affinity of the HDB2 aptamer instead of HDB1, since we wanted to determine the detection limit for affinity that could not be identified using radioactive or fluorescence polarization assays (Figure 2A, Figure S5B, Supporting Information). The K_d-value for all three aptamers was determined in the micromolar range (HDB2: 55.9 ± 3.57 μM, LM1: 38.0 ± 2.10 μM, and LR1: 34.7 ± 1.97 μM, Figure 2C).

In addition, the LR1 aptamer was found to bind to neomycin B and kanamycin B when used in a fluorescence polarization assay, but did not interact with ampicillin, cAMP, arginine, or theophylline (Figure 2D). Therefore, we examined the binding affinity of the LR1 aptamer to kanamycin B. The heat generated by kanamycin B titration in the buffer was again subtracted from kanamycin B titration in the LR1 aptamer solution (Figure S6D, Supporting Information). ITC measurements revealed that the LR1 aptamer had an affinity for kanamycin B of 130.0 ± 30.9 μM, which is almost four times lower than the affinity of LR1 for neomycin B (Figure S6E, Supporting Information).

2.4. Automated Capture Selection for Different Ligands

After having established an automated capture SELEX process, we extended the approach to other small molecule targets. In this context, we used L-arginine and theophylline, which had previously been used in the selection of RNA aptamers.[15,16] Unfortunately, after the fourth round of automated SELEX, the PCR profiles showed a shortening of the DNA, indicating an unsuccessful enrichment process and the occurrence of so-called molecular parasites (Figure S7, Supporting Information). Our hypothesis for the shortening of the DNA was that the initially high target concentration in the transcription mix (90 μM) prevented the transcribed RNA molecules from binding to the capture ODN and instead favoring their binding to the target. As a result, only sequences that dissociated nonspecifically were advanced to the next selection step. These sequences, which did not need the random region for their evolution, could have lost it to amplify more efficiently. This phenomenon did not occur with neomycin B, probably because its binding ability was weakened by the repeated heating and cooling cycles during PCR and prolonged incubation at 37 °C during in vitro transcription reaction.[17] Although all three molecules are relatively stable at 95 °C, repeated heating and cooling can lead to degradation over time. Of the three, theophylline is the most stable up to about 270 °C, and retains much of its structure with moderate temperature variations.[18] L-arginine starts to degrade at about 180 °C,[19] while

neomycin B can degrade at slightly lower temperatures with repeated heat exposure,[20] making neomycin B less thermally stable than theophylline and arginine, which could be the cause for observed selection failure. Of note, lowering the initial concentration of neomycin B to 50 μM and 5 μM or performing 12 selection cycles without the target resulted in a degree of DNA truncation similar to that seen in other unsuccessful selections (Figure S8, Supporting Information).

Based on these observations, we modified the automated capture-SELEX procedure and purified the PCR product from the target before proceeding to the transcription step. To do this, we separated the RT from the amplification step. In the optimized version, RT occurred in the presence of a biotinylated reverse primer and immobilization of the thus biotinylated cDNA to streptavidin-coated magnetic beads (Figure S9, Supporting Information). The supernatant containing the target molecule was then removed and the PCR mix was added to amplify the immobilized cDNA. With the optimized method, the truncation of DNA during SELEX was reduced, although shorter bands occasionally appeared, but they never dominated the library. Remarkably, these by-products did not reappear after reamplification or visualization by denaturing gel electrophoresis, suggesting they could be secondary structures or single-stranded DNA (Figure S10, Supporting Information). We applied the optimized capture-SELEX scheme to 13 target molecules that varied in chemical structure and functionality (**Figure 3**A, Figure S11, Supporting Information). Cherenkov measurements of the enriched libraries showed binding to neomycin B, theophylline, and riboflavin, and to a lesser extent to all other targets except galactose, where the amplified band weakened after round six (Figure S12C, Supporting Information).

NGS analysis of the enriched libraries showed a strong decline of unique sequences for the selection using neomycin B after the fourth selection cycle, whereas for the other targets, a decline in unique sequences only began after the sixth round, and to a much lesser extent (Figure 3B).

2.5. NGS Analysis and Interaction Properties of Monoclonal Sequences

After NGS analysis, we took a deeper look at the enrichment profiles of each selection and its most enriched sequences. We found that several identical sequences were enriched during the course of selections, which target different small molecules (Figure S13, Supporting Information). However, the frequency of these sequences in the enriched libraries was close to zero until the fourth cycle of selection, and most sequences only began to accumulate after the sixth cycle. Some of the sequences (i.e. 1, 3, 4, 6, and 7) were tested for binding, but none of them showed binding to the tested targets (data not shown). We hypothesized that for the selections with little enrichment success, well-amplifying sequences were preferentially enriched, independently of the target used, so that the enriched sequences were identical for selections targeting different ligands.

Next, we searched for the most promising sequences in all selections and examined their binding. As shown in Figure S14, Supporting Information, the 100 most enriched sequences were sorted into different families with no more than 5 point mutations (PM) (only up to six families or 18 families were presented in the case of ppGpp). In addition, common motifs among the 100, the most enriched sequences were identified using the MEME suite tool for motif discovery.[13] In some selections, specific motifs were found and at least one representative sequence of each motif was tested for the binding. In other cases, two to three of the most enriched sequences were tested, trying to avoid sequences that were frequently enriched in several different selections (Figure S13, Supporting Information). Remarkably, the most enriched sequence in the optimized selection approach targeting neomycin B was identical to the HDB12, LM1, and LR5 sequence, which was frequently enriched in all neomycin B selections (Figure S4,S14, Supporting Information).

The interaction of representative sequences from the selections made (marked in Figure S14, Supporting Information with bold) was tested using the fluorescence polarization assay. Among these

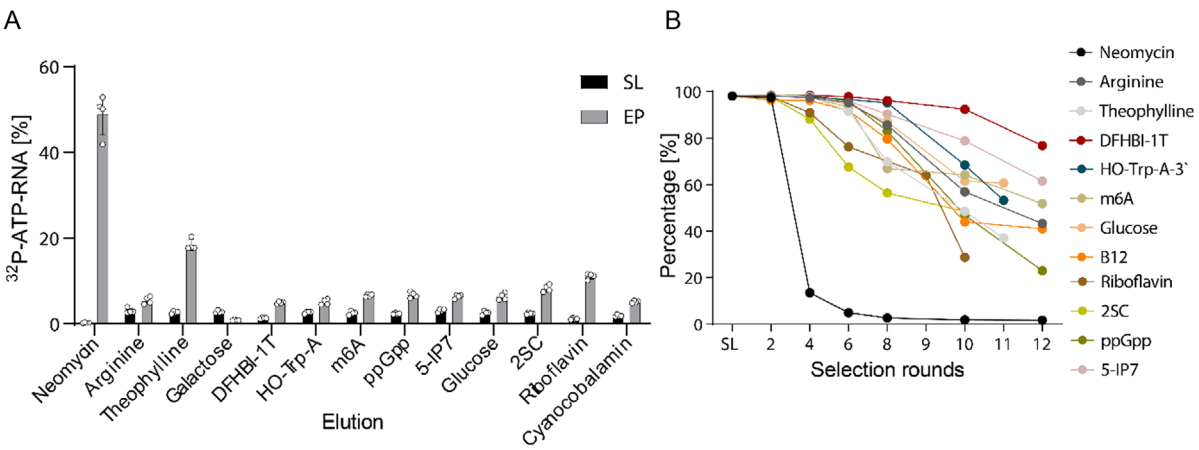

Figure 3. RNA capture SELEX with different small molecule targets. A) Binding comparison of enriched pool (EP) of different small molecule targets. Applied target concentration was 0.1-1 mM. Error bars show standard deviation ($n = 2$). B) Graph of unique sequences in different selection rounds by the selections with different small molecule targets measured by NGS. DFHBI-1 T: 3,5-Difluoro-4-hydroxybenzylidene imidazolinone-1 T,[39] HO-Trp-A: D-Tryptophanyl Adenosine 5′-Monophosphate Phosphoramidate,[37] m6A: N6-Methyladenosine, ppGpp: Guanosine pentaphosphate, 5-IP7: 5-diphospho-myo-inositol pentakisphosphate,[21] 2SC: S-(2-succinyl) cysteine.

sequences, LM1 and I5 from the neomycin B and 5-IP7[21] selections, respectively, showed the strongest binding, while T1, P7, R2, and R3 showed weaker binding to theophylline, ppGpp, and riboflavin, respectively (**Figure 4**A). The remaining tested sequences that did not bind are not shown in the graph. As seen in Figure S15, Supporting Information, different RNA libraries exhibited varying annealing efficiencies toward the capture-ODN. Furthermore, in Figure 4B, monoclonal sequences with identical docking sequences were found to bind to capture-ODNs with different affinities. We then attempted to determine the dissociation constant (K_d) of two binding sequences by the fluorescence polarization method and compared these values with those obtained by ITC measurement. Figure 4C shows that aptamer T1 binds to theophylline with a measured K_d of 54 μM, with no binding observed to the structural

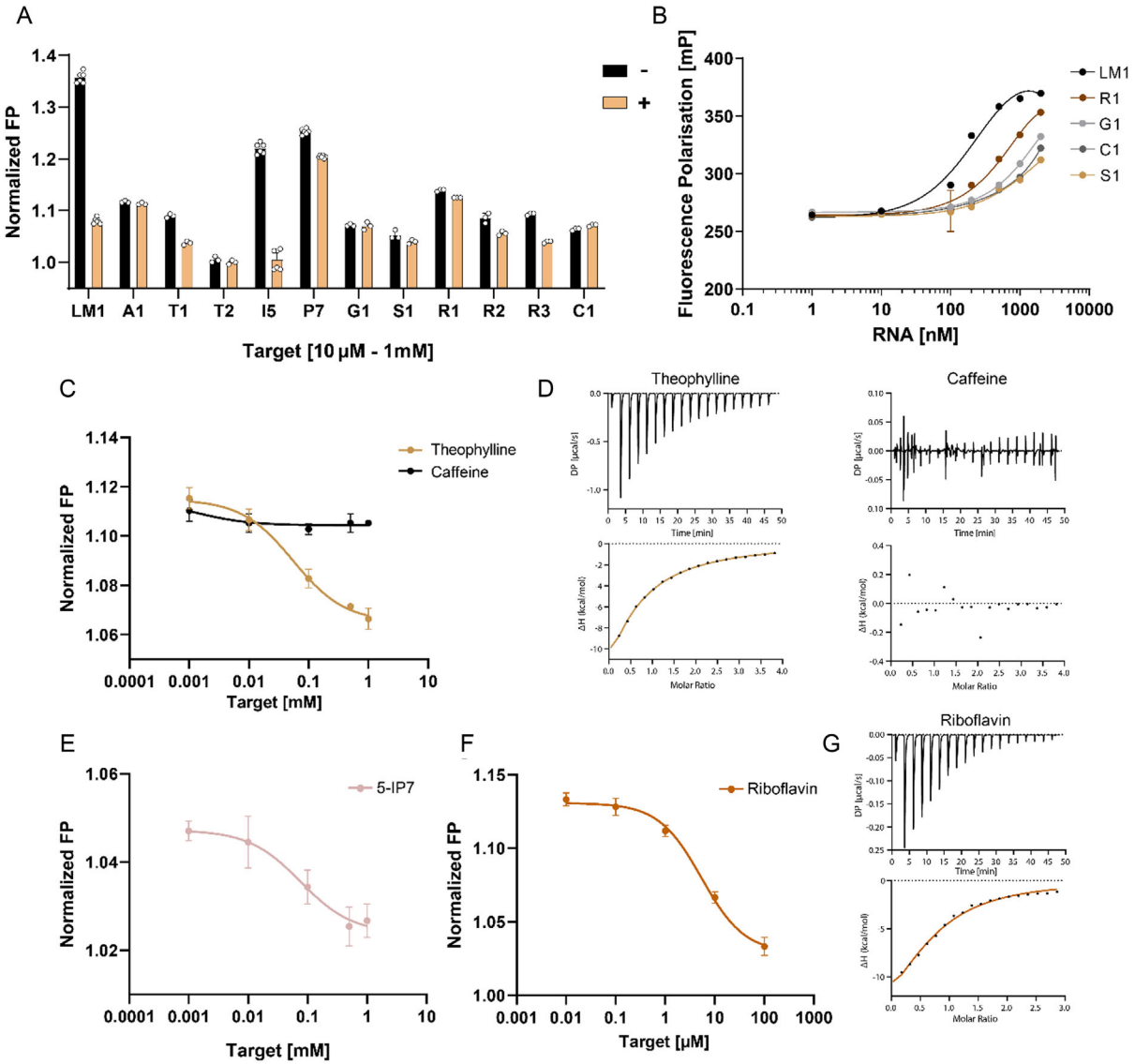

Figure 4. Characterization of monoclonal sequences targeting various small molecule ligands. A) Binding test of various monoclonal sequences targeting ligands such as neomycin B (LM1), arginine (A1), theophylline (T1, T2), 5-IP7 (I5), ppGpp (P7), glucose (G1), S-(2-succinyl) cysteine (S1), riboflavin (R1, R2, R3), and cyanocobalamin (C1). Interaction was measured by FP assay utilizing Cy3-labeled 9-nt complementary oligodeoxynucleotide (ODN). In the assay, 100 nM of Cy3-labeled capture-ODN and 500 nM RNA were used in the absence or presence of target. All values were normalized according to the FP value of Cy3-labeled capture-ODN. Error bars show standard deviation ($n = 3$). B) Annealing efficiency of different monoclonal sequences to the corresponding 9-nt complementary ODN. Efficiency was measured by FP assay. In the assay, 100 nM of Cy3-labeled capture-ODN and 500 nM RNA were used. Error bars show standard deviation ($n = 3$). C) Concentration-dependent binding of theophylline or caffeine to T1 aptamer measured by FP. The estimated K_d of T1 aptamer binding to theophylline determined by the assay was ≈54 μM. The fluorescence change was fitted to inhibitor vs. response model. Error bars show standard deviation ($n = 3$). D) Thermodynamic properties of the interaction of theophylline or caffeine with the T1 aptamer measured by ITC. The determined K_d of T1 aptamer binding to theophylline was 70.3 ± 6.33 μM. 1 mM of theophylline or caffeine was titrated to 50 μM of T1 aptamer. E) Concentration-dependent binding of 5-IP7 to I5 aptamer measured by FP. The estimated K_d determined by the assay was ≈76 μM. The fluorescence change was fitted to inhibitor versus response model. Error bars show standard deviation ($n = 3$). F) Concentration-dependent binding of riboflavin to R3 aptamer measured by FP. The estimated K_d determined by the assay was ≈5 μM. The fluorescence change was fitted to inhibitor versus response model. Error bars show standard deviation ($n = 3$). G) Thermodynamic properties of the interaction of riboflavin and R3 aptamer measured by ITC. The determined K_d was 9.88 ± 1.09 μM. 300 μM of riboflavin was titrated to 20 μM of R3 aptamer.

analog caffeine. Likewise, ITC-measured interaction of T1 and theophylline yielded a K_d-value of 70.3 ± 6.33 μM, with no interaction observed for caffeine (Figure 4D). Similarly, Figure 4E shows concentration-dependent binding of 5-IP7 to aptamer I5, resulting in a calculated K_d-value of 76 μM. We attempted to determine the binding affinity of the I5 aptamer using ITC, but the experiment was unsuccessful due to the precipitation of the target at high concentration. Finally, we tested the interaction of riboflavin and aptamer R3 by fluorescence polarization, which resulted in a K_d-value of 5 μM, and the interaction measured by ITC yielded a value of 9.88 ± 1.09 μM (Figure 4 G).

3. Discussion

In our study, we sought to automate the selection of RNA aptamers that bind small molecules by applying capture SELEX. Our initial focus was on gaining a thorough understanding of the various capture SELEX methods described in previous work and using this information to adapt the process to an automated format.[8,11] The results of our experiments indicated that LDB selection resulted in sequence enrichment with stronger recovery of RNA in the presence of neomycin B compared to HDB selection (Figure 1D). This difference in specific recovery of RNA species clearly demonstrates that LDB selection outperforms HDB selection and that the density of capture-ODNs on the beads plays an important role in the enrichment of RNA libraries during the capture SELEX procedure. We hypothesize that the reason for the lower efficiency of HDB selection is that numerous free ODNs remain on the beads, causing the captured RNA to bind to the next available ODN instead of dissociating and binding to the target. This assumption is consistent with the fact that target molecules prevent the RNA from rebinding to the capture-ODNs on the beads after dissociation, rather than playing a more active role in destabilizing the duplex structure between the capture-ODN and the docking sequence in the RNA library. Furthermore, we have successfully applied this methodology to the robotic platform and performed it using neomycin B as a model target.

To characterize the enriched sequences of all three different selections (manual and automated) with neomycin B in more detail, we performed NGS analysis and compared the most enriched sequences. Although we used the same library and the same target, we enriched different sequences in all three selections. Nevertheless, some motifs and one sequence were retained in all three selections (Figure S4, Supporting Information). Since we did not find many dominating motifs in the enriched libraries (Figure S4B, Supporting Information), we decided to test the binding of the first two most enriched sequences in each of the selections, where at least one sequence contained the motifs one to four (Figure S4, Supporting Information) and both sequences were present in either all three selections or both LDB selections. All six sequences showed binding to neomycin B, but the HDB1 and HDB2 sequences, both of which were enriched in HDB selection, showed very weak binding. To confirm these results and determine the K_d for subsequent ITC measurement, we performed target-dependent displacement of a representative aptamer (HDB1, LM1, and LR1) from fluorescently labeled capture-ODNs using different concentrations of neomycin B (Figure 2, Figure S6A, Supporting Information). The affinities determined were 4 μM and 3 μM for aptamers LM1 and LR1, respectively, which were about ten times lower as the results obtained by ITC measurement (38.0 ± 2.10 μM and 34.7 ± 1.97 μM for LM1 and LR1 aptamer, respectively).

However, the affinities obtained were lower than those previously reported for neomycin B-binding RNA aptamers ($K_d \approx 100$ nM),[12] which were selected using an immobilized target. This condition could allow for more stringent separation of binding and nonbinding sequences. In accordance with this notion are results of selections with the capture SELEX method, which targets structurally similar aminoglycoside antibiotics and resulted in micromolar affinity DNA aptamers.,[8] but low micromolar affinity has also been reported in other capture SELEX aptamer publications.[22–27] This could be due to the nature of the small molecule targets, which have fewer functional groups with which to interact. However, aptamers with much stronger affinities have been reported in studies using immobilized small molecule targets.[28–30] Nevertheless, in some published studies using the capture SELEX method aptamers have been obtained that bound to their ligands in the nanomolar range.[31–33] Most of these studies describe well-designed and target-specific selection procedures that take into account the initial target concentration and usage of several structurally similar analogs for counter-selection in their selection approach.[32,33] Alkhamis and Xiao[33] performed several selection experiments with flunixin. Their results suggest that using lower initial target concentrations and reducing its concentration very sharply during the selection could lead to an enrichment of aptamers with stronger affinity. They also employed a well-thought-out counter-selection strategy, demonstrating its importance.

We also applied the automated selection strategy to select aptamers that target other ligands (Figure 3). Although we were able to enrich aptamers for some ligands, all tested aptamers still bind in the micromolar range (Figure 4). Therefore, we believe that adjusting the ligand concentration specifically for each target could improve the affinity of selected candidates and increase the overall success rate. The high-throughput platform would also allow several selection experiments to be carried out simultaneously for each target, since, as we have also shown in Figure S8, Supporting Information, if the starting target concentration is too low, this could lead to the loss of binding sequences and to the appearance of selection artifacts, for example, truncation of the library in the early selection cycles. To improve the specificity of selected aptamers, one could introduce additional elution with counter targets or add the counter targets to the washing buffer solution, although neomycin B and theophylline binding aptamers selected with the current method show fairly specific interactions with respective targets (Figure 2A and Figure 4C,D). Another way to improve the affinity of enriched aptamers would be to gradually extend the capture-ODN:RNA complex by using longer capture-ODNs in the selection procedure. This way, ligand interaction would have to prevent rebinding of RNAs mediated by longer base-pairing sites, thus directing selection toward more tightly binding aptamers. The studies mentioned above, which yielded aptamers in the nanomolar range, also used the position of the docking

sequence at the 5′ end of the library.[32,33] This could also contribute to the enrichment of aptamers with higher affinity. However, no studies have yet been carried out in which the length and position of the docking sequence and its effects on the enrichment of high-affinity binding aptamers are systematically investigated. We therefore believe that our platform, which allows multiple selection processes and is operator-independent, enables deeper exploration and a better understanding of the SELEX process.

We also presented a quick and easy fluorescence polarization assay that serves as a cost-effective alternative to time-consuming radioactive binding assays because it does not require RNA labeling and expensive magnetic beads. A further advantage was the possibility of automation with spectrophotometric plate readers attached to the pipetting station. Using enriched libraries and monoclonal sequences for neomycin B, we optimized the length of the capture-ODN that produced the greatest change in fluorescence between the absence and presence of the ligands (Figure S5, Supporting Information). Shortening of the capture-ODN to 9-nt still ensured that the RNA bound well to the ODN, but at the same time also prevented the rebinding of the RNA to the capture-ODN in the presence of the ligand. We used the same length of the capture-ODN to test the binding of other monoclonal sequences targeting different ligands (Figure 4A), but for some sequences we observed very weak binding to the capture-ODN. We tested the concentration-dependent annealing of several monoclonal sequences, and although all sequences had the same complementary docking sequence to the capture-ODN, the annealing kinetics was quite different than for the LM1 aptamer (Figure 4B). Therefore, we believe that a specific adjustment of the aptamer concentration could help to verify binding when a shorter capture-ODN length is used.

In summary, we have demonstrated a fast and fully automated process for selecting RNA aptamers for small molecules without the need to immobilize the target. Furthermore, we see potential for adapting this procedure to the selection of DNA aptamers or even chemically modified DNA aptamers, for example, clickmers.[34,35] In a very recent publication, an automated procedure to gain DNA aptamers binding to a glycoprotein was established.[36] In a similar manner, our platform could also be extended to generate peptide- or protein-binding RNA aptamers using the automated capture-SELEX approach described here. Although our method has proven effective for most targets tested, we anticipate that by further optimization of conditions, such as target concentration and washing procedures, we will increase the success rate of this selection method and enrich high-affinity aptamers. The automated process allows for rapid screening of aptamer targetability of specific targets, and thus provides a unique approach to stratify targets for further development and selection procedures.

4. Experimental Section

Materials

Antibiotics Neomycin B, ampicillin, and kanamycin B were purchased from Roth, Germany. Theophylline, L-arginine, galactose, S-(2-Succinyl)-L-cystein (2-SC), cyanocobalamin, and cAMP were purchased from Sigma-Aldrich, Germany. D-Tryptophanyl Adenosine 5′-Monophosphate Phosphoramidate (HO-Trp-A-3′)[37] was provided by Clemens Richerts (University of Stuttgart) and N6-Methyladenosine (m6A) by Mark Helm (University of Mainz). Guanosine pentaphosphate (ppGpp) and 5-diphospho-*myo*-inositol pentakisphosphate (5-IP7)[21] were provided by Henning Jessen and Andreas Meyer (University of Freiburg and University of Lausanne). N6-Methyladenine was purchased from Cayman Chemical, USA and DFHBI-1 T from Bio-Techne, Germany. Other chemicals were purchased from Roth, Germany.

Selection Using HDBs Approach

Oligodeoxynucleotide (ODN) beads were prepared by first washing 10 mg of Dynabeads *M*-280 Streptavidin (Thermo Fisher Scientific) 3-times with Binding and Washing buffer (5 mM Tris, 0.5 mM EDTA, 1 M NaCl) and resuspending them in 1 mL of 5 μM ODN solution in BWB buffer (for sequence information see *Manual preparation of RNA-oligo-beads complexes for the initial round*). The mixture was incubated on a rotator for 1 h at room temperature. Afterward, ODN-beads were washed 3-times with 1 mL of 40 mM Tris buffer pH 7.9 and resuspended in 150 μl. 22.5 μl of prepared ODN-beads (1.5 mg beads, 600 pmol ODN) were mixed with 750 pmol of RNA library in the final concentration of 40 mM Tris pH 7.9 with 35 mM Mg^{2+} and incubated overnight at 37 °C and 900 rpm (for preparation of RNA library see *Manual preparation of RNA-oligo-beads complexes for the initial round*). The rest of the ODN-beads solution was stored at 4 °C for following rounds. The next day, supernatant was discarded and the beads were washed 6-times with 200 μl and 3-times for 5 min with 100 μl of the selection buffer (primer binding sites (PBS), 3 mM Mg^{2+} pH 7.4). Next, 50 μl of 1 mM neomycin B solution in the selection buffer was added to the beads and incubated for 15 min at 21 °C and 900 rpm. After incubation, 45 μl of the eluate was removed from the beads and mixed with RT-PCR solution (1x GoTaq buffer, 1.35 mM Mg^{2+}, 2 mM DTT, 1 μM forward primer, 1 μM reverse primer, 0.3 mM dNTPs, GoTaq Polymerase (Promega)). The program for RT-PCR is described in the *Automated selection*. After amplification, 10 μl of the PCR product was transferred to the transcription mix (40 mM Tris pH 7.9, 5 mM DTT, 35 mM Mg^{2+}, 2.5 mM NTPs, 0.5 mg oligo-beads, T7-RNA polymerase (homemade)). The in vitro transcription ran for 1.5 h at 37 °C and 900 rpm. Next, the supernatant was removed and the beads were washed 3-times for 5 min with 100 μl for of the selection buffer as done in the beginning of the round. Repeated rounds were done in the same way with increasing stringency by decreasing target concentration (1–0.5 mM), decreasing time of incubation of beads with the target solution (15–5 min), and decreasing the transcription time (1.5–0.5 h). The selection was done for 12 rounds.

Manual Preparation of RNA-Oligo-Beads Complexes for the Initial Round

The design of primer-binding sites was taken from Breuers et al.[6] and 12-nt DS design from Stoltenburg et al.[8] The DS was placed between 10- and 30-nt random region. Library was purchased as single-stranded DNA from Ella biotech, Germany (5′-GGGAGAGGAGGGA GATAGATATCAA-N10-TGAGGCTCGATC-N30-TTTCGTGGATGCCACAGG AC-3′). Forward primer with T7 promotor (5′-AATTCTAATACGACTCACT ATAGGGAGAGGAGGGAGATAGATATCAA-3′), reverse primer (5′-GTCC TGTGGCATCCACGAAA-3′), and biotinylated 12-nt capture oligo-deoxynucleotide (ODN) (5′-biotin-18spacer–GATCGAGCCTCA-3′) were provided by Ella Biotech, Germany. First, RNA library was prepared by a large-scale PCR of 10 mL by using 1 nmol of synthetized ssDNA pool. PCR was performed with the program: (1) 95 °C 2 min, (2) 95 °C 1 min, (3) 56 °C 1 min, (4) 72 °C 1 min, and (5) 72 °C 3 min, with repeated steps 2−4 for 5 cycles (1x GoTaq buffer, 1.5 mM Mg^{2+}, 1 μM reverse primer, 1 μM forward primer, 0.3 mM dNTPs, 5 U GoTaq polymerase (Promega)). Produced DNA was purified by phenol/chloroform extraction followed

by ethanol precipitation. One-quarter of the DNA was used for 1 mL of in vitro transcription (40 mM Tris pH 7.9, 5 mM DTT, 35 mM Mg^{2+}, 2.5 mM NTPs, T7 polymerase (homemade)). The solution was incubated at 37 °C overnight. The next day, the RNA was precipitated by ethanol precipitation and the pellet was resuspended in 4x PAA buffer (5.8 M Urea, 0.1 M EDTA, 10 % glycerol). RNA was separated from other nucleic acids on 10 %urea PAGE electrophoresis and the isolated band was crushed and shaken in 0.3 M NaOAc pH 5.9 for 2 h at 65 °C. Afterward, the RNA solution was sifted through the syringe with glass wool to remove gel particles. Finally, the RNA solution was precipitated by Ethanol precipitation and the RNA was resuspended in ddH_2O and stored at −20 °C. For the initial round of selection, the RNA was manually captured to the beads. 1.5 nmol of RNA and 1.5 nmol of 12-nt capture ODN was mixed in 100 μl selection buffer (PBS, 3 mM Mg^{2+} pH 7.4) and left to anneal by applying 50 °C for 15 min and slowly cooling down to 30 °C for 45 min with gentle shaking. In the meantime, 2.5 mg of Dynabeads *M*-280 Streptavidin (ThermoFisher Scientific, USA) was washed 3-times with 500 μl selection buffer by DynaMag-2 Magnet (ThermoFisher Scientific, USA). Finally, the beads were resuspended in 50 μl selection buffer and mixed with RNA-ODN solution. The mixture was incubated for 30 min at 21 °C with gentle shaking to allow RNA-ODN complexes to be coupled to the beads. Afterward, the supernatant was discarded and 100 μl of fresh selection buffer was added to the beads.

Selection Using LDBs Approach

The selection was done manually in the same way as described in *Manual preparation of RNA-oligo-beads complexes for the initial round* with following selection described in *Automated selection*. Neomycin B concentration during the selection was 1−0.05 mM. The amount of Dynabeads *M*-280 Streptavidin used in selection round 2−12 was 1 mg.

Robot Preparation

The selection process was done on Biomek NXp station (Beckman Coulter, USA) including different ALPs positions (heating/cooling devices, freezing device, magnet, and reservoir holder), a gripper, and a spin-8 pipette. A PCR cycler (Biometra, Germany) and a hotel, where filter tips (Beckman Coulter, USA) were stored, were connected to the Biomek NXp station with a gripper hand and a moving lane. The software, which was used for the programming of the selection process, was Biomek Software 4.1 and SAMI EX 4.1. All reagents were stored at 4 °C and enzymes at −25 °C. Reagents were stored in 96-well PCR plates (Starlab, Germany) and were sealed with X-Pierce film (Sigma-Aldrich, Germany). All selection steps were performed in 96-well PCR plates (Eppendorf, Germany). The magnetic station included magnetic rings suited for 96-well plate. To prevent evaporation of the liquid in the PCR cycler, a removable auto-sealing plate lid was utilized (Biorad, USA). The selection buffer was stored in a reservoir (Beckman Coulter, Germany). Pipettes calibration was done before initiation and after each selection round. The room was climatized to 19 °C to decrease evaporation of the liquid.

Automated Selection

Before the start of the selection, all required reagents as target solution, RT-PCR mix, transcription mix, beads solution, selection buffer (PBS, 3 mM Mg^{2+} pH 7.4, in the case of 5-IP7 and ppGpp selection, ICB buffer [12 mM HEPES, pH 7.7, 135 KCl, 10 mM NaCl, 3 mM $Mg(OAc)_2$] was used), and enzymes were prepared, aliquoted in plates and stored at either 4 °C (reagents), −25 °C (enzymes), or at room temperature (buffer). The whole volume of RNA-oligo-beads solution (described in *Manual preparation of RNA-oligo-beads complexes for the initial round*) was transferred to the incubation plate and placed to the Biomek NXp pipetting station. The solution was first incubated for 5 min at 21 °C with gentle shaking. Then, the plate was moved to the magnet position and allowed beads for 2 min to be moved to the magnet. The solution was discarded and 100 μl of fresh selection buffer was added to the beads. Plate was moved to the standard position and the beads were pipetted several times up and down. The plate was again moved to the magnet position and the same procedure was repeated once again. After the beads were washed for the third time, the supernatant was discarded and 50 μl of 1 mM target solution in the selection buffer was added to them. The solution was pipetted few times up and down and incubated for 15 min at 21 °C and 900 rpm. Afterward, plate was moved to the magnet and 45 μl of the eluate was transferred to the 53 μl of RT-PCR mix with the final concentration of: 1x GoTaq buffer, 1.35 mM Mg^{2+}, 2 mM DTT, 1 μM forward primer, 1 μM reverse primer, and 0.3 mM dNTPs. The mix was first heated up to 65 °C for 5 min to break the secondary structure of the RNA. Then, 1 μl of M–MLV enzyme (Promega, USA) and 1 μl GoTaq polymerase (Promega, USA) were added to the mixture and RNA was reverse transcribed and amplified with the program: 1) 55 °C 10 min, 2) 95 °C 2 min; 3) 95 °C 1 min, 4) 56 °C 1 min, 5) 72 °C 1 min, and 6) 72 °C 3 min, with repeated 3-5 steps. Afterward, 10 μl of the PCR product was transferred to the 38 μl of the transcription mix with final concentration: 40 mM Tris pH 7.9, 5 mM DTT, 2.5 mM NTPs, 25 mM Mg^{2+}, 4 μM 12-nt capture oligodeoxynucleotide (ODN), and the rest of the PCR product was stored at 4 °C. 1 μl of T7-RNA polymerase (NEB, USA) was added to the transcription mixture and the in vitro transcription was performed for 2 h at 37 °C with gentle shaking. Afterward, half of the transcription mixture was discarded (25 μl) and 100 μl of 0.5 mg beads solution was added to it in final concentration of 1x PBS with 5 mM Mg^{2+}. The mixture was incubated for 30 min to allow RNA-ODN complexes and beads to interact. Finally, the beads were washed 3-times with 100 μl of the selection buffer as done in the beginning of the round. Repeated rounds were done in the same way with increasing stringency by decreasing target concentration (1–0.05 mM), decreasing time of incubation of beads with the target solution (15–5 min), and decreasing the transcription time (2–1 h). The selection was done for 12 rounds.

Reverse Transcription and PCR Performance on Beads

45 μl of the eluate with dissociated RNA and target was transferred to the 54 μl of RT mix: 1x *M*-MLV buffer, 0.5 μM biotinylated reverse primer, 0.5 mM dNTPs. Biotinylated reverse primer was purchased from Ella Biotech, Germany (5′-biotin-18spacer-GTCCTGTGGCATCCACG AAA-3′). First, the mixture without the *M*-MLV enzyme (Promega, USA) was heated up to 65 °C for 5 min to break the secondary structure of the RNA. Afterward, enzyme was added and RT was performed for 15 min at 40 °C. Next, 0.25 mg Dynabeads *M*-280 Streptavidin (ThermoFisher Scientific, USA) was added to the RT mix and was incubated for 30 min at 21 °C with gentle shaking. The supernatant was removed and a fresh PCR mix was added to the beads. PCR was performed for different number of PCR cycles with the program: 1) 95 °C 2 min; 2) 95 °C 1 min, 3) 56 °C 1 min, 4) 72 °C 1 min, and 5) 72 °C 3 min, with repeated 2−4 step. After the PCR, the solution was removed from the beads.

Radioactive Binding Studies

RNA was prepared as described in *Manual preparation of RNA-oligo-beads complexes for the initial round* in lower volume (300 μl) of PCR and transcription solution and was purified on a small 10% Urea-PAGE gel. 75 pmol of pure RNA was used for 5′ end labeling of the RNA. First, RNA was dephosphorylated, 5′-labeled with γ-^{32}P- ATP (Perkin Elmer, USA), and purified with polyacrylamide gel electrophoresis. Next, one quarter of the RNA (app. 15 pmol) was mixed with 15 pmol of 12-nt complementary oligo in the selection buffer

(PBS + 3 mM Mg^{2+}, pH 7.4). The solution was incubated for 1 h by heating up to 50 °C for 15 min and slowly cooling down to 30 °C with gentle shaking to allow RNA and oligos to hybridize. In the meantime, 0.5 mg of Dynabeads *M*-280 Streptavidin was washed 3-times with the selection buffer by using DynaMag-2 Magnet and finally resuspended in 50 μl of the selection buffer. RNA-oligos solution was then mixed with beads solution and incubated for 30 min at 21 °C with gentle shaking, so the biotinylated oligos and streptavidin coupled beads could interact. Afterward, the supernatant was removed and saved for measurement. Beads were washed 3-times with 100 μl of selection buffer and each fraction was saved for the measurement. Finally, 50 μl of 1 mM target solution was added to the beads and was incubated for 15 min at 21 °C and 900 rpm. Eluate was removed from beads and both fractions were saved for measurement. 1 mL of ddH_2O was added to each fraction and measured by liquid scintillation counter (Perkin Elmer, USA). Final result was calculated as a percentage of the sum of all fractions: supernatant, three washes, elution, and beads. Graph design and statistics were performed using GraphPad Prism 8 software.

NGS

The starting library, the selection round pool 2, 4, 6, 8, 10, and 11 or 12 were used for NGS. The protocol was taken from Tolle and Mayer.[38] Pools were amplified with different primers synthetized by Ella Biotech, Germany, each having a unique 6-nucleotides extension at the 5′ prime end, which was used as a barcode for further NGS analysis. A PCR reaction mix was prepared for each pool and for an additional No Template Control (NTC), using a proofreading *Pfu*-Polymerase (homemade). 1 μM of reverse and 1 μM of forward primer with the same index sequence were added to the PCR master mix. The mix was split and the DNA template or water for NTC was added to it. DNA was amplified with a normal PCR program, described in *Manual preparation of RNA-oligo-beads complexes for the initial round*. PCR product was purified with Nucleospin Gel and PCR clean-up columns (Macherey Nagel, Germany) according to the manufacturer's instructions. 0.125 μg of each DNA was mixed together and used for the following step. Next, adapter needed for immobilization and processing of the sample on the Illumina instruments was ligated to the DNA sequences using TruSeq DNA PCR-Free Sample Preparation Kit LT (Illumina, USA). Ligation was done according to manufacturer instructions applying three procedures: "End Repair", "Adenylation", and "Adapter Ligation". The ligated products were afterward separated on an agarose gel, cutting out only the longest sequence (app. 210 bp) with ligated adapters on both sides. The DNA was purified from the gel using Nucleospin gel and PCR clean-up columns, following manufacturer instructions. Finally, DNA was eluted with the resuspension buffer (TruSeq DNA PCR-Free Sample Preparation Kit LT) and was used for illumina sequencing with NextSeq500 with High Output v2 chemistry. NGS analysis was done by in-house designed software AptaNext. Graph design was performed using GraphPad Prism 8 software.

RNA Displacement from Complementary Fluorescence Labeled Oligodeoxynucleotides by Target Addition Measured by Fluorescent Polarization

5′-Cy3 labeled oligodeoxynucleotides (ODN) were purchased from Ella Biotech, Germany. Sequences of different oligo lengths are provided in Table 2, Supporting Information. Polarization assay was performed in final volume of 50 μl of (100 nM Cy3-ODN, 500 nM RNA, 0.1−1 mM target) in 1xPBS with 3 mM Mg^{2+} and 0.005% Tween 20. First, RNA and target were mixed together and incubated for 30 min at 21 °C and 500 rpm. Second, Cy3-ODN was added and incubated for another 30 min at 21 °C and 500 rpm. Finally, the solution was transferred to the Corning 96 Well Half-Area Microplate (Sigma Aldrich, Germany) and was measured by *Tecan Ultra* Micro Plate Reader (Tecan, Switzerland) at excitation light 535 nm, and emission light 595 nm. The fluorescence polarization (FP) values were always normalized to the value of the 100 nM Cy3-ODN sample. Graph design was performed using GraphPad Prism 8 software.

ITC Measurement

The RNA for affinity measurement was prepared by in vitro transcription. After ethanol precipitation, the RNA was resuspended in the binding buffer and further washed several times with the same buffer on the 3 K Amicon Ultra 0.5 mL Centrifugal Filters (Merck, Germany). Different concentrations of ligands in the syringe were titrated to different aptamer concentrations in the sample cell, dependently of the ligand-aptamer pair. For the titrations with neomycin B- and kanamycin-aptamers pairs, we titrated the ligand in 38 injections: first injection of 0.4 μl and subsequent 37 injections of 1 μl. With theophylline- and riboflavin-aptamer pairs, we titrated the ligand in 38 injections 0.4 μl and subsequent 18 injections of 2 μl. The affinity was measured on MicroCalTM PEAQ-ITC (Malvern Panalytical, UK) with power of 10 μcal/sec and spacing time 180 sec. Graph design was performed using GraphPad Prism 8 software.

Acknowledgements

This project was supported by funds from the Deutsche Forschungsgemeinschaft (DFG, MA/4221 7−1 to G.M.) and the ERC ("IntraMAP" 101140898 to G.M.). The authors thank Mark Helm, Clemens Richerts, Andreas Meyer, and Henning Jessen for providing compounds used in the automated capture SELEX process.

Conflict of Interest

The authors declare no conflict of interest.

Data Availability Statement

The data that support the findings of this study are available from the corresponding author upon reasonable request.

Keywords: aptamers · automation · capture-systematic evolution of ligands by exponential enrichment

[1] C. Tuerk, L. Gold, *Science* **1990**, *249*, 505.
[2] A. D. Ellington, J. W. Szostak, *Nature* **1990**, *346*, 818.
[3] R. Stoltenburg, C. Reinemann, B. Strehlitz, *Biomol. Eng.* **2007**, *24*, 381.
[4] L. Civit, I. Theodorou, F. Frey, H. Weber, A. Lingnau, C. Gröber, M. Blank, C. Dambrune, J. Stunden, M. Beyer, *Sci. Rep.* **2019**, *9*, 4976.
[5] J. Mi, Y. Liu, Z. Rabbani, Z. Yang, B. Sullenger, B. Clary, *Cancer Res.* **2008**, *68*, 4744.
[6] S. Breuers, L. L. Bryant, T. Legen, G. Mayer, *Methods* **2019**, *161*, 3.
[7] A. Schmitz, A. Weber, M. Bayin, S. Breuers, V. Fieberg, M. Famulok, G. Mayer, *Angew. Chem., Int. Ed.* **2021**, *60*, 10279.
[8] R. Stoltenburg, N. Nikolaus, B. Strehlitz, *J. Anal. Methods Chem.* **2012**, *2012*, 415697.
[9] G. Mayer, B. Wulffen, C. Huber, J. Brockmann, B. Flicke, L. Neumann, D. Hafenbradl, B. M. Klebl, M. J. Lohse, C. Krasel, *Rna* **2008**, *14*, 524.
[10] A. Hunsicker, M. Steber, G. Mayer, J. Meitert, M. Klotzsche, M. Blind, W. Hillen, C. Berens, B. Suess, *Chem. Biol.* **2009**, *16*, 173.
[11] A. Boussebayle, F. Groher, B. Suess, *Methods* **2019**, *161*, 10.

[12] M. G. Wallis, U. von Ahsen, R. Schroeder, M. Famulok, *Chem. Biol.* **1995**, *2*, 543.
[13] T. L. Bailey, J. Johnson, C. E. Grant, W. S. Noble, *Nucleic Acids Res.* **2015**, *43*, W39.
[14] T. Legen, G. n. Mayer, *ACS Sens.* **2024**, *9*, 753.
[15] A. Geiger, P. Burgstaller, H. Von der Eltz, A. Roeder, M. Famulok, *Nucleic Acids Res.* **1996**, *24*, 1029.
[16] R. D. Jenison, S. C. Gill, A. Pardi, B. Polisky, *Science* **1994**, *263*, 1425.
[17] Á. Kerek, B. G. Ecsedi, Á. Szabó, Z. Szimrók, B. Paliczné Kustán, Á. Jerzsele, G. Nagy, *Antibiotics* **2024**, *13*, 549.
[18] P. Szterner, B. Legendre, M. Sghaier, *J. Therm. Anal. Calorim.* **2010**, *99*, 325.
[19] I. M. Weiss, C. Muth, R. Drumm, H. O. Kirchner, *BMC Biophysics.* **2018**, *11*, 1.
[20] N. Hodges, J. Singh, *J. Pharm. Pharmacol.* **1978**, *30*, 737.
[21] I. Pavlovic, D. T. Thakor, J. R. Vargas, C. J. McKinlay, S. Hauke, P. Anstaett, R. C. Camuña, L. Bigler, G. Gasser, C. Schultz, *Nat. Commun.* **2016**, *7*, 10622.
[22] J. A. Martin, J. L. Chávez, Y. Chushak, R. R. Chapleau, J. Hagen, N. Kelley-Loughnane, *Anal. Bioanal. Chem.* **2014**, *406*, 4637.
[23] H. Wang, J. Wang, L. Xu, Y. Zhang, Y. Chen, H. Chen, R. Pei, *Anal. Methods* **2016**, *8*, 8461.
[24] A. Zhang, D. Chang, Z. Zhang, F. Li, W. Li, X. Wang, Y. Li, Q. Hua, *Molecules* **2017**, *22*, 383.
[25] N. Komarova, M. Andrianova, S. Glukhov, A. Kuznetsov, *Molecules* **2018**, *23*, 3159.
[26] L. Gu, H. Zhang, Y. Ding, Y. Zhang, D. Wang, J. Liu, *Smart Mol.* **2023**, *1*, e20230007.
[27] Y. Zhao, A. Z. Li, J. Liu, *Environ. Health* **2023**, *1*, 102.
[28] J. S. Paige, *Science* **2011**.
[29] J. R. Lorsch, J. W. Szostak, *Biochemistry* **1994**, *33*, 973.
[30] L. Barthelmebs, J. Jonca, A. Hayat, B. Prieto-Simon, J.-L. Marty, *Food Control* **2011**, *22*, 737.
[31] A. Boussebayle, D. Torka, S. Ollivaud, J. Braun, C. Bofill-Bosch, M. Dombrowski, F. Groher, K. Hamacher, B. Suess, *Nucleic Acids Res.* **2019**, *47*, 4883.
[32] N. Nakatsuka, K.-A. Yang, J. M. Abendroth, K. M. Cheung, X. Xu, H. Yang, C. Zhao, B. Zhu, Y. S. Rim, Y. Yang, *Science* **2018**, *362*, 319.
[33] O. Alkhamis, Y. Xiao, *J. Am. Chem. Soc.* **2022**, *145*, 194.
[34] F. Tolle, G. M. Brändle, D. Matzner, G. Mayer, *Angew. Chem. Int. Ed.* **2015**, *54*, 10971.
[35] M. Ondruš, V. Sýkorová, L. Bednárová, R. Pohl, M. Hocek, *Nucleic Acids Res.* **2020**, *48*, 11982.
[36] Y. Zhang, S. Zhang, Z. Ning, X. Lin, N. Duan, Z. Wang, S. Wu, *J. Agric. Food Chem.* **2024**, *72*, 28148.
[37] O. Doppleb, J. Bremer, M. Bechthold, C. Sánchez Rico, D. Göhringer, H. Griesser, C. Richert, *Chem.– Eur. J.* **2021**, *27*, 13544.
[38] F. Tolle, G. Mayer, *In Nucleic Acid Aptamers*, Springer **2016**, pp. 77–84.
[39] G. S. Filonov, J. D. Moon, N. Svensen, S. R. Jaffrey, *J. Am. Chem. Soc.* **2014**, *136*, 16299.

Manuscript received: March 27, 2025
Revised manuscript received: June 13, 2025
Version of record online:

Supplementary information

Robotic-assisted selection of RNA aptamers binding to small molecules

Tjasa Legen[1,2], Günter Mayer[1,2]*

[1]Life and Medical Sciences Institute (LIMES), University of Bonn, Germany
[2]Center of Aptamer Research and Development (CARD), University of Bonn, Germany

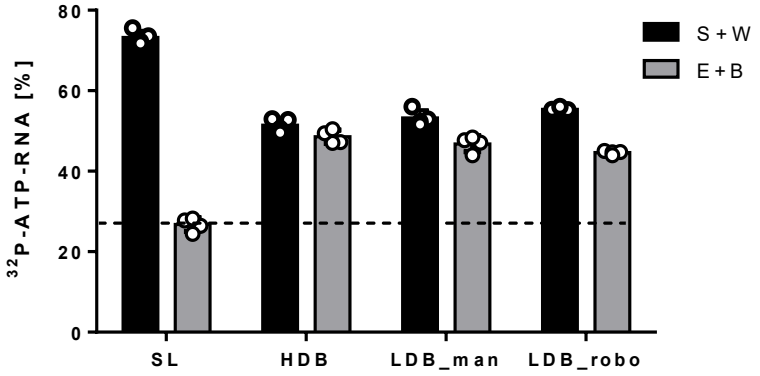

Figure S1. Annealing efficiency of the starting library (SL) and enriched pools selected for neomycin B by different strategies. During the selection, annealing efficiency of enriched sequences increases. Error bars show standard deviation (n=2). S+W: Sum of supernatant and three washing fractions, E+B: Sum of elution and beads fraction. HDB: selection with high-density beads, LDB: selection with low-density beads, man: manual selection, robo: robotic selection.

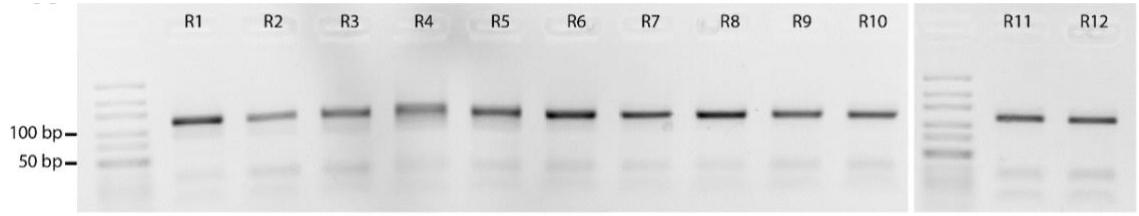

Figure S2. PCR profile of different selection rounds of robotic assisted selection targeting neomycin B. PCR product was loaded on a 4% Agarose gel with Ultra-low range ladder.

Table S1. Summary of SELEX conditions utilized in the selections targeting neomycin B

SELEX round	Target concentration	IVT time	Washing	Incubation time
1	1 mM	50°C-30°C	1x100 µl: 5 min; 2x100 µl	15 min
2		2 h	3x100 µl	
3				
4		1.5 h		
5	0.5 mM			10 min
6				
7				
8		1 h		
9	50 µM			5 min
10				
11				
12				

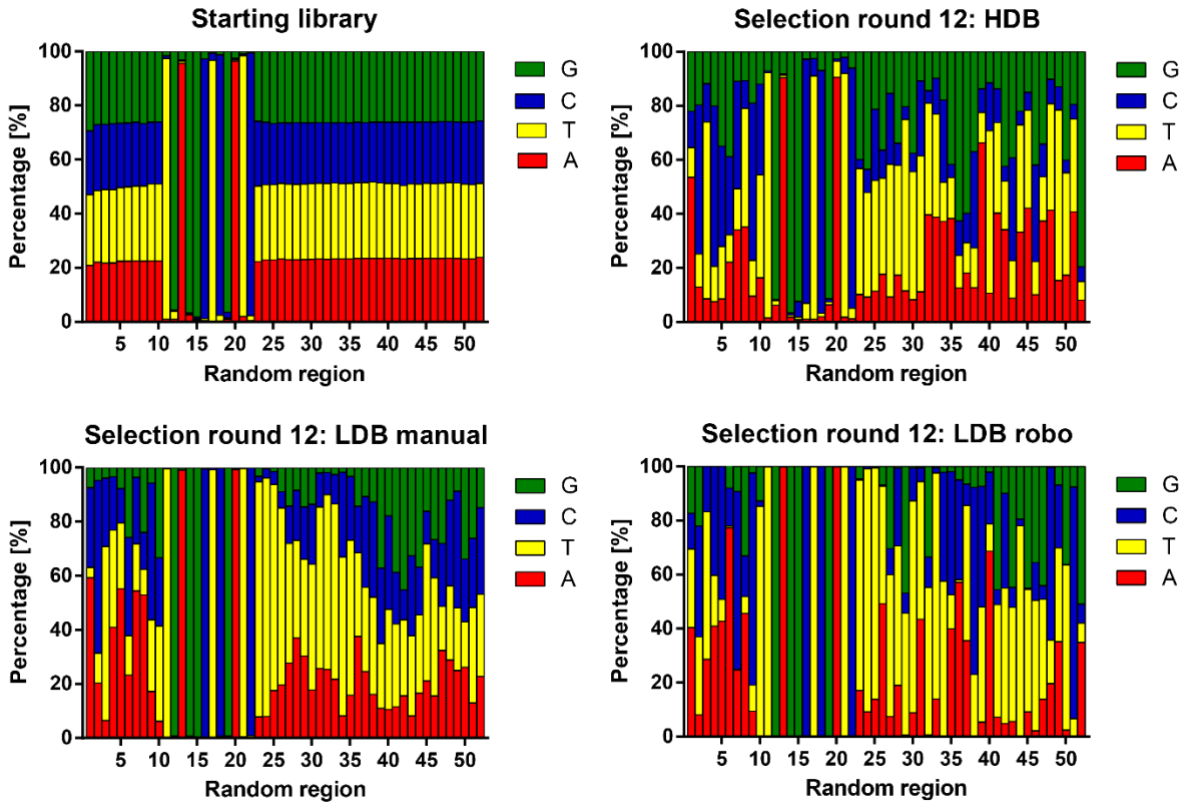

Figure S3. Nucleotide distribution in the random region of starting library, round 12 (R12) high-density beads (HDB) selection, R12 low-density beads (LDB) manual selection, and R12 LDB robotic selection targeting neomycin B measured by next-generation sequencing (NGS).

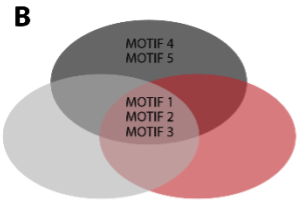

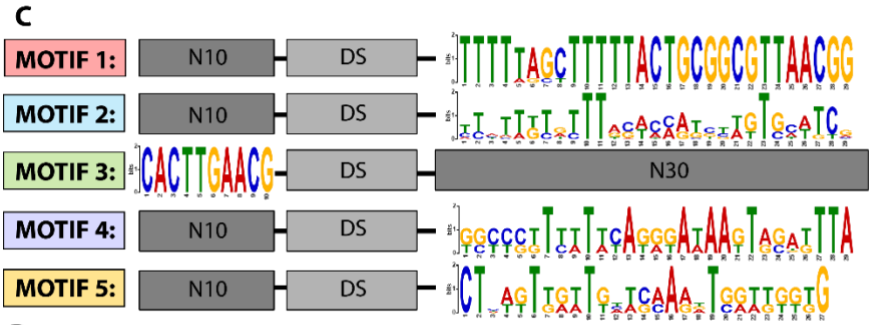

D

HDB_1	ACCCCATCT	**TGAGGCTCGATC**	GGCTCGTTTTTCAGGGATAAGTAGATTTAG
HDB_2	ACCGGCACC	**TGAGGCTCGATC**	TTTGTTTGCAAAGGGCATTGCATCGATGTG
HDB_3	ACTCCCATCT	**TGAGGCTCGATC**	GGCTCGTTTTTCAGGGATAAGTAGATTTAG
HDB_4	ACCGGCACC	**TGAGGCTCGATC**	TTTGTTTGCAAAGGGCATTGCATCGATGTG
HDB_5	GGGTACTGA	**TGAGGCTCGATC**	TGGATAGTTACGGCACACCTCGACCAAAAG
HDB_6	GGTGTACTGA	**TGAGGCTCGATC**	TGGATAGTTACGGCACACCTCGACCAAAAG
HDB_7	ATTCACTCC	**TGAGGCTCGATC**	TGGCTCAGTGAATGCACCAGTTGGTTTGGG
HDB_8	TATTCACTCC	**TGAGGCTCGATC**	TGGCTCAGTGAATGCACCAGTTGGTTTGGG
HDB_9	ACCCCATCT	**TGAGGCTCGATC**	GGCTCGTTTTTTCAGGGATAAGTAGATTTAG
HDB_10	ACTCCCATCT	**TGAGGCTCGATC**	GGCTCGTTTTTTCAGGGATAAGTAGATTTAG
HDB_11	CACGAACG	**TGAGGCTCGATC**	TTTTTAGCTTTTTACTGCGGCGTTAACGGT
HDB_12	CACTTGAACG	**TGAGGCTCGATC**	TTTTTAGCTTTTTACTGCGGCGTTAACGGT
HDB_13	ACCCGTAAC	**TGAGGCTCGATC**	GCAATTTTATATATATGAAGGGCATCGTAGT
HDB_14	ACTCCGTAAC	**TGAGGCTCGATC**	GCAATTTTATATATATGAAGGGCATCGTAG
HDB_15	ACCCGGCCC	**TGAGGCTCGATC**	TTTGTTTGCAAAGGGCATTGCATCGATGTGT
HDB_16	ACCCGGCTCC	**TGAGGCTCGATC**	TTTGTTTGCAAAGGGCATTGCATCGATGTG
HDB_17	CGCTGTACT	**TGAGGCTCGATT**	GTTGTTTTTGAAAATGATGGTTGGTCCATAT
HDB_18	CTGCTGTACT	**TGAGGCTCGATT**	GTTGTTTTTGAAAATGATGGTTGGTCCATA
HDB_19	GCACCT	**TGAGGCTCGATC**	ATTTGTTGATCAAAGTCGATGGTGACTGGGTT
HDB_20	ACTCTGGCAT	**TGAGGCTCGATC**	GTTTAGTTGTTTTTATTGTTGAGTTCCTGC

LM_1	CACTTGAACG	**TGAGGCTCGATC**	TTTTTAGCTTTTTACTGCGGCGTTAACGGT
LM_2	ACTAACAGTC	**TGAGGCTCGATC**	TTTTGCAGAAACTTTCGTCTTTTGGCTATC
LM_3	CACTTGAACG	**TGAGGCTCGATC**	TTTTTAGCTTTTTTACTGCGGCGTTAACGGT
LM_4	ACTTAATTCG	**TGAGGCTCGATC**	TTAGCTTTTTTCAGTCACTAGCATCTAGTA
LM_5	ACTAACAGAC	**TGAGGCTCGATC**	TTTTTTAACAACCAAACATGTGTCGTCCAC
LM_6	ACTAAGCACT	**TGAGGCTCGATC**	TTTTACACTTTTTGGCCTAGCATTCATCTT
LM_7	ACTAAACACT	**TGAGGCTCGATC**	TTTATTGTATTTACACCATCTTGTGCATCA
LM_8	ACTACGCACT	**TGAGGCTCGATC**	TTTAAAACTTTTTTCACTGGGCTAACACCT
LM_9	ACTAACAGTC	**TGAGGCTCGATC**	TTTTAATGATTTTTCACTGTGTCGGTCATC
LM_10	GTCCAACACT	**TGAGGCTCGATC**	AAATAACTTTAACCACTGAGCATGCCACCA
LM_11	ACTTGCACTT	**TGAGGCTCGATC**	TTTTCAATTTCACTGGGTATTCAGAAGTCG
LM_12	CTTCATCAAA	**TGAGGCTCGATC**	TTTTTATTTAACCATCTGTAAGCATTTACG
LM_13	ACTCATTATT	**TGAGGCTCGATC**	TTTATCAGTTTTTCACCTGAGTATTCATGC
LM_14	ACTAACCACT	**TGAGGCTCGATC**	TTTTTATCACTTTTAGAGTCTGAACGCATC
LM_15	CTTCAGTGCT	**TGAGGCTCGATC**	TTTTGTTCCAGTTTATGGCGTAAGCGATTG
LM_16	GCTAACACTC	**TGAGGCTCGATC**	TTTTCATATTCTTTTACCTGGCGCATCACA
LM_17	ACTAGTAACT	**TGAGGCTCGATC**	TTACTTTATACTCAATGTGGCTTTGCAACT
LM_18	GAATCCAG	**TGAGGCTCGATC**	TTTTTAATTTTTCATTCCTAGCATCGCGTT
LM_19	CTTGAACACT	**TGAGGCTCGATC**	TTTTGCTTAATTCACCTTGTCATTCTCGAA
LM_20	CATAACA	**TGAGGCTCGATC**	TTTACTATTCTTTTATCCGTGTCAGCACAC

LR_1	ACTAAACACT	**TGAGGCTCGATC**	TTTATTGTATTTACACCATCTTGTGCATCA
LR_2	TTACCACGCT	**TGAGGCTCGATC**	TTTTGCTTTGTCCATCTAGTGTTGTCTGCG
LR_3	GGTTCCGCAT	**TGAGGCTCGATC**	AAAACTTTTCATCATTCTGTGTACGTCTCG
LR_4	GGCCAAATCT	**TGAGGCTCGATC**	ATTGAACAATTCCATGTCATTGTGTAGTCC
LR_5	CACTTGAACG	**TGAGGCTCGATC**	TTTTTAGCTTTTTACTGCGGCGTTAACGGT
LR_6	CGTCCAACTG	**TGAGGCTCGATC**	TTAATTTTCGACTAGTTCCAAGGCATCTTG
LR_7	ACTACCAGTT	**TGAGGCTCGATC**	GTTTTAGCTTTTAGTCAATTGTGTCATTCG
LR_8	GGCTCACAGC	**TGAGGCTCGATC**	TTTTGTTAACCGGCGTTGTGGCTAATCATG
LR_9	TCCACTACGT	**TGAGGCTCGATC**	TACTTTTTTCGTTTCGTGGATGC
LR_10	GGCCAAACTT	**TGAGGCTCGATC**	ATTCATCATTTTCATGCCAGTGGATATACG
LR_11	CACTTGAACG	**TGAGGCTCGATC**	TTTTTTAGCTTTTTACTGCGGCGTTAACGG
LR_12	CACTTGAACG	**TGAGGCTCGATC**	TTTTTAGCTTTTAGTCAATTGTGTCATTCG
LR_13	CTTCACACAC	**TGAGGCTCGATC**	ACCTTTAGTCTTTTACTTGTAGCTTGCACG
LR_14	ACTAAACACT	**TGAGGCTCGATC**	TTTATTGTATTTACACCATCTTGTGCATCG
LR_15	CACTTGAACG	**TGAGGCTCGATC**	TTTTTAGCTTTTTACTGCGGCGTTAACGG
LR_16	ACTAAACACT	**TGAGGCTCGATC**	TTTTGCTTTGTCCATCTAGTGTTGTCTGCG
LR_17	TTACCACGCT	**TGAGGCTCGATC**	TTTATTGTATTTACACCATCTTGTGCATCA
LR_18	CACTTGAACG	**TGAGGCTCGATC**	TTTTTAGCTTTTTACTGCGGCGTTAACGGC
LR_19	CACTTGAACG	**TGAGGCTCGATC**	GTTTTAGCTTTTAGTCAATTGTGTCATTCG
LR_20	CACTTGAACG	**TGAGGCTCGATC**	TTTTTAGCTTTTTACTGCGGCGTTAACGGG

Figure S4. The sequence analysis of high-density beads (HDB) selection, low-density beads (LDB) manual selection, and LDB robotic selection for neomycin B. A) Common sequence in different selection strategies among 20 the most enriched sequences of each selection. Dark grey: HDB selection; light grey: LDB manual selection; red: LDB robotic selection. **B)** Common motifs in different selection strategies among 20 the most enriched sequences of each selection. For motifs search, MEME suite tool for motif discovery was utilized.[1] **C)** Motif sequence and positions of the motifs in the enriched sequences. **D)** Highlighted motif sequences in the 20 the most enriched sequences in each neomycin selection (HDB: High-density beads, LM: Low-density beads manual, LR: Low-density beads robotic). With the black arrow, the sequences found among all three selections are marked and with the red arrow, the sequence common in LM and LR selection.

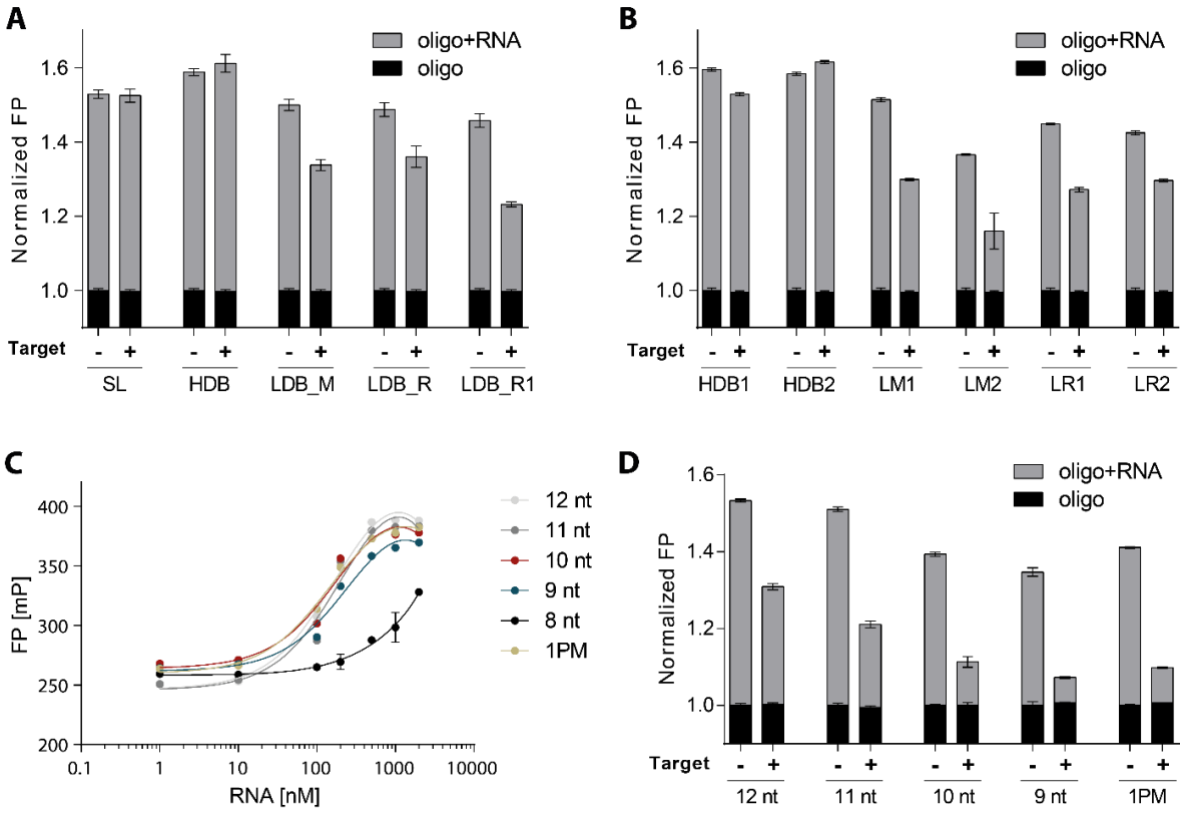

Figure S5. Optimization of fluorescence polarization assay for binding studies using enriched pool and monoclonal sequences binding to neomycin B. A) Binding of enriched pools to neomycin target obtained by different selections measured

by fluorescence polarization assay. For assay, 100 nM of Cy3 labelled capture oligodeoxynucleotide (ODN) and 500 nM RNA was used in the absence or presence of 100 µM neomycin. The FP-values were normalized according to the value of free Cy3-ODN. Error bars show standard deviation (n=3). SL: starting library, HDB: Selection with high-density beads, LDB_M: Manual selection with low-density beads, LDB_R: Robotic selection with low-density beads, LDB_R1: Robotic selection with low-density beads and RT-PCR performed on magnetic beads (see **Supp. Fig. 9**). **B)** Binding of different monoclonal sequences to neomycin B target obtained by different selections measured by fluorescence polarization assay. For assay, 100 nM of Cy3 labelled capture ODN and 500 nM RNA was used in the absence or presence of 100 µM Neomycin. The FP-values were normalized according to the value of free Cy3-ODN. Error bars show standard deviation (n=3). HDB: Sequences obtained by high-density selection, LM: Sequences obtained by manual low-density selection, LR: Sequences obtained by robotic low-density selection. **C)** Annealing efficiency of RNA to different length ODNs measured by fluorescent polarization. For the annealing, different concentration of neomycin B aptamer LM1 were used during 30 min incubation at 21°C in PBS with 3 mM Mg^{2+}. Concentration of the ODNs was constant 100 nM. The FP-values were normalized according to the value of free Cy3-ODN. Error bars show standard deviation (n=3). The data were fitted in non-linear fit model. By the 8-nt capture ODN, there is only a weak annealing observed. nt: nucleotide, 1PM: one point mutation in 12-nt oligonucleotide. **D)** LM1 aptamer displacement from different lengths of ODNs by binding to the neomycin B target. The concentration of ODN and aptamer LM1 was 100 nM and 500 nM, respectively. Concentration of neomycin was 100 µM. The FP-values were normalized according to the value of free Cy3-ODN. Error bars show standard deviation (n=3). The highest decrease in the fold-change of FP is by the 9-nt ODN.

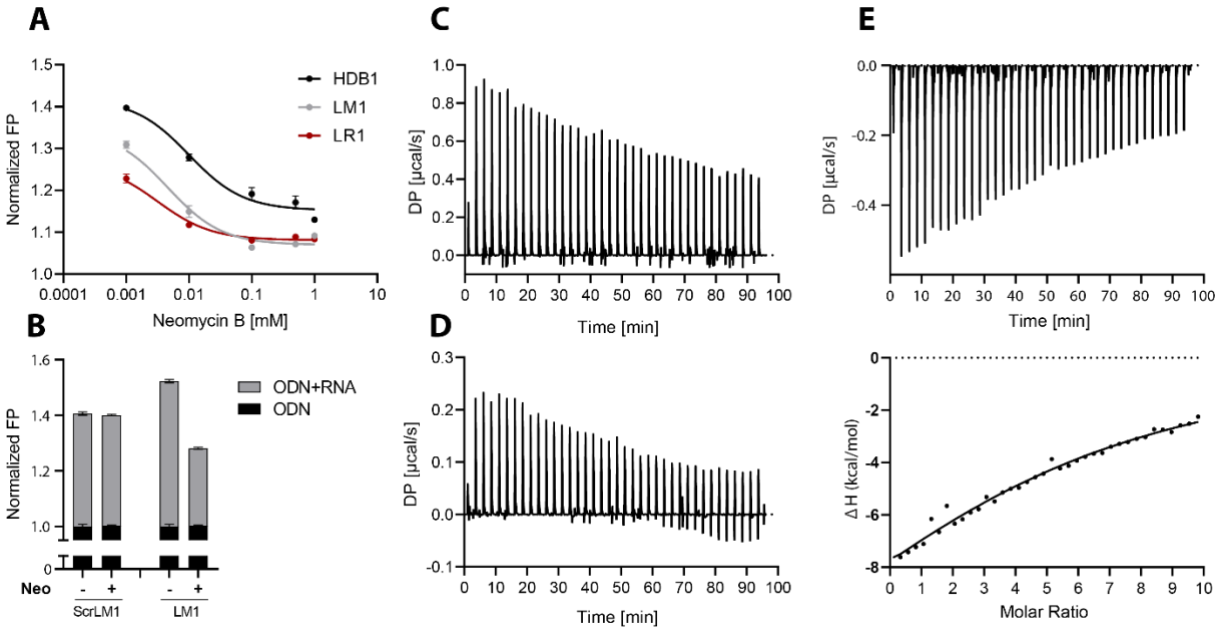

Figure S6. Binding affinity measurement by isothermal titration calorimetry (ITC). A) Concentration dependent binding of neomycin B to HDB1, LM1 and LR1 aptamer measured by fluorescence polarization. The FP-values were normalized according to the value of free Cy3-ODN. Error bars show standard deviation (n=3). The estimated K_d determined by the assay was approximately 10 µM, 4 µM and 3 µM, respectively. The fluorescence change was fitted to inhibitor vs. response model. FP: fluorescence polarization. **B)** Binding of scrabbled LM1 (ScrLM1) and LM1 sequences to neomycin B measured by fluorescence polarization assay. The FP-values were normalized according to the value of free Cy3-ODN. Error bars show standard deviation (n=3). **C)** Neomycin B (1 mM) titration to PBS + 3 mM Mg^{2+} buffer. DP: differential power. **D)** Kanamycin (1 mM) titration to PBS + 3 mM Mg^{2+} buffer. **E)** LR1 and kanamycin interaction. K_d is 130.0 ± 30.9 µM. For the measurement 20 µM of RNA and 1 mM of target was used.

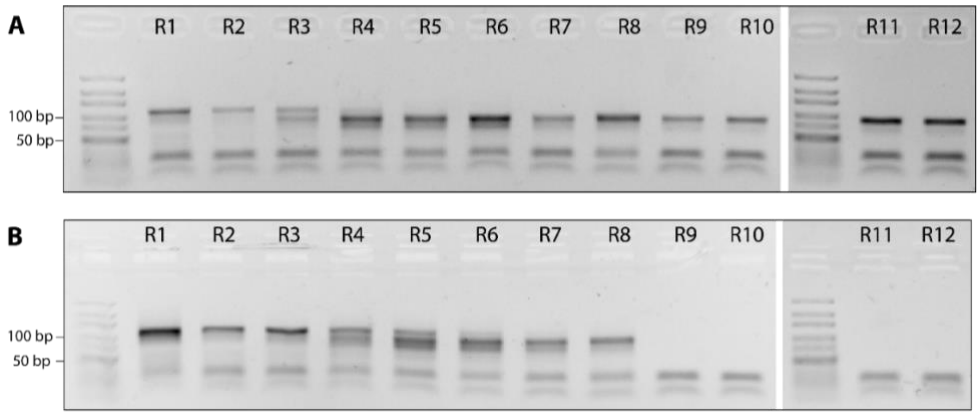

Figure S7. PCR profile of different rounds of robotic assisted selection targeting L-arginine (A) and theophylline (B). Both selections lead to truncation of the RNA library or even to loss of the product band.

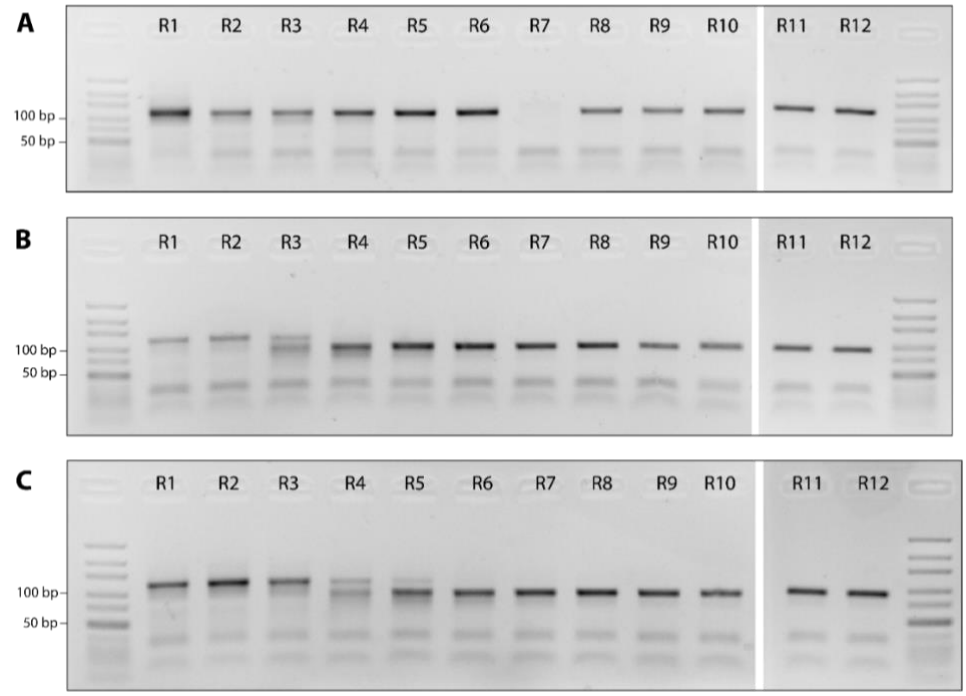

Figure S8. PCR profile of different rounds of automated selection targeting A) neomycin B with initial concentration of 50 µM, B) neomycin B with initial concentration of 5 µM, and C) only selection buffer (PBS + 3 mM Mg^{2+}). By initial target concentration as low as 5 µM (B), the library length shortens indicating unsuccessful selection, the same being observed in the selection using no target molecule (C). PCR product was loaded on a 4% Agarose gel with Ultra-low range ladder.

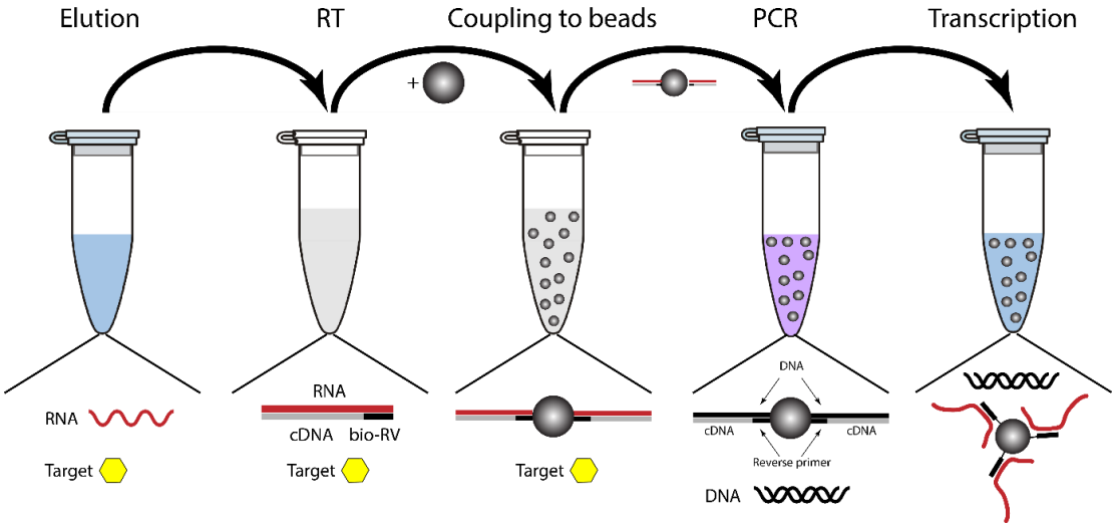

Figure S9. Separation of reverse transcription (RT) and amplification step of dissociated sequences during capture SELEX process to remove remaining target molecule. Elution mix with dissociated RNA and target molecule is mixed with the reverse transcription (RT) solution, which contains biotinylated reverse primer. Generated biotinylated-cDNA (bio-cDNA) is then captured by addition of streptavidin (SA) beads to the RT solution to remove the solution with the target molecule. Next, polymerase chain reaction (PCR) mix is added to the beads with captured cDNA template. After amplification, an aliquot of PCR product is added as a template for the *in vitro* transcription (IVT) reaction, where the transcribed RNA is directly annealed to the biotinylated-capture oligodeoxynucleotide present in the IVT mixture and subsequently captured to SA-beads.

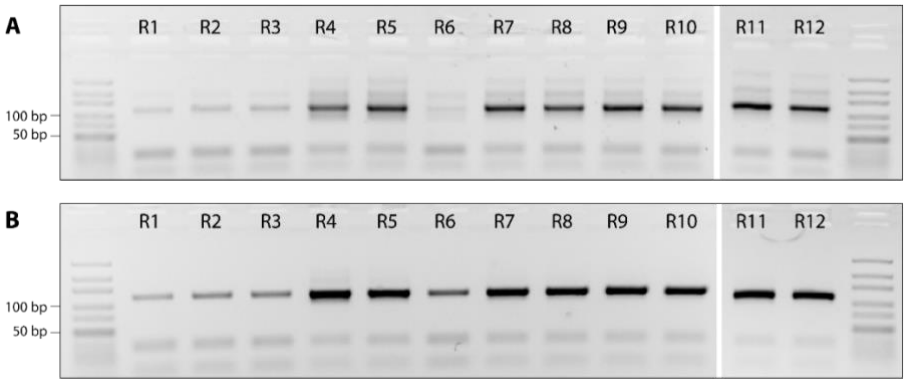

Figure S10. PCR profile of automated selection with a new strategy keeping RT and PCR reaction separated for removal of target molecule (A) and re-amplification of PCR product (B). All additional bands visible in the gel A disappear after the re-amplification (gel B) indicating that those bands were either RNA or single-stranded DNA sequences. The utilized target in the SELEX was neomycin B. PCR product was loaded on a 4% Agarose gel with Ultra-low range ladder.

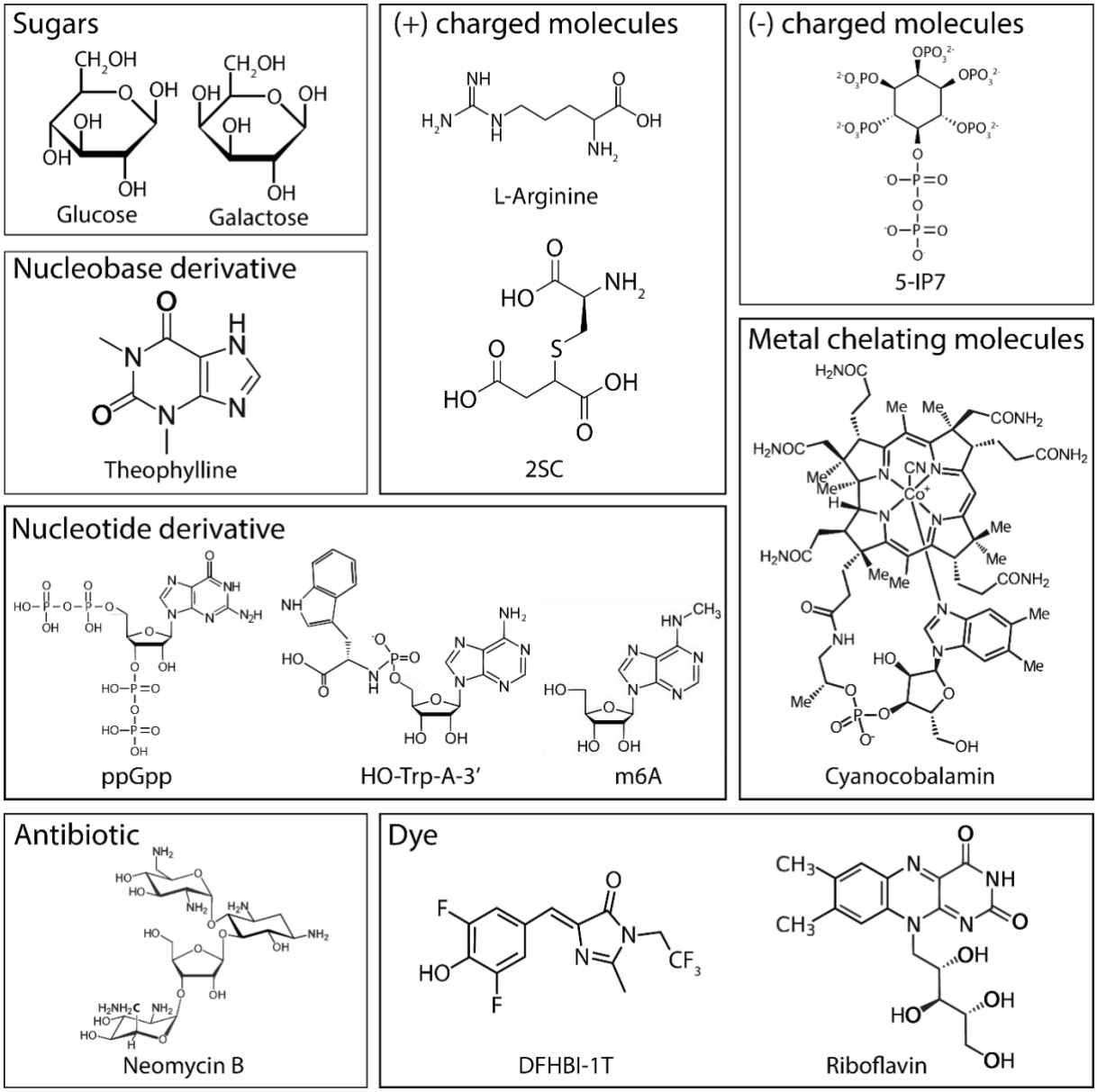

Figure S11. Structure and characterization of small molecule targets according to their functionality or functional groups. Different structural or functional moieties were chosen for the automated selection to investigate versatility of selection ability. 2SC: S-(2-succinyl) cysteine, DFHBI-1T: 3,5-Difluoro-4-hydroxybenzylidene imidazolinone-1T,[2] HO-Trp-A-3': D-Tryptophanyl Adenosine 5'-Monophosphate Phosphoramidate,[3] m6A: N6-Methyladenosine, 5-IP7: 5-diphospho-*myo*-inositol pentakisphosphate,[4] ppGpp: Guanosine pentaphosphate.

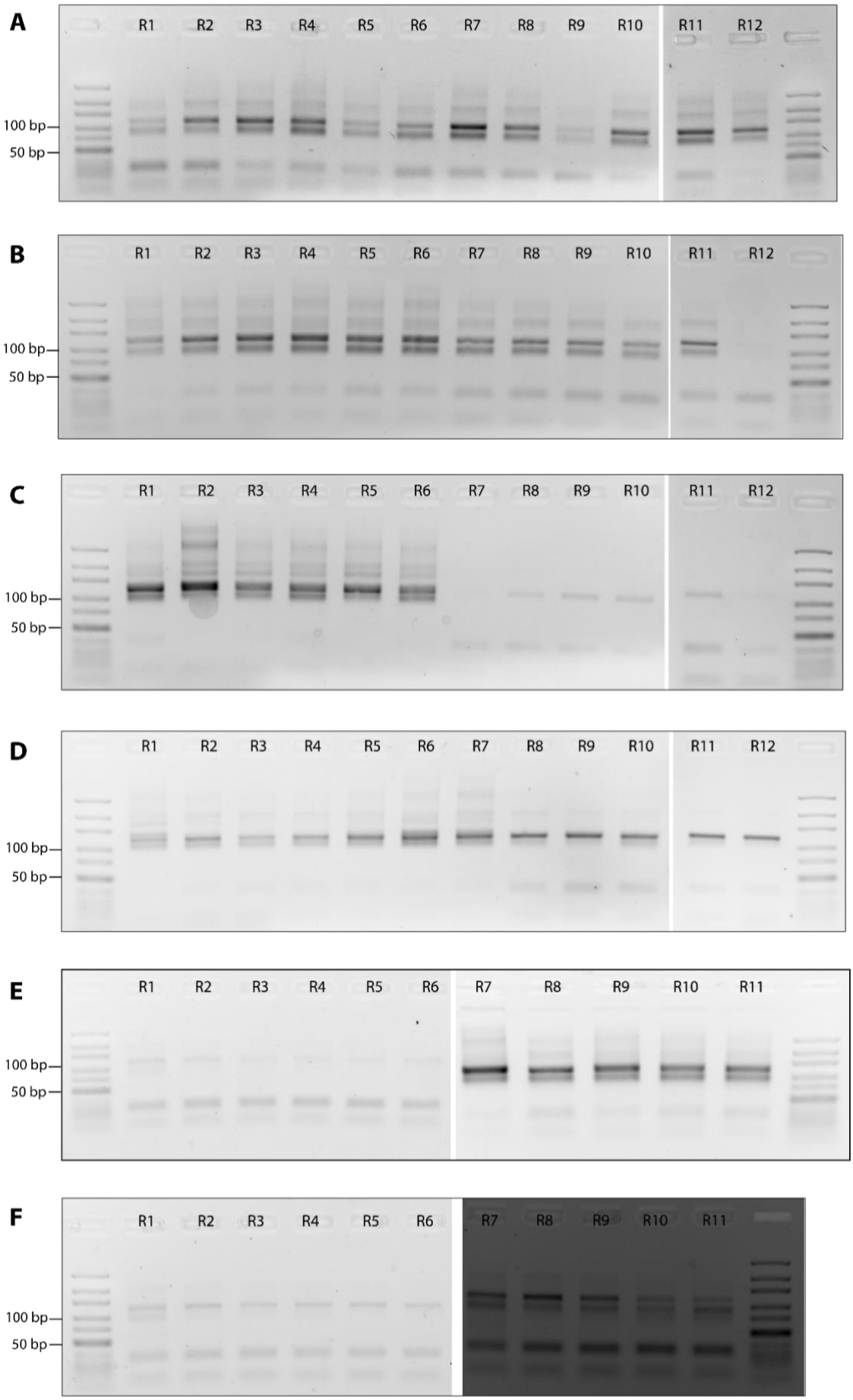
A
R1 R2 R3 R4 R5 R6 R7 R8 R9 R10 R11 R12
100 bp
50 bp
B
R1 R2 R3 R4 R5 R6 R7 R8 R9 R10 R11 R12
100 bp
50 bp
C
R1 R2 R3 R4 R5 R6 R7 R8 R9 R10 R11 R12
100 bp
50 bp
D
R1 R2 R3 R4 R5 R6 R7 R8 R9 R10 R11 R12
100 bp
50 bp
E
R1 R2 R3 R4 R5 R6 R7 R8 R9 R10 R11
100 bp
50 bp
F
R1 R2 R3 R4 R5 R6 R7 R8 R9 R10 R11
100 bp
50 bp

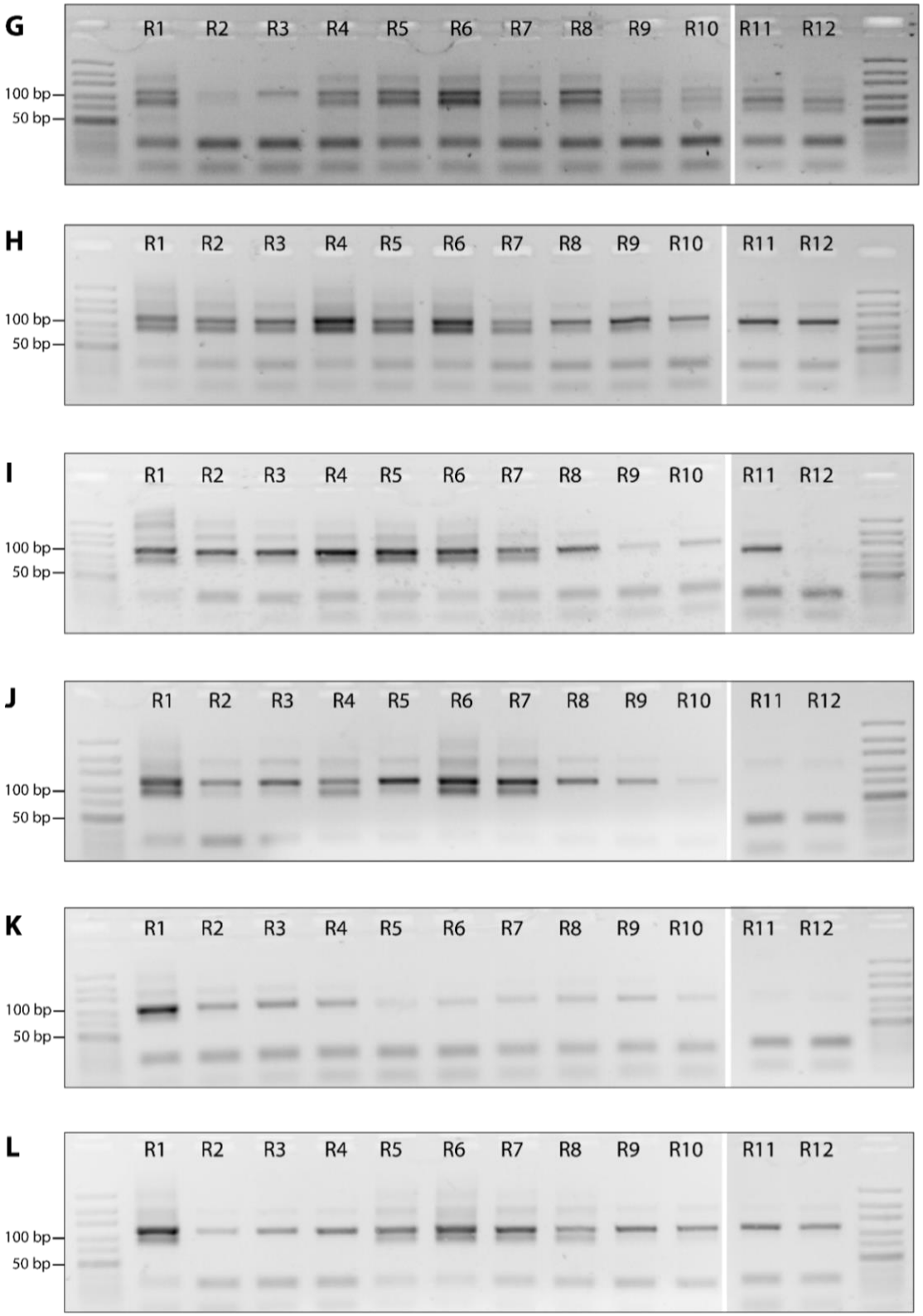

Figure S12. PCR profile of automated selection with various small molecule targets. A) Arginine, **B)** Theophylline, **C)** Galactose, **D)** 3,5-Difluoro-4-hydroxybenzylidene imidazolinone-1T (DFHBI-1T),[2] **E)** D-Tryptophanyl Adenosine 5'-Monophosphate Phosphoramidate (HO-Trp-A-3'),[3] **F)** N6-Methyladenosine (m6A), **G)** Guanosine pentaphosphate (ppGpp), **H)** 5-diphospho-*myo*-inositol pentakisphosphate (5-IP7),[4] **I)** Glucose, J) S-(2-succinyl) cysteine (2SC), **K)** Riboflavin, and **L)** Cyanocobalamin.

No.	Sequence	Arginine	Theo	DFHBI-1T	2SC	Riboflav	Cyanoco	Glucose	HO-Trp	m6A	5-IP7	ppGpp
1	GGAACGGTAATGAGGCTCGATCGAATTAGACCGCCTTGATTCCCTCGTGGCG	0	0	0.0869	0.2749	0.0042	0.2666	0.0405	0.0202	0.3329	9.1016	48.9888
2	CTATCGCTTGTGAGGCTCGATCTTTATGTGCCCCTCCTTCAGGTTGGCGTCT	0	0	0	0	0	0	0	0.0554	0.1967	0	0
3	GGGATGTCGTGAGGCTCGATCAATGTATTTTGCTCCCTGCTCGGTGGTTCC	0	0	0	0.2227	0.0021	0.034	0.3061	0	0.3138	0	0.0106
4	CCACGCTGGTGAGGCTCGATCACGGAGACTTCATTTCCCATTGTTGTGTGG	0.2252	0	0	0	0	0	0	0.586	1.8388	0.0124	0.907
5	GCTATCTAGTTGAGGCTCGATCAGTGTACCATACTTTCTTCTCCCACCGGCA	0	0	0.0228	0.0224	0	0.0059	0.0979	0	0.0536	0	0
6	ATCTATCCGATGAGGCTCGATCCAGTGCTTTTGCTCTCTAGAGTCATTCACG	0	0	0.2513	0.0077	0	0.8026	0.0586	0	0	0	0
7	CCGGTATCTATGAGGCTCGATCTTCTTACTACCTTCTCTTCAGGTCGGCGCCG	0	0	0	0	0	0.0221	0.0052	1.108	0.7844	0	0.0301

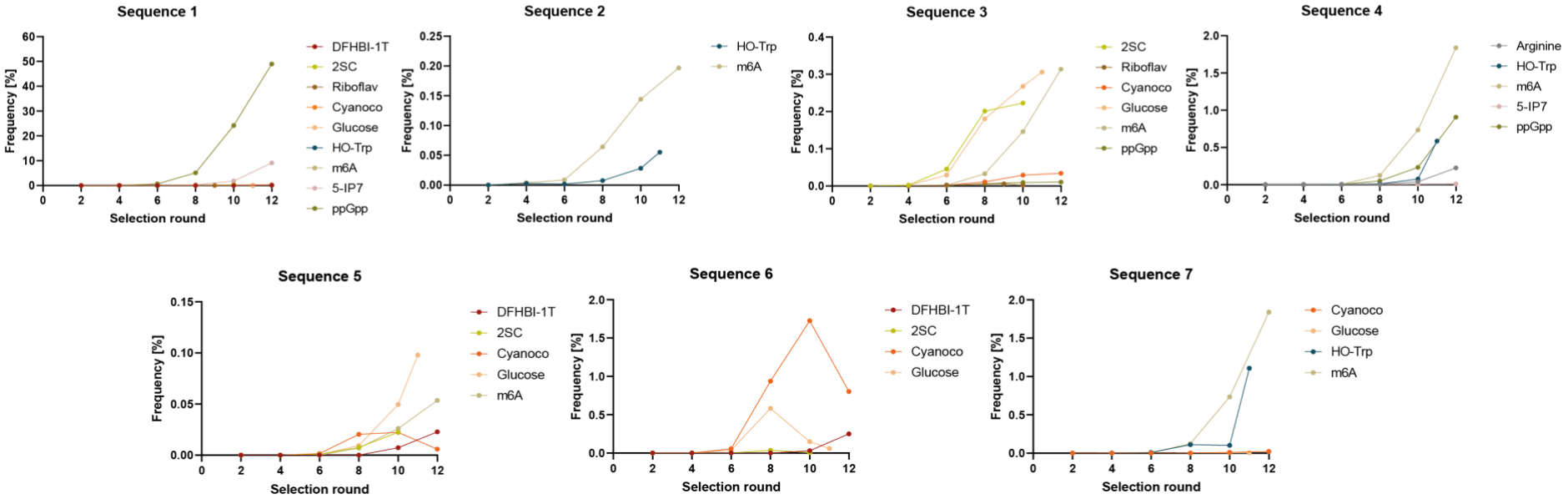

Figure S13. Enrichment of parasitic non-binding sequences in different selections. In the table, seven sequences are listed, which were found among several selections targeting different molecules. The enrichment of each sequence in different selection is shown in the graphs below. DFHBI-1T: 3,5-Difluoro-4-hydroxybenzylidene imidazolinone-1T,[2] Theo: Theophylline, 2SC: S-(2-succinyl) cysteine, Riboflav: Riboflavin, Cyanoco: Cyanocobalamin, HO-Trp: D-Tryptophanyl Adenosine 5'-Monophosphate Phosphoramidate,[3] m6A: N6-Methyladenosine, 5-IP7: 5-diphospho-*myo*-inositol pentakisphosphate,[4] ppGpp: Guanosine pentaphosphate.

Neomycin B			Frequency [%]						
	FAMILY	SEQUENCE	Round 2	Round 4	Round 6	Round 8	Round 10	Round 12	PM
LM1 → **N1**	Neo1	CACTTGAACGTGAGGCTCGATCTTTTTAGCTTTTTTACTGCGGCGTTAACGGT	0.0204	3.4954	12.0294	13.8122	20.7139	23.1198	0
N9	Neo1	CACTTGAACGTGAGGCTCGATCTTTTTAGCTTTTTTTACTGCGGCGTTAACGG	0.0004	0.1079	0.3815	0.4596	0.9392	1.3032	2
N10	Neo1	CACTTGAACGTGAGGCTCGATCTTTTTAGCTTTTTACTGCGGCGTTAACGGTT	0.066	9.7189	20.4801	14.2551	4.0027	1.0151	2
...	Neo1								
N2	Neo2	CCACTACGTTGAGGCTCGATCTTTTGCTTTGTCCATCTAGTGTTGTCTGCGT	0.0001	0.0778	0.4855	1.5797	6.6098	19.6315	0
N3	Neo2	ACCACGCTTGAGGCTCGATCTTTTGCTTTGTCCATCTAGTGTTGTCTGCGT	0.0222	6.9117	16.6203	24.6762	23.6135	13.4118	5
N6	Neo2	CACCACGCTTGAGGCTCGATCTTTTGCTTTGTCCATCTAGTGTTGTCTGCGT	0.0001	0.0595	0.2981	0.661	1.9265	4.1765	3
...	Neo2								

Arginine			Frequency [%]						
ID	FAMILY	SEQUENCE	Round 2	Round 4	Round 6	Round 8	Round 10	Round 12	PM
A1	Arg1	CCACTTCGGATGAGGCTCGATCAACTCCCGTTATAGTCTGGGCAATCGCTGG	0	0	0.0006	0.0155	0.1648	1.4959	0
4 → A2	Arg2	CCACGCTGGTGAGGCTCGATCACGGAGACTTCATTTCCCATTGTTGTGTGGT	0	0	0.0004	0.0044	0.0391	0.2252	0
A3	Arg3	GCCCCACGTCTGAGGCTCGATCTACTTGAGTTCATTCTTCATGCATCCCGCG	0	0	0.0001	0.0003	0.0182	0.1678	0
A4	Arg4	GACCTGCTCGTGAGGCTCGATCCTCCTAATTAGTGCCGTCGGTCGTCCCGCG	0	0	0.0002	0.0031	0.0277	0.1656	0
A5	Arg5	CCATGCCCCGTGAGGCTCGATCACTCCCAGACCTGTAGTTCGCGTCCCGTGC	0	0.0001	0.0013	0.0082	0.0591	0.136	0

Theophylline			Frequency [%]						
ID	FAMILY	SEQUENCE	Round 2	Round 4	Round 6	Round 8	Round 10	Round 11	PM
T1	Theo1	CTATCGCTTGTGAGGCTCGATCTTTATGTGCCCCTCCTTCAGGTTTGGCGTCT	0	0.0002	0.0272	1.1351	7.6954	10.6657	0
T12	Theo1	CTATCGCTTGTGAGGCTCGATCTTTATGTGCCCCTCCTTCAGGTTTGGCGCCT	0	0	0.0001	0.0133	0.121	0.2351	1
T29	Theo1	CTATCGCTTGTGAGGCTCGATCTTTATGTGCCCCTCCTTCAGGCTTGGCGTCT	0	0	0	0.0052	0.0478	0.1018	1
T44	Theo1	CTATCGCTTGTGAGGCTCGATCTTTATGTGCCCCTCCTTCAGGTTTTGGCGTC	0	0	0	0.0069	0.0424	0.0752	2
T72	Theo1	CTATCGCTTGTGAGGCTCGATCTTTATGTGCCCCTCCTCCAGGTTTGGCGTCT	0	0	0.0001	0.0031	0.03	0.0465	1
T85	Theo1	CTATCGCTTGTGAGGCTCGATCTTTATGTGCCCCTCCTTCGGGTTTGGCGTCT	0	0	0.0001	0.0046	0.0322	0.0385	1
T2	Theo2	CAGGGCAATTTGAGGCTCGATCTAGCGCCGTGCCCTCGCTCAGTTGGCGTCG	0	0.0001	0.0093	0.2888	1.0288	1.4868	0
T3	Theo3	GCACCAATCTGAGGCTCGATCGTTTATGTGCCCCGACTCTTTAGGTGGTGG	0	0	0.0059	0.341	1.0824	1.4262	0
T4	Theo4	GTGCAGAATTTGAGGCTCGATCTACAAAACGCCTGCATCCTCTGATCGTGGC	0	0.0001	0.004	0.1284	0.3827	0.672	0
T5	Theo5	GAGTGATATATGAGGCTCGATCATTTACCATACCCTGCTCTGTCTTAGGTGG	0	0.0001	0.0039	0.1131	0.3723	0.6314	0

DFHBI-1T			Frequency [%]						
ID	FAMILY	SEQUENCE	Round 2	Round 4	Round 6	Round 8	Round 10	Round 12	PM
6 → D1	DFHBI1	ATCTATCCGATGAGGCTCGATCCAGTGCTTTTGCTCTCTAGAGTCATTCACGT	0	0	0.0002	0.0009	0.0307	0.2513	0
1 → D2	DFHBI2	GGAACGGTAATGAGGCTCGATCGAATTAGACCGCCTTGATTCCCTCGTGGCG	0	0	0.0006	0.0033	0.0243	0.0869	0
D3	DFHBI3	GAAGACCCCTGAGGCTCGATCCATCAAACAGATTCTTCATGATGTCGATGCT	0	0	0	0.0006	0.0122	0.0804	0
D4	DFHBI4	GGCGCACCCCTGAGGCTCGATCTTGGTTGAAATATGCGCTGCGATGGTCGTC	0	0	0	0.0004	0.008	0.0578	0
D5	DFHBI5	GCCAACCCCTTGAGGCTCGATCTAGTGTGAGAAACTGGCTTGATGTCTACCCT	0	0	0	0.0006	0.0035	0.0254	0

	HO-Trp-A			Frequency [%]						
	ID	FAMILY	SEQUENCE	Round 2	Round 4	Round 6	Round 8	Round 10	Round 11	PM
7 →	**H1**	HO1	CCGGTATCTATGAGGCTCGATCTTCTTACTACCTTCTCTTCAGGTCGGCGCCT	0.0001	0.0017	0.0091	0.0111	0.1033	1.108	0
4 →	**H2**	HO2	CCACGCTGGTGAGGCTCGATCACGGAGACTTCATTTCCCATTGTTGTGTGGT	0	0.0014	0.0018	0.0103	0.0755	0.586	0
	H3	HO3	CCCAACCTATTGAGGCTCGATCCGCTGTTCTTTGGGTGGCTGTCTCTCCGCCT	0	0	0	0.0017	0.0126	0.0774	0
	H4	HO4	CCACGAATCTTGAGGCTCGATCAGATCTCCCTCGATCTATTCTGTGTGGCGTT	0	0	0	0.0009	0.0098	0.0742	0
	H5	HO5	GCAGCTCTACTGAGGCTCGATCTTTATCTTGCTATGCATTTCTAGCCCCTCCT	0	0	0.0018	0.0009	0.0171	0.0615	0

	m6A			Frequency [%]						
		FAMILY	SEQUENCE	Round 2	Round 4	Round 6	Round 8	Round 10	Round 12	PM
4 →	**m1**	m6A1	CCACGCTGGTGAGGCTCGATCACGGAGACTTCATTTCCCATTGTTGTGTGGT	0	0.0009	0.0058	0.1245	0.7344	1.8388	0
	m3	m6A1	CCACGCTGGTGAGGCTCGATCACGGAGACTTCATCTCCCATTGTTGTGTGGT	0	0.0001	0.0005	0.0386	0.2769	0.7538	1
	m17	m6A1	CCACGCTGGTGAGGCTCGATCATGGAGACTTCATTTCCCATTGTTGTGTGGT	0	0	0	0.0036	0.0173	0.0473	1
7 →	**m2**	m6A2	CCGGTATCTATGAGGCTCGATCTTCTTACTACCTTCTCTTCAGGTCGGCGCCT	0	0	0.0014	0.0305	0.3374	0.7844	0
1 →	**m4**	m6A4	GGAACGGTAATGAGGCTCGATCGAATTAGACCGCCTTGATTCCCTCGTGGCG	0	0.0009	0.0033	0.0578	0.1686	0.3329	0
	m79	m6A4	GGAACGGTAATGAGGCTCGATCGAATTAGACCGCCTTGGTTCCCTCGTGGCG	0	0	0	0.0039	0.0083	0.0128	1
3 →	**m5**	m6A5	GGGATGTCGTGAGGCTCGATCAATGTATTTTGCTCCCTGCTCGGTGGTTCCT	0	0	0.0019	0.0328	0.1462	0.3138	0

	Glucose			Frequency [%]						
		FAMILY	SEQUENCE	Round 2	Round 4	Round 6	Round 8	Round 10	Round 11	PM
	G1	Glu1	CCACGCTGGTGAGGCTCGATCACGGAGACTTCATTTCCCATTGTTGTGTGGT	0	0.0001	0.0033	0.0508	0.2121	0.409	0
	G9	Glu1	CCACGCTGGTGAGGCTCGATCACGGAGACTTCATTTCCCATTGTTTGTGTGG	0	0	0.0002	0.0035	0.0153	0.0304	2
	G2	Glu2	CCACTTCGGATGAGGCTCGATCAACTCCCGTTATAGTCTGGGCAATCGCTGG	0	0.0005	0.0205	0.1449	0.2636	0.3108	0
	G58	Glu2	CCACTTCGGATGAGGCTCGATCAACTCCCATTATAGTCTGGGCAATCGCTGG	0	0	0.0004	0.003	0.0057	0.0075	1
	G87	Glu2	CCACTTCGGATGAGGCTCGATCAACTCCCGTTATAGTCTTGGCAATCGCTGG	0	0	0.0003	0.0013	0.0031	0.0038	1
3 →	**G3**	Glu3	GGGATGTCGTGAGGCTCGATCAATGTATTTTGCTCCCTGCTCGGTGGTTCCTT	0	0.0018	0.0291	0.1805	0.2679	0.3061	0
	G78	Glu3	GGGATGTCGTGAGGCTCGATCAATGTATTTTGCTCCTGCTCGGTGGTTCCTT	0	0	0.0005	0.0029	0.0047	0.0057	2
	G85	Glu3	GGATGTCGTGAGGCTCGATCAATGTATTTTGCTCCCTGCTCGGTGGTTCCTT	0	0	0.0003	0.0016	0.0031	0.0041	2
	G90	Glu3	GGGATGTCGTGAGGCTCGGTCAATGTATTTTGCTCCCTGCTCGGTGGTTCCT	0	0	0.0002	0.0014	0.002	0.0028	1
	G4	Glu4	ACACCTGAATTGAGGCTCGATCTTATTAACACCTCATCAGGAACAACACCCG	0	0	0.0002	0.0014	0.0429	0.203	0
	G5	Glu5	GCTATCTAGTTGAGGCTCGATCAGTGTACCATACTTTCTTCTCCCACCGGCA	0	0.0001	0.0007	0.0095	0.0496	0.0979	0
	G13	Glu5	GCTATCTAGTTGAGGCTCGATCAGTTTACCATACTTTCTTCTCCCACCGGCA	0	0	0.0002	0.0014	0.0097	0.0232	1
6 →	**G6**	Glu6	ATCTATCCGATGAGGCTCGATCCAGTGCTTTTGCTCTCTAGAGTCATTCACGT	0	0.0013	0.0368	0.5822	0.149	0.0586	0
	S18	Glu6	ATCTATCCGATGAGGCTCGATCCAGTGCCTTTGCTCTCTAGAGTCATTCACGT	0	0	0.0003	0.0042	0.0145	0.0192	1
	S96	Glu6	GTCTATCCGATGAGGCTCGATCCAGTGCTTTTGCTCTCTAGAGTCATTCACGT	0	0.0001	0.0004	0.0093	0.0019	0.0009	1
	S98	Glu6	CTATCCGATGAGGCTCGATCCAGTGCTTTTGCTCTCTAGAGTCATTCACGT	0	0	0.0004	0.0062	0.0019	0.0007	4
	S99	Glu6	ATCTATCCGATGAGGCTCGATCCAGTGCTTTGCTCTCTAGAGTCATTCACGT	0	0	0.0004	0.0063	0.0016	0.0006	2
	S100	Glu6	ATCTATCTGATGAGGCTCGATCCAGTGCTTTTGCTCTCTAGAGTCATTCACGT	0	0	0.0002	0.0029	0.0009	0.0005	1

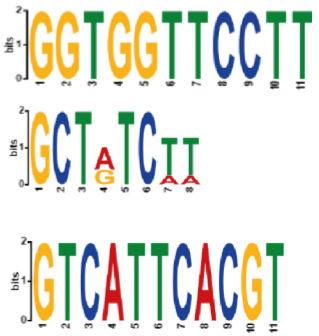

	5-IP7			Frequency [%]						
		FAMILY	SEQUENCE	Round 2	Round 4	Round 6	Round 8	Round 10	Round 12	PM
1 →	I1	IP1	GGAACGGTAATGAGGCTCGATCGAATTAGACCGCCTTGATTCCCTCGTGGCGT	0.0021	0.0043	0.0547	0.297	1.8403	9.1016	0
	I9	IP1	GGAACGGTAATGAGGCTCGATCGAATTAGACCGCCTTGATTCCCTCGTGGCGG	0	0	0.0002	0.0042	0.0265	0.0791	1
	I14	IP1	GGAACGGTAATGAGGCTCGATCGAATTAGACCGCCTTGATCCCCTCGTGGCGT	0	0	0.0002	0.0008	0.0064	0.0456	1
	I18	IP1	GGAACGGTAATGAGGCTCGATCGAATTAGACCGCCTTGATTCCCTCATGGCGT	0	0	0.0006	0.0013	0.0123	0.0417	1
	I19	IP1	GGAACGGTAATGAGGCTCGATCGAATTAGACCGCCTTGATTCCCTCGCGGCGT	0	0	0.0003	0.0006	0.0079	0.0413	1
	I24	IP1	GGAACGGTAATGAGGCTCGATCGAATTAGACCGCCTTGACTCCCTCGTGGCGT	0	0	0.0001	0.0013	0.0055	0.0348	1
	...	IP1								
	I67	IP1	GGAACGGTAATGAGGCTCGATCGATTTAGACCGCCTTGATTCCCTCGTGGCGT	0	0.0001	0.0001	0.0008	0.007	0.0153	1
	I2	IP2	CACGAGTTAATGAGGCTCGATCCAGCATGTCCTCTTCATCGTTTGTGGTGTG	0	0	0.0017	0.0228	0.0732	0.1864	0
	I3	IP3	CTATCAGGTCTGAGGCTCGATCCCTTGGCAGGTGTTCACATCCGGTTCTTGG	0	0	0.0001	0.0055	0.0302	0.125	0
	I4	IP4	CTATCAGGTCTGAGGCTCGATCCGTCAATTGGTCGTGTGCGAGTGTCTACGG	0	0	0.0001	0.001	0.0195	0.1234	0
	I5	IP5	ACGAACGGCATGAGGCTCGATCTACGTTACCCCTCTGACGTTGGCATTTGTG	0	0	0.0006	0.0058	0.0385	0.1052	0
	I6	IP6	CAGGGCAATTTGAGGCTCGATCTAGCGCCGTGCCCTCGCTCAGTTGGCGTCGT	0.0001	0.0009	0.0115	0.0053	0.0767	0.1016	0

	ppGpp			Frequency [%]						
		FAMILY	SEQUENCE	Round 2	Round 4	Round 6	Round 8	Round 10	Round 12	PM
1 →	P1	ppGpp1	GGAACGGTAATGAGGCTCGATCGAATTAGACCGCCTTGATTCCCTCGTGGCGT	0.0016	0.036	0.6512	5.1331	24.1979	48.9888	0
	P3	ppGpp1	GGAACGGTAATGAGGCTCGATCGAATTAGACCGCCTTGATTCCCTCGTGGCGG	0.0001	0.0002	0.0091	0.1095	0.1173	0.7745	1
	P6	ppGpp1	GGAACGGTAATGAGGCTCGATCGAATTAGACCGCCTTGATTCCCTCATGGCGT	0	0.0012	0.0046	0.0135	0.1301	0.301	1
	P12	ppGpp1	GGAACGGTAATGAGGCTCGATCGAATTAGACCGCCTTGATCCCCTCGTGGCGT	0	0	0.0016	0.0175	0.0885	0.2069	1
	P13	ppGpp1	GGAACGGTAATGAGGCTCGATCGAATTAGACCGCCTTGATTCCCTCGTGGTGT	0	0	0.0038	0.0232	0.0867	0.1791	1
	P14	ppGpp1	GGAACGGTAATGAGGCTCGATCGAATTAGACCGCCTTGACTCCCTCGTGGCGT	0	0	0.0006	0.0129	0.08	0.173	1
	...	ppGpp1								
	P96	ppGpp1	GGAACGGTAATGAGGCTCGATCGAATTAGACCGCCTTGATTCCCTCGTGTCGT	0	0	0.0008	0.002	0.0114	0.0178	1
4 →	P2	ppGpp2	CCACGCTGGTGAGGCTCGATCACGGAGACTTCATTTCCCATTGTTGTGTGGT	0	0.0002	0.004	0.0514	0.2318	0.907	0
	P8	ppGpp2	CCACGCTGGTGAGGCTCGATCACGGAGACTTCATCTCCCATTGTTGTGTGGT	0	0	0.0008	0.0115	0.0612	0.2281	1
	P4	ppGpp4	CAGGGCAATTTGAGGCTCGATCTAGCGCCGTGCCCTCGCTCAGTTGGCGTCGT	0.0003	0.0016	0.1984	0.8165	2.1538	0.6938	0
	P101	ppGpp4	CAGGGCAATTTGAGGCTCGATCTAGCGCCGTGCCCTCACTCAGTTGGCGTCGT	0	0	0.0014	0.0058	0.0131	0.0083	1
	P5	ppGpp5	CACGAACCAATGAGGCTCGATCATGGATCCTTCGTCGAACCTGCTGGCGTTG	0	0	0.0022	0.028	0.1791	0.4992	0
	P7	ppGpp7	CAGGAACGGTTGAGGCTCGATCAGATACCCCTCGCTACAATGCGGCATTGGG	0	0	0.002	0.0171	0.0861	0.2846	0
	P9	ppGpp9	CATCCACACATGAGGCTCGATCCATTATCATGGCCTGACTCGTAGTCCTGCG	0	0	0.001	0.0059	0.0496	0.2084	0
	P18	ppGpp18	CTATCAGGTCTGAGGCTCGATCTTCAGTGTGGTAACGCATCCGTTTGTGCGG	0	0	0.0004	0.0095	0.0169	0.1168	0

Riboflavin			Frequency [%]					
ID	FAMILY	SEQUENCE	Round 2	Round 4	Round 6	Round 9	Round 10	PM
R1	Rib1	GTTAGGCTATTGAGGCTCGATCGAAGAAGGAACACACATCTGTCGCTCTGCT	0	0.0005	0	0.2798	5.3896	0
R2	Rib2	GAGGTACGTATGAGGCTCGATCGGAAGGCTGGTCTAGGTCCCGTCCTGACCG	0.0001	0.0001	0	0.0227	5.2139	0
R3	Rib3	GTCGGAGGTATGAGGCTCGATCACGAAGAAGGCCGATTGGGTTACCCTCCTT	0	0.0002	0	0.1351	2.9985	0
R4	Rib4	AGGCGGAAGATGAGGCTCGATCAAGGTAGGCGGTAGAATCTGTCTTCTCGAT	0	0.0001	0	0.0091	1.6036	0
R5	Rib5	GACTTAGCGTGAGGCTCGATCGAAACGGCTATCATTGAGATACTTGCCCCGT	0	0.0004	0	0.1202	1.3797	0

S-(2-succinyl) cysteine			Frequency [%]					
ID	FAMILY	SEQUENCE	Round 2	Round 4	Round 6	Round 8	Round 10	PM
S1	SC1	GGAACGGTAATGAGGCTCGATCGAATTAGACCGCCTTGATTCCCTCGTGGCG	0	0.0003	0.0191	0.1124	0.2749	0
S31	SC1	GGAACGGTAATGAGGCTCGATCGAATTAGACCGCCTTGATTCCCTCGTGGTG	0	0	0.0007	0.0044	0.0083	1
S47	SC1	GGAACGGTAATGAGGCTCGATCGAATTAGACCGCTTTGATTCCCTCGTGGCG	0	0	0.0007	0.0031	0.0066	1
S2	SC2	GGGATGTCGTGAGGCTCGATCAATGTATTTTGCTCCCTGCTCGGTGGTTCC	0	0.0022	0.0456	0.2013	0.2227	0
S72	SC2	AGGATGTCGTGAGGCTCGATCAATGTATTTTGCTCCCTGCTCGGTGGTTCC	0	0	0.0008	0.0034	0.0045	1
S78	SC2	GGGATGTCGTGAGGCTCGATCAATGTATTTTTGCTCCCTGCTCGGTGGTTC	0	0	0.0004	0.0024	0.0036	4
S3	SC3	CCCAACCTATTGAGGCTCGATCCGCTGTTCTTTGGGTGGCTGTCTCTCCGC	0	0.0006	0.0108	0.0724	0.1515	0
S4	SC4	CTATCGCTTGTGAGGCTCGATCTTTATGTGCCCCTCCTTCAGGTTTGGCGT	0	0.0018	0.0218	0.0138	0.0899	0
S75	SC4	CTATCGCTTGTGAGGCTCGATCTTTATGTGCCCCTCCTTCAGGTTTGGCGC	0	0.0001	0.001	0.0019	0.0041	1
S77	SC4	CTATCGCTTGTGAGGCTCGATCTTTATGTGCCCCTCCTTCAGGCTTGGCGT	0	0.0001	0.0008	0.001	0.0036	1
S5	SC5	GTCCGGCCTCTGAGGCTCGATCTTTCTGGCCTGGCTTAGATACGTGCGCTC	0	0	0.0014	0.0167	0.0787	0

Cyanocobalamin			Frequency [%]						
ID	FAMILY	SEQUENCE	Round 2	Round 4	Round 6	Round 8	Round 10	Round 12	PM
C1	Cob1	CCACGCTGGTGAGGCTCGATCACGGAGACTTCATTTCCCATTGTTGTGTGG	0.0001	0.0001	0.0024	0.041	0.2723	1.0699	0
C2	Cob2	GGAGGCTCGATCTTTTAAGTGATTTTATCTCTAGGTCCGCGGTTTCGTGGAT	0.0003	0.0005	0.0025	0.0212	0.1781	0.926	0
C20	Cob2	GGAGGCTCGATCTTTTAAGTGGTTTTATCTCTAGGTCCGCGGTTTCGTGGAT	0	0	0	0.0011	0.0118	0.0617	1
C3	Cob3	ATCTATCCGATGAGGCTCGATCCAGTGCTTTTGCTCTCTAGAGTCATTCACGT	0.0005	0.0007	0.0554	0.9378	1.7265	0.8026	0
C19	Cob3	ATCTATTCGATGAGGCTCGATCCAGTGCTTTTGCTCTCTAGAGTCATTCACGT	0.0001	0.0001	0.0058	0.07	0.1223	0.0639	1
C35	Cob3	ATCTATCCGATGAGGCTCGATCCAGTGCCTTTGCTCTCTAGAGTCATTCACGT	0	0	0.0004	0.0051	0.0297	0.0469	1
C84	Cob3	ATCTATCCGATGAGGCTCGATCCGGTGCTTTTGCTCTCTAGAGTCATTCACGT	0	0	0	0.0036	0.0144	0.0176	1
C99	Cob3	ATCTATCCGATGAGGCTCGATCCAGCGCTTTTGCTCTCTAGAGTCATTCACGT	0	0	0.0016	0.0204	0.0223	0.0059	1
S100	Cob3	GTCTATCCGATGAGGCTCGATCCAGTGCTTTTGCTCTCTAGAGTCATTCACGT	0	0	0	0.0034	0.0089	0.0052	1
C4	Cob4	GGAACGGTAATGAGGCTCGATCGAATTAGACCGCCTTGATTCCCTCGTGGCG	0	0.0002	0.0068	0.0432	0.2214	0.2666	0

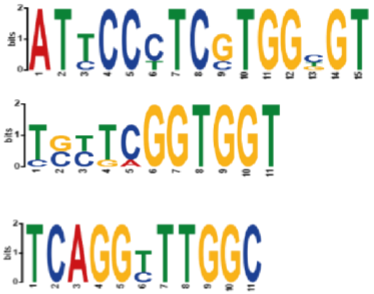

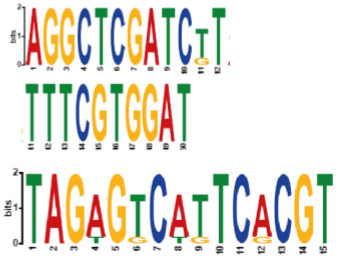

Figure S14. NGS analysis of selections targeting different small molecules. First, 100 the most enriched sequences were sorted in different families with no more than 5-point mutations (PM). Here, only up to first six families are shown or in the case of ppGpp target up to 18 families. Next, different motifs were searched using MEME suite tool for motif discovery.[1] Through different selections, common sequences were found highlighted with the same colour. The common sequences shown in **Supp. Fig. 13** are marked with an arrow and corresponding number. With the bold,

sequences are depicted, which were tested for binding to corresponding target. DFHBI-1T: 3,5-Difluoro-4-hydroxybenzylidene imidazolinone-1T,[2] HO-Trp-A: D-Tryptophanyl Adenosine 5'-Monophosphate Phosphoramidate,[3] m6A: N6-Methyladenosine, 5-IP7: 5-diphospho-*myo*-inositol pentakisphosphate,[4] ppGpp: Guanosine pentaphosphate.

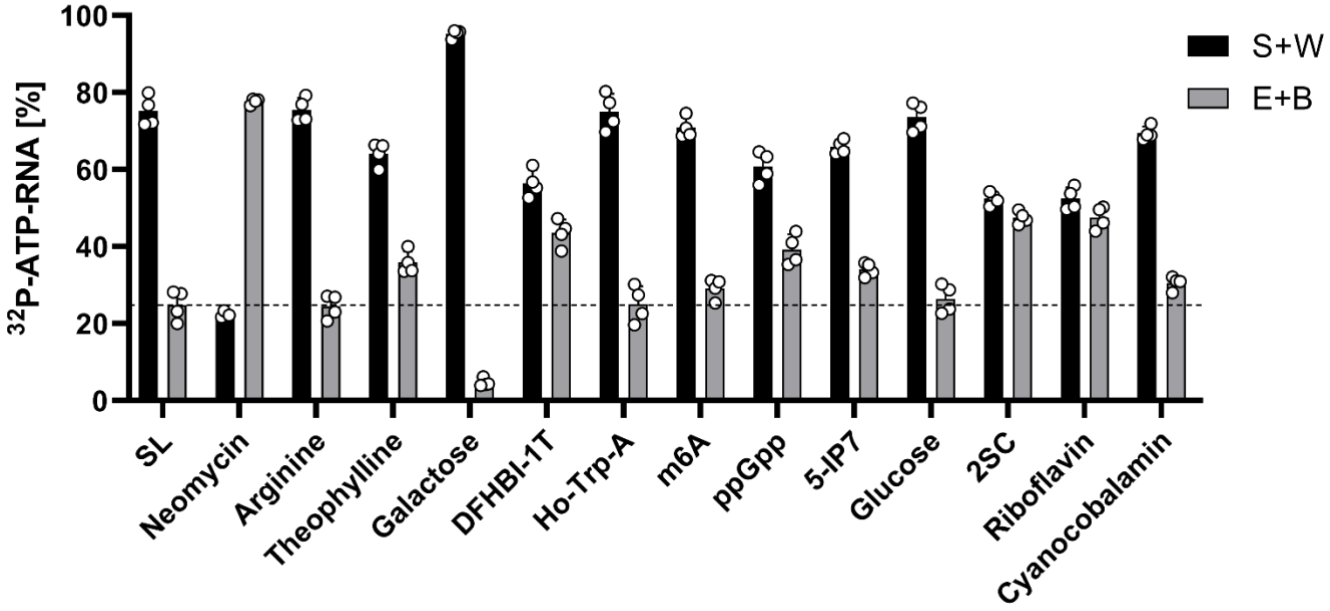

Figure S15. Annealing efficiency of the starting library (SL) and enriched pools selected for different small molecule targets. Annealing efficiency of some enriched pools increases (e.g. neomycin B, theophylline, DFHBI-1T, ppGpp, 2SC, riboflavin), while for mostly failed selections it decreases (e.g. galactose). Error bars show standard deviation (n=2). S+W: Sum of supernatant and three washing fractions, E+B: Sum of elution and beads fraction. DFHBI-1T: 3,5-Difluoro-4-hydroxybenzylidene imidazolinone-1T,[2] HO-Trp-A: D-Tryptophanyl Adenosine 5'-Monophosphate Phosphoramidate,[3] m6A: N6-Methyladenosine, 5-IP7: 5-diphospho-*myo*-inositol pentakisphosphate,[4] ppGpp: Guanosine pentaphosphate, 2SC: S-(2-succinyl) cysteine.

Table S2. List of utilized sequences

Sequence	‘5-‘3
C2 library	GGGAGAGGAGGGAGAUAGAUAUCAA-N40-UUUCGUGGAUGCCACAGGAC
UFZ library	GGGAGAGGAGGGAGAUAGAUAUCAA-N10-UGAGGCUCGAUC-N30-UUUCGUGGAUGCCACAGGAC
Forward primer	AATTCTAATACGACTCACTATAGGGAGAGGAGGGAGATAGATATCAA
Reverse primer	GTCCTGTGGCATCCACGAAA
Bio-ODN	Biotin-18spacer-GATCGAGCCTCA
Cy3-ODN_12nt	Cy3-GATCGAGCCTCA
Cy3-ODN_11nt	Cy3-GATCGAGCCTC
Cy3-ODN_10nt	Cy3-GATCGAGCCT
Cy3-ODN_9nt	Cy3-GATCGAGCC
Cy3-ODN_8nt	Cy3-GATCGAGC
Cy3-ODN_PM	Cy3-GATCGCGCCTCA
Forward NGS primer	6nt index-AGGGAGATAGATATCAA
Reverse NGS primer	6nt index-TGGCATCCACGAAA
HDB1	GGGAGAGGAGGGAGATAGATATCAAACCCCATCTTGAGGCTCGATCGGCTCGTTTTTCAGGGATAAGTAGATTTAGTTTTTCGTGGATGCCACAGGAC
HDB2	GGGAGAGGAGGGAGATAGATATCAAACCGGCACCTGAGGCTCGATCTTTGTTTGCAAAGGGCATTGCATCGATGTGTTTTTCGTGGATGCCACAGGAC
LM1	GGGAGAGGAGGGAGATAGATATCAACACTTGAACGTGAGGCTCGATCTTTTTAGCTTTTTACTGCGGCGTTAACGGTTTTCGTGGATGCCACAGGAC
LM2	GGGAGAGGAGGGAGATAGATATCAAACTAACAGTCTGAGGCTCGATCTTTTGCAGAAACTTTCGTCTTTTGGCTATCTTTCGTGGATGCCACAGGAC
LR1	GGGAGAGGAGGGAGATAGATATCAAACTAAACACTTGAGGCTCGATCTTTATTGTATTTACACCATCTTGTGCATCATTTCGTGGATGCCACAGGAC
LR2	GGGAGAGGAGGGAGATAGATATCAATTACCACGCTTGAGGCTCGATCTTTTGCTTTGTCCATCTAGTGTTGTCTGCGTTTCGTGGATGCCACAGGAC
T1	GGGAGAGGAGGGAGATAGATATCAACTATCGCTTGTGAGGCTCGATCTTTATGTGCCCCTCCTTCAGGTTTGGCGTCTTTCGTGGATGCCACAGGAC
T2	GGGAGAGGAGGGAGATAGATATCAACAGGGCAATTTGAGGCTCGATCTAGCGCCGTGCCCTCGCTCAGTTGGCGTCGTTTCGTGGATGCCACAGGAC
A1	GGGAGAGGAGGGAGATAGATATCAACCACTTCGGATGAGGCTCGATCAACTCCCGTTATAGTCTGGGCAATCGCTGGTTTCGTGGATGCCACAGGAC
I5	GGGAGAGGAGGGAGATAGATATCAAACGAACGGCATGAGGCTCGATCTACGTTACCCCTCTGACGTTGGCATTTGTGTTTCGTGGATGCCACAGGAC
P7	GGGAGAGGAGGGAGATAGATATCAACAGGAACGGTTGAGGCTCGATCAGATACCCCTCGCTACAATGCGGCATTGGGTTTCGTGGATGCCACAGGAC
G1	GGGAGAGGAGGGAGATAGATATCAACCACGCTGGTGAGGCTCGATCACGGAGACTTCATTTCCCATTGTTGTGTGGTTTTCGTGGATGCCACAGGAC
S1	GGGAGAGGAGGGAGATAGATATCAAGGAACGGTAATGAGGCTCGATCGAATTAGACCGCCTTGATTCCCTCGTGGCGTTTCGTGGATGCCACAGGAC
R1	GGGAGAGGAGGGAGATAGATATCAAGTTAGGCTATTGAGGCTCGATCGAAGAAGGAACACACATCTGTCGCTCTGCTTTTCGTGGATGCCACAGGAC
R2	GGGAGAGGAGGGAGATAGATATCAAGAGGTACGTATGAGGCTCGATCGGAAGGCTGGTCTAGGTCCCGTCCTGACCGTTTCGTGGATGCCACAGGAC
R3	GGGAGAGGAGGGAGATAGATATCAAGTCGGAGGTATGAGGCTCGATCACGAAGAAGGCCGATTGGGTTACCCTCCTTTTTCGTGGATGCCACAGGAC
C1	GGGAGAGGAGGGAGATAGATATCAACCACGCTGGTGAGGCTCGATCACGGAGACTTCATTTCCCATTGTTGTGTGGTTTTCGTGGATGCCACAGGAC

Reference

[1] T. L. Bailey, J. Johnson, C. E. Grant, W. S. Noble. "The MEME suite" *Nucleic acids research* **2015**, *43*, W39-W49.

[2] G. S. Filonov, J. D. Moon, N. Svensen, S. R. Jaffrey. "Broccoli: rapid selection of an RNA mimic of green fluorescent protein by fluorescence-based selection and directed evolution" *J Am Chem Soc* **2014**, *136*, 16299-16308.

[3] O. Doppleb, J. Bremer, M. Bechthold, C. Sánchez Rico, D. Göhringer, H. Griesser, C. Richert. "Determining the Diastereoselectivity of the Formation of Dipeptidonucleotides by NMR Spectroscopy" *Chemistry–A European Journal* **2021**, *27*, 13544-13551.

[4] I. Pavlovic, D. T. Thakor, J. R. Vargas, C. J. McKinlay, S. Hauke, P. Anstaett, R. C. Camuña, L. Bigler, G. Gasser, C. Schultz. "Cellular delivery and photochemical release of a caged inositol-pyrophosphate induces PH-domain translocation in cellulo" *Nature communications* **2016**, *7*, 10622.

APPENDIX B

Modular Approach for Rapid Identification of RNA-Based Sensors

Tjasa Legen[1,2] and Günter Mayer[1,2]

Received: September 29, 2023
Published online: January 22, 2024

DOI: https://doi.org/10.1021/acssensors.3c02060

Own contributions

- Design and planning of experiments
- Execution of experiments
- Evaluation of experimental results
- Drafting of the manuscript

[1] Life and Medical Sciences Institute (LIMES), University of Bonn, 53121, Germany
[2] Center of Aptamer Research and Development (CARD), University of Bonn, 53121, Germany

ACS SENSORS

pubs.acs.org/acssensors

Article

Modular Approach for Rapid Identification of RNA-Based Sensors

Tjasa Legen and Günter Mayer*

Cite This: *ACS Sens.* 2024, 9, 753−758

Read Online

ACCESS | Metrics & More | Article Recommendations | Supporting Information

ABSTRACT: Detection of metabolites in real time and in whole cells requires effective molecular sensors. In this regard, fluorogenic light-up RNAs have recently become important tools for small-molecule detection in cells. However, the construction of light-up RNA sensors is an arduous task that requires structural knowledge of both the sensor and reporter RNA. De novo strategies for selecting sensors from RNA libraries are limited and are mostly restricted to known aptamers and riboswitches. Here, we provide a solution to this problem by developing a capture-SELEX variant that allows the obtained libraries and aptamers to be linked to fluorogenic RNAs in a modular and allosteric manner. The approach is generally applicable and allows for rapid modular allosteric assembly with green- or red-shifted fluorogenic RNAs.

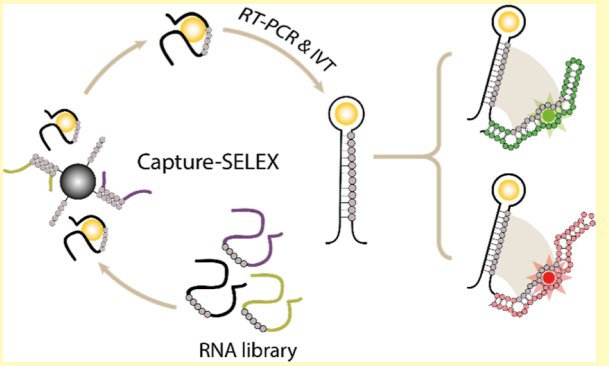

KEYWORDS: *fluorogenic RNA sensor, capture-SELEX, light-up RNA aptamers, thiamine pyrophosphate, broccoli aptamer*

Capture-SELEX is a selection variant in which the RNA library used is immobilized via an embedded docking sequence that hybridizes to a capture oligodeoxynucleotide (ODN) (Figure 1A).[1] The binding sequences are then isolated by addition of the target molecule in solution, resulting in a conformational change of the RNA and thus a reduced ability of the docking sequence to bind to the capture-ODN.[2] We took advantage of these properties and designed RNA libraries with docking sequences complementary to the fluorogenic RNA Broccoli (Figure 1A).[3] We designed five different libraries (SE4−SE12) with 4−12 nt complementary regions to Broccoli while retaining a 12 nt docking sequence to allow capture-SELEX (Supporting Information Figure S1). We tested the intrinsic sensing ability of these libraries by adding the corresponding capture-ODNs in solution (Supporting Information Figure S2A). All libraries exhibited low intrinsic fluorescence, and the addition of the capture-ODN resulted in turn-on values of up to 1.4, with the SE8 library being the most sensitive (Supporting Information Figure S2A). The libraries with a 4 or 6 nt complementary region did not respond to the capture-ODN (Supporting Information Figure S2A). Next, we included four linker regions in the design (L1−L4) that were previously shown to increase sensor signaling (Supporting Information Figure S2B).[4] Libraries with linkers L3−4 showed a strong increase in Broccoli fluorescence in the presence of the capture-ODN (Supporting Information Figure S2C−E), whereas a control library without complementarity to Broccoli did not respond to the addition of the capture-ODN (Supporting Information Figure S2E). As shown in Supporting Information Figure S2C−E, linker 3 provided the highest turn-on values by ensuring optimal stability of the incorporated Broccoli aptamer in the case of all tested libraries and was therefore used for subsequent incorporation to selected aptamers. Based on these data, we selected the library SE8 for capture-SELEX (Figure 1A, Supporting Information Figure S3) and identified RNA aptamers that bind to the metabolite thiamine pyrophosphate (TPP). TPP was chosen because it has been used previously to generate sensors based on natural TPP-binding riboswitches.[4,5] The selection was performed with the SE8 library, excluding the Broccoli sequence. We chose this approach because capture-SELEX might be limited in the presence of the Broccoli domain. The inclusion of Broccoli can restrict the hybridization of the docking sequence of the RNA library to the capture-ODN and, thus, could interfere with the capture step in the absence of a target molecule. Similarly, the replacement of Broccoli with other fluorogenic RNAs, e.g., Red Broccoli, could be less modular than when performing SELEX in the absence of the fluorogenic RNA domain. We started the selection with a TPP concentration of 1 mM as higher concentrations have been shown to interfere with Broccoli function (Supporting Information Figure S3A,B). The enrichment of TPP-binding RNA aptamers was confirmed by fluorescence polarization measurements using a Cy3-labeled capture-ODN (Figure 1B, Supporting Information Figure S4). Of note, the capture-ODN used in this binding assay has only 8 nt complementary to Broccoli as the 12 nt complementary ODN does not allow a

Received: September 29, 2023
Revised: December 19, 2023
Accepted: January 10, 2024
Published: January 22, 2024

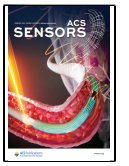

https://doi.org/10.1021/acssensors.3c02060
ACS Sens. 2024, 9, 753−758

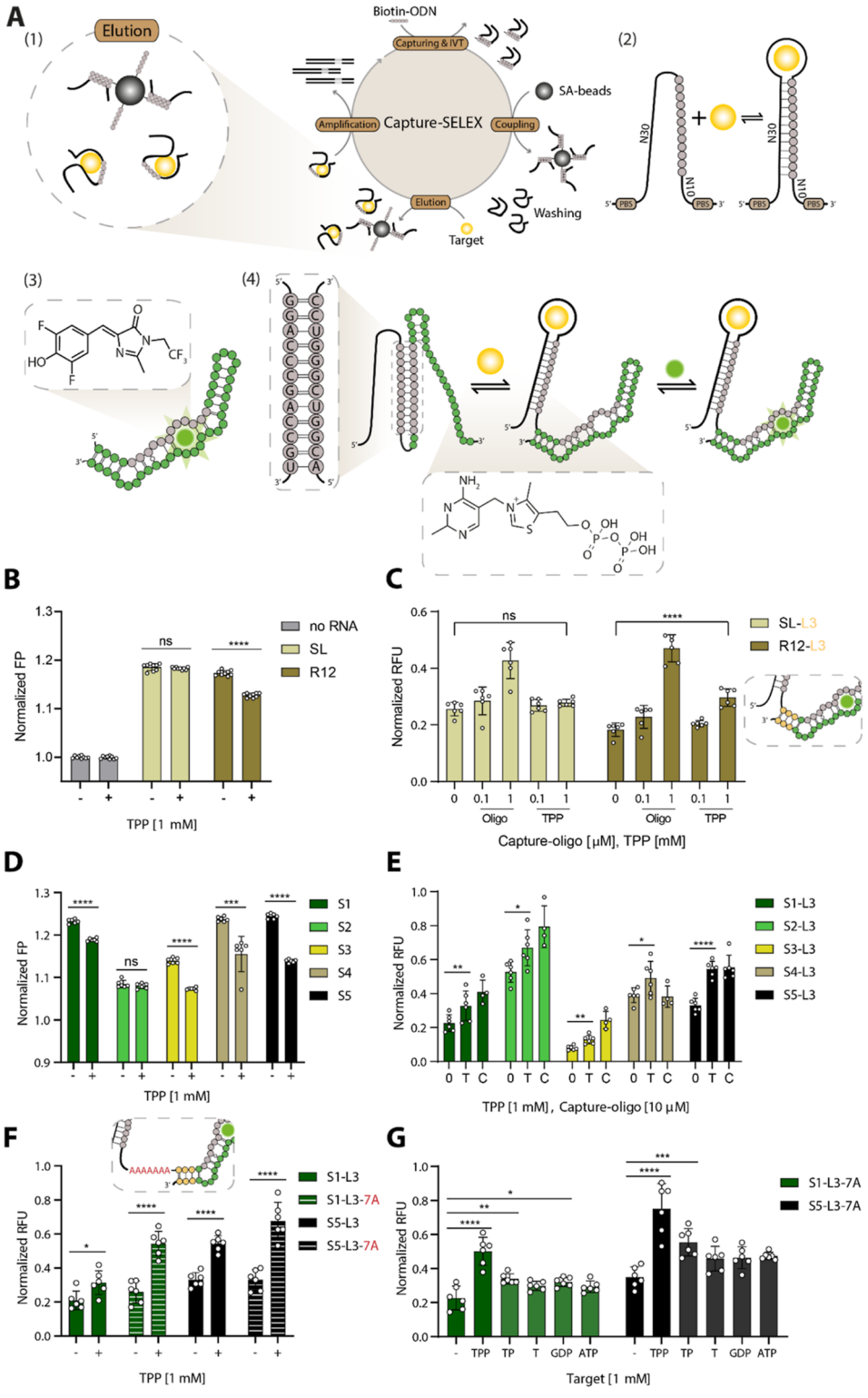

Figure 1. De novo selection of light-up RNA sensors. (A) Schematic of the selection design based on (1) Capture-SELEX, which allows for the selection of ligands free in solution by immobilization of the library through a complementary capture-ODN to the matrix. In our selection, the RNA library was hybridized to a biotinylated capture-ODN (biotin-ODN), and the complex was captured on streptavidin-coated magnetic beads (SA-beads). Subsequently, noncaptured sequences were removed, and bound sequences were recovered from the beads by the addition of the target molecule. The revered sequences were reverse transcribed, amplified, and in vitro transcribed (IVT) in the presence of capture-ODN for the next selection cycle. (2) RNA library consists of two primer-binding sites (PBS) and a random region of 40 nucleotides (N30 + N10). The random region is divided by a docking sequence highlighted in gray, which is a defined part in the library used for the hybridization to the biotinylated ODN. (3) DFHBI-1T molecule, shown in a dotted square, binds to the Broccoli aptamer and thereby emits green fluorescence. The region in the Broccoli aptamer highlighted in gray was used as a module, complementary to the docking sequence in the RNA library. (4) This module allows the docking sequence of the library or an identified aptamer from the library to hybridize to Broccoli in the absence of the target molecule. Upon addition of the target, a conformational change in the aptamer is induced, thereby enabling the folding and binding of Broccoli to DFHBI-1T, which results in an

https://doi.org/10.1021/acssensors.3c02060
ACS Sens. 2024, 9, 753−758

Figure 1. continued

increased fluorescence signal. TPP was utilized as a target in a proof-of-principle selection, and its structure is shown in a dotted square. (B) Fluorescence polarization assays to measure the binding of the starting library and the RNA library from selection cycle 12 to TPP. Binding was measured by using 100 nM Cy3-labeled capture-ODN that is complementary to 8-nucleotides of the RNA. All values were normalized to the polarization values of the Cy3-capture-ODN. *P*-values were calculated using the unpaired *t*-test; ****: $p < 0.0001$. Error bars indicate standard deviations ($n = 3$). (C) Allosteric control of the binding of DFHBI-1T to Broccoli by TPP. Broccoli was connected to the libraries via linker 3 (−3) shown in a dotted square with orange. All values were normalized according to the sample with Broccoli and the corresponding amount of capture-ODN or TPP. *P*-values were calculated using the unpaired *t*-test comparing the values of SL-L3 and R12-L3 without oligo and TPP and values with 1 mM of TPP; ****: $p < 0.0001$. Error bars indicate standard deviations ($n = 3$). SL: starting library; R12: RNA library from selection cycle 12. (D) Interaction of monoclonal sequences S1−S5 with TPP measured by fluorescence polarization. All values were normalized to the polarization value of the Cy3-capture-ODN. *P*-values were calculated using the unpaired *t*-test; ***: $p = 0.0007$, ****: $p < 0.0001$. Error bars indicate standard deviations ($n = 2$). (E) Allosteric control of the binding of DFHBI-1T to Broccoli by TPP. Broccoli was connected to the aptamers with linker 3 (−3). All values were normalized to Broccoli and the corresponding amount of capture-ODN or TPP. *P*-values were calculated using the unpaired *t*-test; *: $p = 0.0167$ (S2), 0.0444 (S4), **: $p = 0.0326$ (S1), $p = 0.0020$ (S3), ****: $p < 0.0001$ (S5). Error bars indicate standard deviations ($n = 3$). (F) Allosteric control of DFHBI-1T binding to sensors S1 and S5 (with linker 3 extension—L3) without or with a 7-nucleotide-long A linker (−7A) shown in a dotted square upon addition of TPP. All values were normalized to Broccoli or to Broccoli with TPP. *P*-values were calculated using the unpaired *t*-test (*: $p = 0.0169$, ****: $p < 0.0001$). Error bars indicate standard deviations ($n = 3$). (G) Specificity of sensors S1 and S5 including a 7A linker. All values were normalized to Broccoli or Broccoli in the presence of the indicated molecules. *P*-values were calculated using the one-way ANOVA and Dunnett's multiple comparisons test (*: $p = 0.0122$, **: $p = 0.025$, ***: $p = 0.0009$, ****: $p = 0.0001$). Error bars indicate standard deviations ($n = 3$). TPP: thiamine pyrophosphate, TP: thiamine monophosphate, T: thiamine, GDP: guanosine diphosphate, ATP: adenosine triphosphate.

significant decrease in fluorescence polarization values, likely due to the hybridization energy being greater than the energy released upon interaction with the TPP molecule (Supporting Information Figure S4B). By linking the enriched library to Broccoli using the linker L3, a TPP-dependent increase in fluorescence was detected (Figure 1C), indicating a proof-of-concept at the library level. We next analyzed the enriched population by next-generation sequencing (NGS) and examined the five most abundant sequences (S1−S5, Supporting Information Figure S3C−G) and the sequences with the highest rate of enrichment from rounds 8−12 (Supporting Information Figure S5A−E) for TPP binding by fluorescence polarization. Sequence S5_M had *a* point mutation (C to U) within the docking sequence (Supporting Information Figure S3G), which was critical for performance (Supporting Information Figure S6) and was corrected for all subsequent studies. Consequently, the characterized sequence S5 has the same docking sequence as all the other sequences tested. The sequences S1, S3, S4, S5, S9, and S29 showed TPP-dependent binding (Figure 1D, Supporting Information Figure S5F), of which S1, S2, S3, and S5 enabled induction of fluorescence when connected to Broccoli via linker L3 and TPP was added (Figure 1E, Supporting Information Figure S5G). These results confirmed our concept and demonstrated that rationally designed RNA libraries can be used for selection to identify individual sequences capable of binding to a target molecule and control Broccoli folding allosterically while coupled to it. Although the enrichment profile from the NGS data shows that the individual sequences were not highly enriched (e.g., the most abundant sequence accounted for 4% of all sequences in the library), we still observed a significant increase in fluorescence signal with the addition of TPP to the RNA library from selection cycle 12, underlining the sensitivity of the approach (Figure 1B,C).

After demonstrating the de novo selection of RNA aptamers that can be modularly linked to fluorogenic RNAs and allowing allosteric control of binding to DFHBI-1T, we proceeded with sensors S1 and S5 as they have low background fluorescence and higher induction values to further optimize performance. We inserted different numbers of A nucleotides between the aptamer and the Broccoli domain to change the proximity of the docking sequence and the helix structure in Broccoli and to provide additional flexibility for facilitation of helix formation upon TPP interaction.[4] The addition of A nucleotides increased the TPP-mediated induction of fluorescence significantly, with 7 nucleotides being most effective (Supporting Information Figure S4). Sensors S1 and S5 showed a significant increase in the TPP response (Figure 1F), whereas the fluorescence of the sensors in the absence of TPP was not altered (Figure 1F). Remarkably, both sensors responded specifically to TPP and thiamine phosphate (TP), but not to thiamine (T) or the unrelated metabolites guanosine diphosphate (GDP) or adenosine triphosphate (ATP), whereas S5 was found to be slightly more specific (Figure 1G). Finally, we determined the affinity of the aptamers S1 and S5 for TPP by isothermal titration calorimetry (Supporting Information Figure S8). S1 and S5 bind TPP with similar affinities, 479 ± 136 and 462 ± 94.8 μM, respectively, which are much lower than the affinity of the natural TPP riboswitch.[5] To further prove allosteric activation of the sensor by TPP binding, we introduced point mutations into the region of S1 and S5 complementary to Broccoli, which led to a strong loss of sensing ability and which have been shown similarly in Geraci et al. (Supporting Information Figures S9 and S10).[6]

To demonstrate the modularity of the approach, we exchanged Broccoli by Red Broccoli since both fluorogenic RNAs share common motifs (Figure 2A).[7] We connected all sequences (Supporting Information Figures S3F and S5A) to Red Broccoli via linker L3 and tested them for TPP-dependent induction of fluorescence (Supporting Information Figure S11). Among them, sensor S5 revealed the best performance (Supporting Information Figure S11). We used S1 and S5 and optimized the sensor performance by introducing different numbers of A nucleotides, as described above when using Broccoli. Of these variants, S5 showed the strongest induction of fluorescence with 5 As, whereas S1 was less sensitive (Figure 2B). Furthermore, the Red Broccoli variant of S5 with a linker L3 extension and an additional 5A linker (S5−L3−7A) revealed a concentration-dependent induction by TPP (Figure 2C) and a specificity profile comparable to that of the Broccoli variant (Figure 2D).

DISCUSSION

In the first part of our study, we evaluated the molecular design of the sensor library. From five libraries (SE12−4) differing in

https://doi.org/10.1021/acssensors.3c02060
ACS Sens. 2024, 9, 753−758

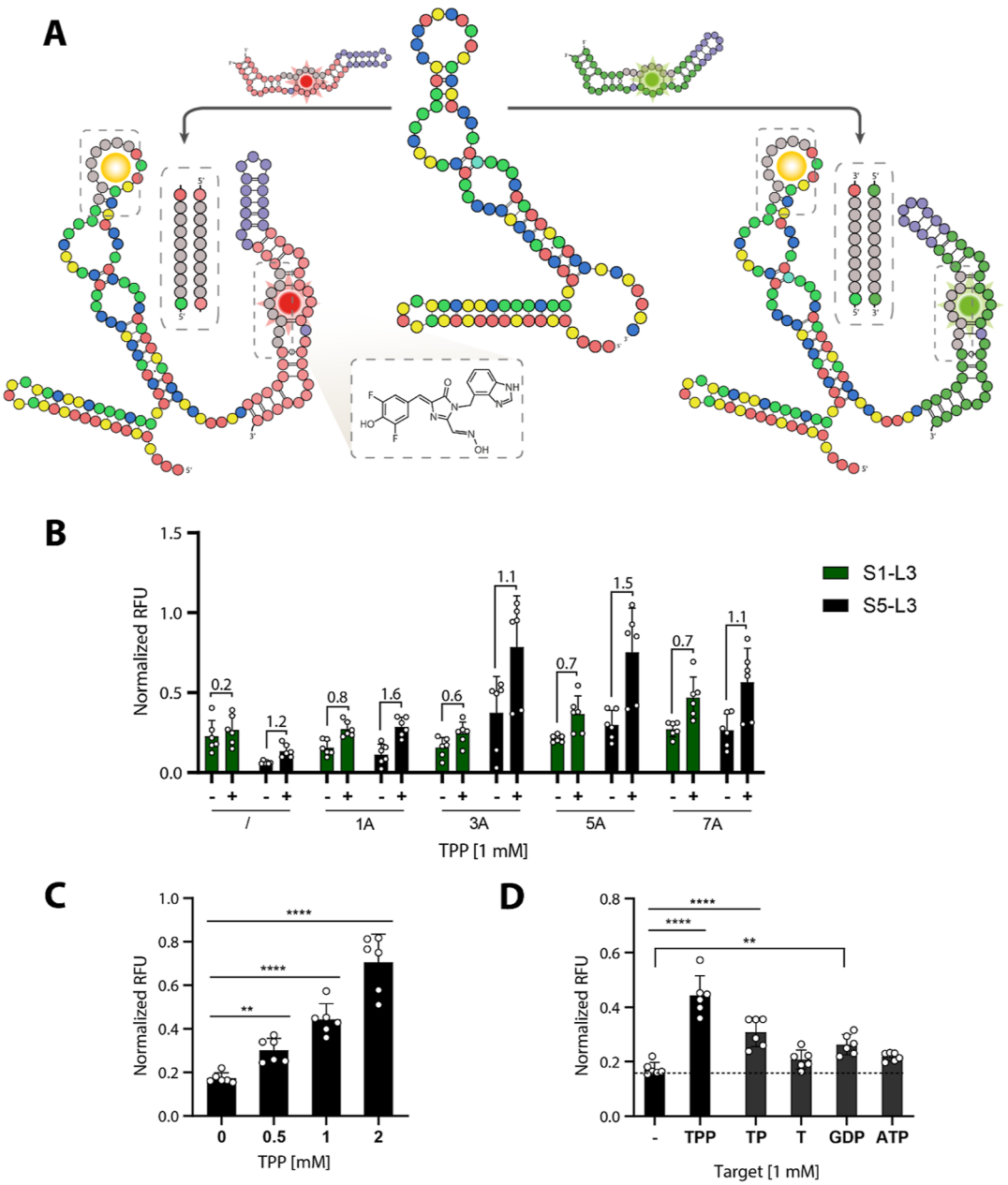

Figure 2. Fusion of S1 and S5 aptamers with Red Broccoli aptamers. (A) Predicted secondary structure and adaptation of the S5 aptamer to a red-shifted sensor. Nucleotide positions highlighted in red in Broccoli (left) and in green in Broccoli (right) are identical, whereas the nucleotide positions marked in purple are different. Red Broccoli and Broccoli aptamers are linked to the S5 aptamer on its 3′-end. In the absence of the TPP target and OBI (structure shown in a dotted box) or DFHBI-1T fluorophore, respectively, the complementary region highlighted in gray of the S5 aptamer and Red Broccoli or Broccoli aptamers hybridize. (B) Fluorescence intensity of the Red Broccoli sensors with the aptamer domains S1 and S5 in the absence or presence of TPP. Red Broccoli and S1 and S5 aptamers were connected by different numbers of A nucleotides. All values were normalized to Red Broccoli in the absence and presence of TPP. The addition of normalized Red Broccoli bars with and without TPP is omitted due to the clearer presentation of the graph. Turn-on values were calculated for each pair of F_0 and F_T: TO = $(F_T - F_0)/F_0$, where TO is the turn-on, F_T is the fluorescence of the sample with TPP, and F_0 is the fluorescence without TPP. Error bars indicate standard deviations ($n = 3$). (C) Concentration dependency of the Red Broccoli S5-L3−5A sensor upon addition of TPP. All values were normalized to the Red Broccoli. *P*-values were calculated using the one-way ANOVA and Dunnett's multiple comparisons test (**: $p = 0.0316$, ****: $p < 0.0001$). Error bars indicate standard deviations ($n = 3$). (D) Specificity of the Red Broccoli variant of sensors S5-L3−5A. All values were normalized according to Red Broccoli with the indicated molecules. *P*-values were calculated using the one-way ANOVA and Dunnett's multiple comparisons test (**: $p = 0.0063$, ****: $p < 0.0001$, ns: T and ATP). Error bars indicate standard deviations ($n = 3$). TPP: thiamine pyrophosphate, TP: thiamine monophosphate, T: thiamine.

the length (12−4 nt) of the complementary sequence hybridizing with Broccoli, SE8 was selected. SE4 and SE6 made weak contact with Broccoli, which resulted in increased fluorescence levels in the absence of the capture-ODN, whereas significantly stronger interactions, as demonstrated by libraries SE10 and SE12, did result in limited induction of fluorescence by capture-ODN addition (Supporting Information Figure S2A). The addition of linker residues between the RNA library and the Broccoli domain increased the performance of the sensors. Based on turn-on values, library SE12-L3 showed the

https://doi.org/10.1021/acssensors.3c02060
ACS Sens. 2024, 9, 753−758

best performance. However, we were concerned that a lower affinity between the RNA aptamers and the small target molecule might not efficiently affect the hybridization of a 12 nt docking sequence to Broccoli. This concern was also partially confirmed by the fluorescence anisotropy measurements (Supporting Information Figure S4B), in which TPP could not disrupt the hybridization of a 12 nt capture-ODN with the RNA library from selection cycle 12, whereas an 8 nt capture-ODN hybridization could (Figure 1B). These data indicate that using SE8 was the appropriate choice; however, further optimization might be possible by a more elaborate linker design and selection.

The NGS analysis of the selection cycles showed no strong enrichment of individual sequences and still a relatively high number of unique sequences (Figure S3D−G). As we could not identify common motifs in the enriched sequence populations, we tested five of the most enriched sequences and four sequences with the highest enrichment rate from selection cycles 8 to 12, in which the TPP concentration was reduced and the highest enrichment rates for sequences with high affinity were expected (Figure S5). However, the latter sequences showed a negligible turn-on signal upon addition of TPP. On the contrary, the best-performing sequences are two of the five most abundant sequences. This is in contrast to previous observations showing that the most abundant sequences are not always the best-performing ones, but this observation probably relates to the overall low enrichment levels of individual sequences.[8−10]

In some cases, the incorporated Broccoli domain exceeds the fluorescence signal of the parental Broccoli used for normalization. There could be several reasons for this. First, the incorporated Broccoli becomes more stable due to the addition of the linker (e.g., L3). Second, the higher TPP concentration (>1 mM) has an inhibitory effect on Broccoli function, which might be more pronounced in the free Broccoli used for normalization (Supporting Information Figure S3B). Third, the addition of capture-ODNs, which mimic the function of TPP, not only successfully disrupts the hybridization of the docking sequence with Broccoli but also affects the Broccoli structure of free Broccoli used for normalization.

Intracellular expression of fluorescent RNA sensors enables the real-time monitoring of cell metabolism. While higher intrinsic green fluorescence in cells could interfere with Broccoli signaling, Red Broccoli emits a higher-wavelength fluorescent signal, at which cell autofluorescence is much lower.[7] Nevertheless, the modest turn-on signal intensity of the S5 sensor and the detection of TPP in the mM range might make the detection of cellular TPP concentrations that are in the μM range difficult.[11] Furthermore, the detection of thiamine and its phosphate esters in whole blood samples is an important diagnostic tool for the detection of thiamine deficiency causing beriberi disease.[12] Although TPP is the predominant form and accounts for approximately 90% of the 60−120 μg/L total thiamine present in whole blood, the detection sensitivity of the S5-sensor might still be limited.[13,14] Using the SE12 library, which has lower background fluorescence (Figure 2C), and adjusting the selection strategy with a lower TPP concentration might drive the selection to sensors with lower fluorescence in the absence of TPP, a greater dynamic range, and the higher affinity required for cellular and diagnostic purposes. Alternatively, error-prone PCR to mutate S5 or the generation of degenerated libraries based on S5 could be used to reselect higher affinity variants of S5 that might be applicable in cells and diagnostic assays.

In summary, we describe a convenient approach in which aptamers that bind to small molecules are selected de novo and linked to reporter RNAs, resulting in fluorogenic sensors. The approach is modular, as demonstrated by its compatibility with two fluorogenic reporter RNAs. The performance of the obtained sensors is limited by the affinity of the ligand (TPP), which in the case shown is in the triple-digit micromolar range. However, this value can be lowered by optimized selection schemes or by using degenerate libraries for reselection purposes.[15] Nevertheless, effective sensors could be obtained even with lower-affinity aptamers. The method described can be adapted to other fluorogenic RNAs, such as pepper or chili, which have different spectral properties.[16,17] Due to the modular design of our method, it could be effectively combined with droplet sorting procedures that enable the identification of optimally performing sensors within the enriched libraries.[6,18] Particularly in regard to the relatively low enrichment profile of the used capture-SELEX approach, this combination might be advantageous. Likewise, a combination with cellular screening approaches utilizing advanced expression systems, such as Tornado, would allow for screening the libraries for those sensors that perform best in a cellular environment.[19]

■ ASSOCIATED CONTENT

Supporting Information

The Supporting Information is available free of charge at https://pubs.acs.org/doi/10.1021/acssensors.3c02060.

Experimental details, materials, and methods; design and annealing properties of five different sensor libraries; optimization of the library for sensor selection; selection of the RNA sensor targeting TPP; binding of the starting pool and round 12 pool to TPP; binding and sensing characterization of additional monoclonal sequences; binding and sensing characterization of S5_M-enriched sequence and S5; addition of poly(A) linkers between S1 aptamer sequence and Broccoli; thermodynamic binding properties of aptamer S and S5 to TPP; S1 aptamer with different numbers of point-mutations; S5 aptamer with different numbers of point-mutations; allosteric binding of OBI to Red Broccoli; and list of utilized sequences (PDF)

■ AUTHOR INFORMATION

Corresponding Author

Günter Mayer − *Life and Medical Sciences, University of Bonn, 53121 Bonn, Germany; Center of Aptamer Research and Development, University of Bonn, 53121 Bonn, Germany;* orcid.org/0000-0003-3010-4049; Email: gmayer@uni-bonn.de

Author

Tjasa Legen − *Life and Medical Sciences, University of Bonn, 53121 Bonn, Germany; Center of Aptamer Research and Development, University of Bonn, 53121 Bonn, Germany;* orcid.org/0009-0001-7776-627X

Complete contact information is available at: https://pubs.acs.org/10.1021/acssensors.3c02060

Author Contributions

T.L. designed and conducted the experiments and analyzed the data. G.M. conceived the study and designed and supervised the experiments. T.L. and G.M. wrote the manuscript.

Notes

The authors declare no competing financial interest.

■ ACKNOWLEDGMENTS

This work was supported by funding from the German Research Council (DFG, MA3442/7-1).

■ REFERENCES

(1) Stoltenburg, R.; Nikolaus, N.; Strehlitz, B. Capture-SELEX: selection of DNA aptamers for aminoglycoside antibiotics. *J. Anal. Methods Chem.* **2012**, *2012*, 1−14.
(2) Boussebayle, A.; Groher, F.; Suess, B. RNA-based Capture-SELEX for the selection of small molecule-binding aptamers. *Methods* **2019**, *161*, 10−15.
(3) Filonov, G. S.; Moon, J. D.; Svensen, N.; Jaffrey, S. R. Broccoli: rapid selection of an RNA mimic of green fluorescent protein by fluorescence-based selection and directed evolution. *J. Am. Chem. Soc.* **2014**, *136* (46), 16299−16308.
(4) You, M.; Litke, J. L.; Jaffrey, S. R. Imaging metabolite dynamics in living cells using a Spinach-based riboswitch. *Proc. Natl. Acad. Sci. U.S.A.* **2015**, *112* (21), No. E2756.
(5) Winkler, W.; Nahvi, A.; Breaker, R. R. Thiamine derivatives bind messenger RNAs directly to regulate bacterial gene expression. *Nature* **2002**, *419* (6910), 952−956.
(6) Geraci, I.; Autour, A.; Pietruschka, G.; Shiian, A.; Borisova, M.; Mayer, C.; Ryckelynck, M.; Mayer, G. n. Fluorogenic RNA-Based Biosensor to Sense the Glycolytic Flux in Mammalian Cells. *ACS Chem. Biol.* **2022**, *17* (5), 1164−1173.
(7) Li, X.; Mo, L.; Litke, J. L.; Dey, S. K.; Suter, S. R.; Jaffrey, S. R. Imaging intracellular S-adenosyl methionine dynamics in live mammalian cells with a genetically encoded red fluorescent RNA-based sensor. *J. Am. Chem. Soc.* **2020**, *142* (33), 14117−14124.
(8) Weber, A. M.; Kaiser, J.; Ziegler, T.; Pilsl, S.; Renzl, C.; Sixt, L.; Pietruschka, G.; Moniot, S.; Kakoti, A.; Juraschitz, M.; et al. A blue light receptor that mediates RNA binding and translational regulation. *Nat. Chem. Biol.* **2019**, *15* (11), 1085−1092.
(9) Schütze, T.; Wilhelm, B.; Greiner, N.; Braun, H.; Peter, F.; Mörl, M.; Erdmann, V. A.; Lehrach, H.; Konthur, Z.; Menger, M.; et al. Probing the SELEX process with next-generation sequencing. *PLoS One* **2011**, *6* (12), No. e29604.
(10) Civit, L.; Taghdisi, S. M.; Jonczyk, A.; Haßel, S. K.; Gröber, C.; Blank, M.; Stunden, H. J.; Beyer, M.; Schultze, J.; Latz, E.; et al. Systematic evaluation of cell-SELEX enriched aptamers binding to breast cancer cells. *Biochimie* **2018**, *145*, 53−62.
(11) Nakayama, H.; Hayashi, R. Biosynthesis of thiamine pyrophosphate in Escherichia coli. *J. Bacteriol.* **1972**, *109* (2), 936−938.
(12) Wiley, K. D.; Gupta, M. *Vitamin B1 Thiamine Deficiency*; University of Arkansas for Medical Sciences, 2019.
(13) Losa, R.; Sierra, M.; Fernández, A.; Blanco, D.; Buesa, J. Determination of thiamine and its phosphorylated forms in human plasma, erythrocytes and urine by HPLC and fluorescence detection: a preliminary study on cancer patients. *J. Pharm. Biomed. Anal.* **2005**, *37* (5), 1025−1029.
(14) Talwar, D.; Davidson, H.; Cooney, J.; St. JO'Reilly, D. Vitamin B1 status assessed by direct measurement of thiamin pyrophosphate in erythrocytes or whole blood by HPLC: comparison with erythrocyte transketolase activation assay. *Clin. Chem.* **2000**, *46* (5), 704−710.
(15) (a) Mohsen, M. G.; Midy, M. K.; Balaji, A.; Breaker, R. R. Exploiting natural riboswitches for aptamer engineering and validation. *Nucleic Acids Res.* **2023**, *51* (2), 966−981. (b) Yang, K.; Mitchell, N. M.; Banerjee, S.; Cheng, Z.; Taylor, S.; Kostic, A. M.; Wong, I.; Sajjath, S.; Zhang, Y.; Stevens, J.; et al. A functional group-guided approach to aptamers for small molecules. *Science* **2023**, *380* (6648), 942−948.
(16) Chen, X.; Zhang, D.; Su, N.; Bao, B.; Xie, X.; Zuo, F.; Yang, L.; Wang, H.; Jiang, L.; Lin, Q.; et al. Visualizing RNA dynamics in live cells with bright and stable fluorescent RNAs. *Nat. Biotechnol.* **2019**, *37* (11), 1287−1293.
(17) Steinmetzger, C.; Palanisamy, N.; Gore, K. R.; Höbartner, C. A multicolor large stokes shift fluorogen-activating RNA aptamer with cationic chromophores. *Chem. —Eur. J.* **2019**, *25* (8), 1931−1935.
(18) Baret, J.-C.; Miller, O. J.; Taly, V.; Ryckelynck, M.; El-Harrak, A.; Frenz, L.; Rick, C.; Samuels, M. L.; Hutchison, J. B.; Agresti, J. J.; et al. Fluorescence-activated droplet sorting (FADS): efficient microfluidic cell sorting based on enzymatic activity. *Lab Chip* **2009**, *9* (13), 1850−1858.
(19) Litke, J. L.; Jaffrey, S. R. Highly efficient expression of circular RNA aptamers in cells using autocatalytic transcripts. *Nat. Biotechnol.* **2019**, *37* (6), 667−675.

https://doi.org/10.1021/acssensors.3c02060
ACS Sens. 2024, 9, 753−758

Supporting information

A modular approach for rapid identification of RNA-based sensors

Tjasa Legen[1,2] and Günter Mayer[1,2]*

* to whom correspondence should be addressed: gmayer@uni-bonn.de

[1] Life and Medical Sciences, University of Bonn, 53121 Bonn, Germany

[2] Center of Aptamer Research and Development, University of Bonn, 53121 Bonn, Germany

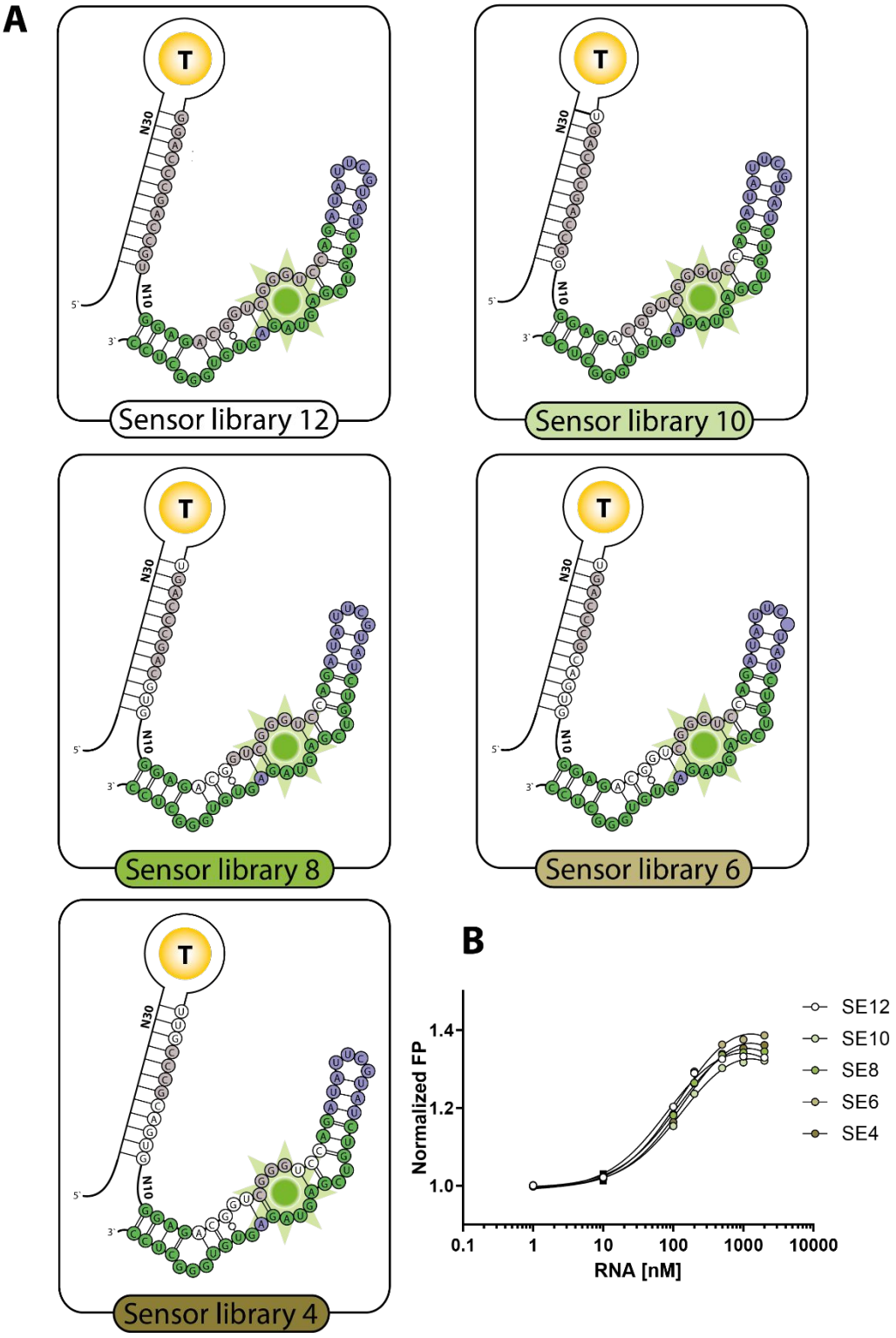

S1. Design and annealing properties of five different sensor libraries. A) Sensor libraries (SE) with different lengths of complementary part to Broccoli. The docking sequence of the libraries (grey and white nucleotides) is always 12 nt long, however the Broccoli complementary part (grey nucleotides) is 12 nt to 4 nt long (SE12-4). T: Small molecule target. **B)** Annealing efficiency of sensor libraries (SE) (without Broccoli sequence) to corresponding capture oligodeoxynucleotides (ODN). The assay is based on the fluorescence polarization (FP) of free versus hybridized Cy3-labelled capture ODN. Assay was performed with 100 nM Cy3-labelled capture ODN. All values were normalized according to the FP value of capture ODN alone.

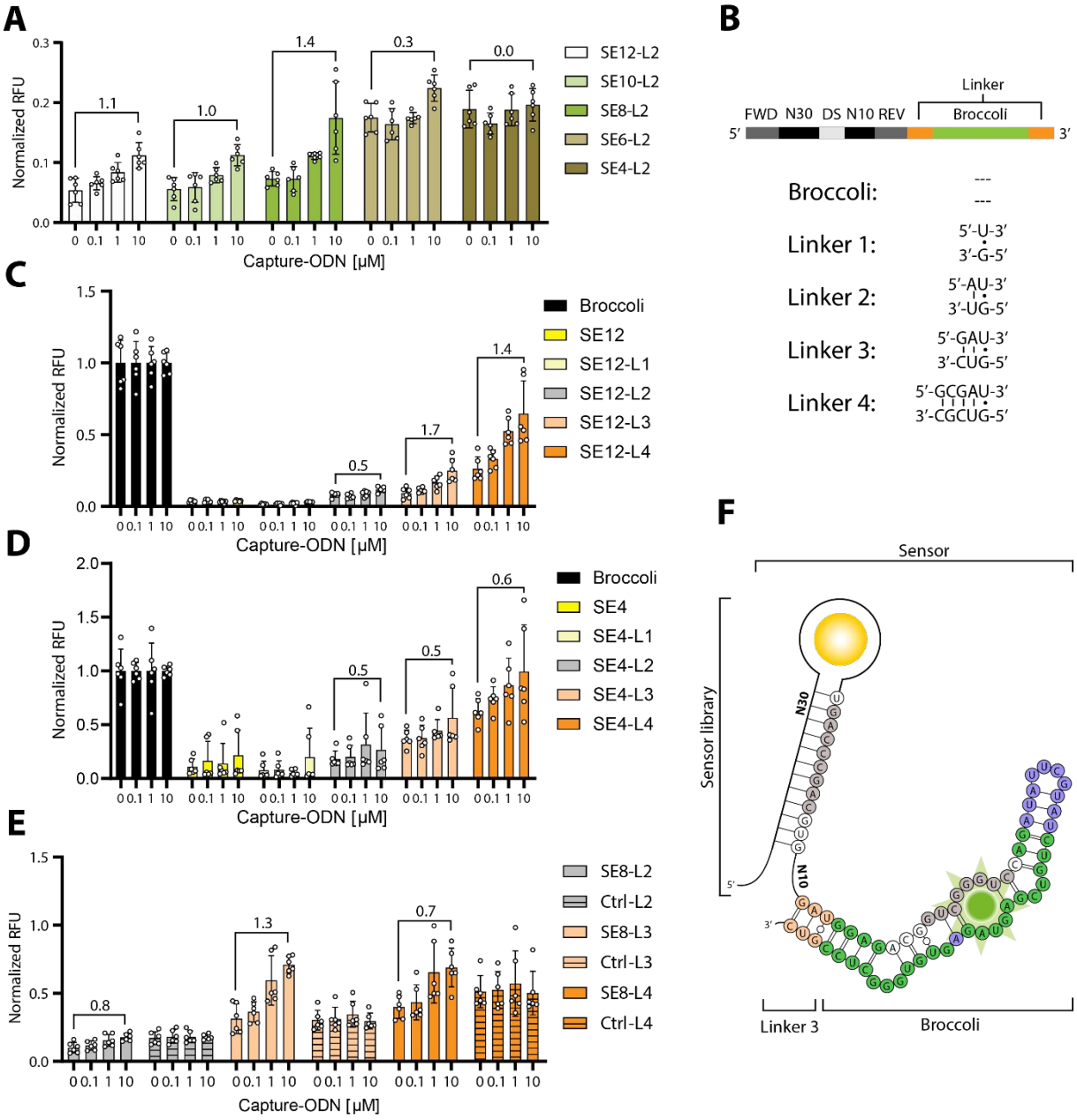

S2. Optimization of the library for sensor selection. A) Allosteric control of DFHBI-1T binding to Broccoli connected to different sensor libraries (SE) upon addition of 12-nt capture-oligodeoxynucleotide (ODN). Since no signal was observed while connecting libraries to the Broccoli aptamer (see C-D, SE12 and SE4), the Broccoli was extended with linker 2 (-L2) in this experiment (for linker design see B). For each sensor library, corresponding capture-ODN was used with full complementarity to the docking sequence. All values were normalized according to the sample with Broccoli and corresponding capture-ODN concentration. To see the differences more clearly, we omitted placing the Broccoli bars on the graph. Turn-on values (TO) were calculated for each pair of F_0 and F_{10}, TO=(F_{10}- F_0)/ F_0 where TO is the turn-on, F_{10} is the fluorescence of sample with 10 μM ODN and F_0 is the fluorescence without ODN. Error bars indicate standard deviations (n = 3). **B)** Representation of different Broccoli extension linkers, which were introduced to the library via PCR. FWD: forward primer-binding site, N30/10: random region, DS: docking sequence, REV: reverse primer-binding site. **C-D)** Allosteric control of DFHBI-1T binding to Broccoli in SE12 (C) and SE4 (D) with different Broccoli linkers. Complementarity of capture-ODN to the docking sequence was utilized for inducement of Broccoli folding. Values were normalized to the signal of Broccoli with corresponding capture-ODN concentration. TO values were calculated for each pair of F_0 and F_{10} the same as explained by A. Error bars indicate standard deviations (n = 3). **E)** Allosteric control of DFHBI-1T binding to SE8 with linkers 2-4 extension upon addition of 12-nt capture ODN. As a control, a library with no complementarity to Broccoli was utilized (Ctrl). All values were normalized according to the sample with Broccoli and corresponding capture ODN concentration. Broccoli bars were not

included in the graph due to the lack of space. TO values were calculated for each pair of F_0 and F_{10} the same as explained by A. Error bars indicate standard deviations (n = 3) **F)** Schematic representation of Sensor 8, which contains Broccoli extended with linker 3 and SE8 library (SE8-L3). This design was the most optimal for the subsequent aptamer selection.

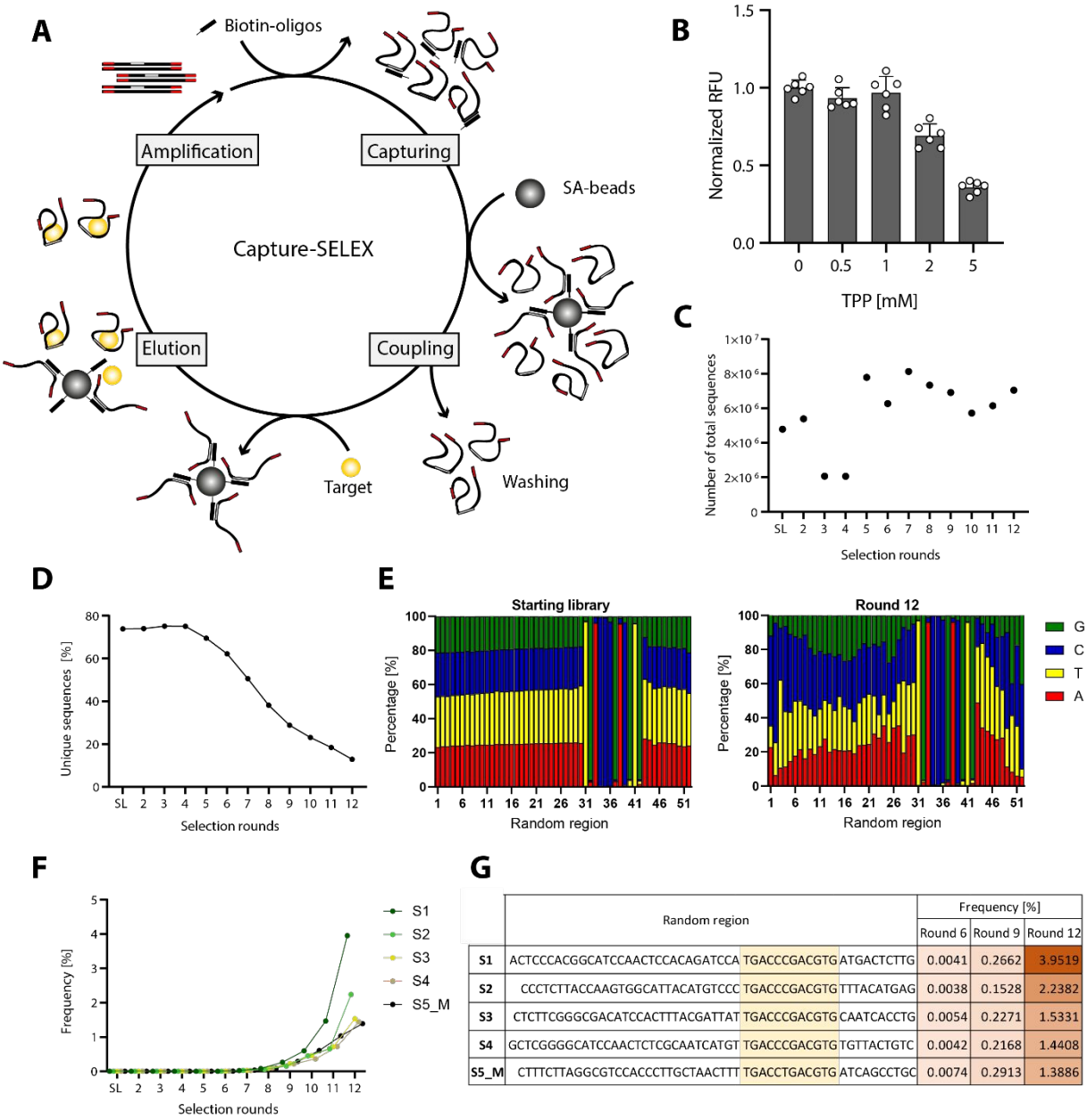

	Random region	Frequency [%]		
		Round 6	Round 9	Round 12
S1	ACTCCCACGGCATCCAACTCCACAGATCCA TGACCCGACGTG ATGACTCTTG	0.0041	0.2662	3.9519
S2	CCCTCTTACCAAGTGGCATTACATGTCCC TGACCCGACGTG TTTACATGAG	0.0038	0.1528	2.2382
S3	CTCTTCGGGCGACATCCACTTTACGATTAT TGACCCGACGTG CAATCACCTG	0.0054	0.2271	1.5331
S4	GCTCGGGGCATCCAACTCTCGCAATCATGT TGACCCGACGTG TGTTACTGTC	0.0042	0.2168	1.4408
S5_M	CTTTCTTAGGCGTCCACCCTTGCTAACTTT TGACCTGACGTG ATCAGCCTGC	0.0074	0.2913	1.3886

S3. Selection of RNA sensor targeting Thiamine pyrophosphate (TPP). A) Scheme of RNA Capture SELEX. Main steps are 1) Capturing of RNA library (without Broccoli) to capture oligodeoxynucleotides (ODN) during transcription, 2) Coupling of RNA-ODN duplexes on magnetic beads and removing of weakly bound sequences, 3) Elution of binding sequences by addition of a target solution, and 4) Reverse transcription and amplification of dissociated sequences. SA: streptavidin. **B)** Signal of DFHBI-1T binding to the Broccoli aptamer in the presence of TPP. Concentration of DFHBI-1T and Broccoli RNA was 10 µM and 1 µM, respectively. Error bars indicate standard deviations (n = 3). **C)** Number of total sequences in each selection round obtained by Next-generation sequencing. **D)** Percentage of unique sequences in different selection rounds measured by Next-generation sequencing. **E)** Nucleotide distribution of the random region in the starting library and after 12 selection rounds. **F)** Frequency of top five enriched sequences through 12 selection rounds. **G)** Table of top five enriched sequences with corresponding sequence of the random region. Docking sequences are highlighted in yellow.

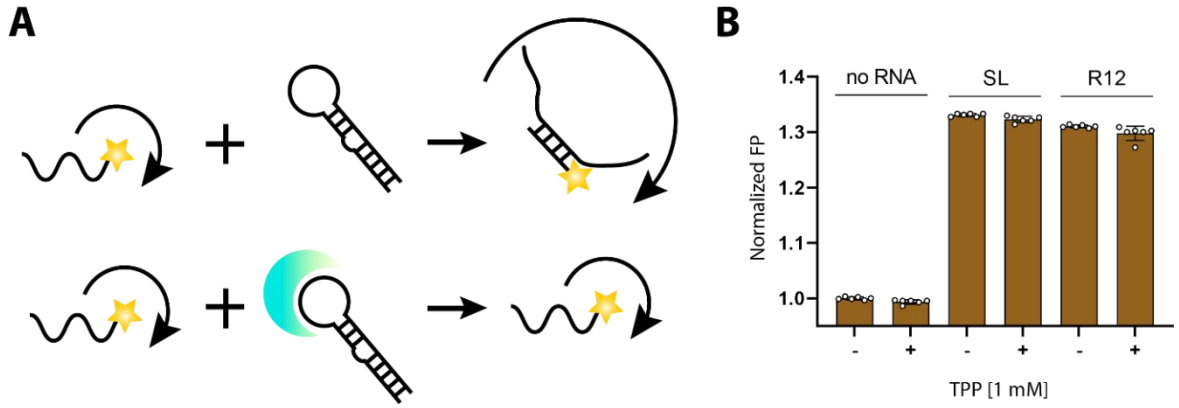

S4. Binding of the starting pool and round 12 pool to TPP measured by fluorescence polarization (FP) assay. A) Principle of fluorescence polarization assay. When the Cy3-labelled capture-oligodeoxynucleotide (ODN) annealed to the RNA the rotation slows down and consequently the fluorescence polarization increases. If the target is bound to the RNA, more of the capture ODN is free thereby the fluorescence polarization decreases. **B)** Binding was measured by using 100 nM Cy3-labelled capture ODN with 12 nt complementarity to RNA. All values were normalized according to the FP value of Cy3-labelled capture ODN. Error bars indicate standard deviations (n = 3).

A

	SEQUENCE	Round 6	Round 8	Round 10	Round 12	R12/R6	R12/R8
S1	ACTCCCACGGCATCCAACTCCACAGATCCA TGACCCGACGTG ATGACTCTTG	0.0041	0.0818	0.5984	3.9519	963.878	48.31174
S2	CCCTCTTACCAAGTGGCATTACATGTCCC TGACCCGACGTG TTTACATGAG	0.0038	0.0579	0.4529	2.2382	589	38.6563
S3	CTCTTCGGGCGACATCCACTTTACGATTAT TGACCCGACGTG CAATCACCTG	0.0054	0.089	0.4599	1.5331	283.9074	17.22584
S4	GCTCGGGGCATCCAACTCTCGCAATCATGT TGACCCGACGTG TGTTACTGTC	0.0042	0.0989	0.3602	1.4408	343.0476	14.56825
S5_M	CTTTCTTAGGCGTCCACCCTTGCTAACTTT TGACCTGACGTG ATCAGCCTGC	0.0074	0.0879	0.6044	1.3886	187.6486	15.7975
S9	CCTTCCATCCACGAATCGCTACCCCGCCAA TGACCCGACGTG ATTATTAGCC	0.0024	0.0347	0.2357	1.0347	431.125	29.81844
S20	CCTGACTCTAGGCATTCACGGACTCCCAGA TGACCCGACGTG ACTTCGATGA	0.0006	0.0076	0.0559	0.369	615	48.55263
S29	CATCTGCTGTGACAAACACGATATCTGTCC TGACCCGACGCG ATCACCCCTC	0.0000	0.001	0.0178	0.226	n.a.	226
S44	ACTCTTACAGCTGCATTCACGAGAACGCCC TGACCCGACGTG TACTTAACTG	0.0001	0.0033	0.0258	0.1461	1461	44.27273

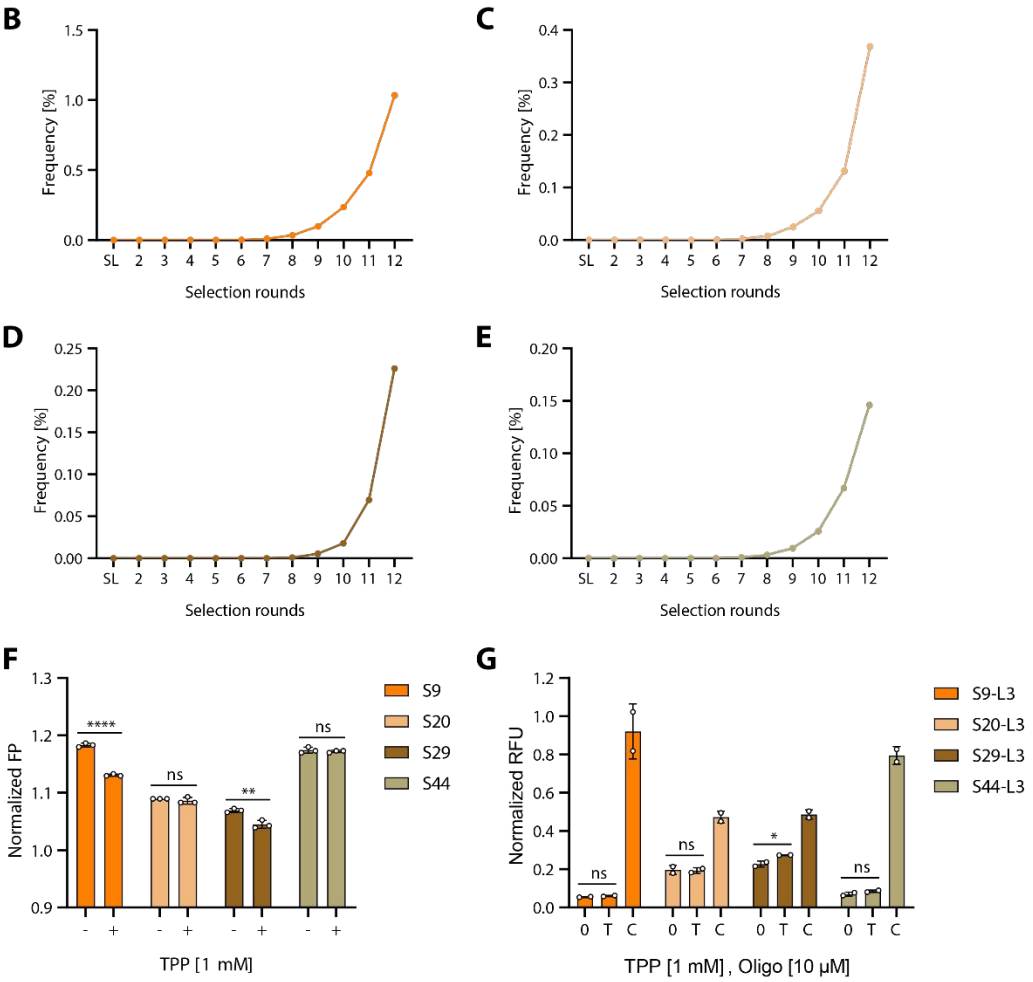

S5. Binding and sensing characterization of additional monoclonal sequences S9, S20, S29, and S44. A) Enrichment table with sequence frequency in round 6, 8, 10, and 12 and enrichment fold change from round 6 and 8 to round 12. Docking sequences are highlighted in yellow. **B-E)** Graph of enrichment through selection rounds of sequences S9 (B), S20 (C), S29 (D), and S44 (E). **F)** Binding of S9, S20, S29, and S44 sequences measured by fluorescence polarization assay. P-values were calculated using the unpaired t-test; **: p=0.0053, ****: p<0.0001. Error bars indicate standard deviations (n = 1). **G)** Allosteric control of DFHBI-1T binding to a Broccoli with linker 3 extension in the presence of TPP in constructs connected to S9, S20, S29, and S44 sequence. P-values were calculated using the unpaired t-test; *: p=0.0497. Error bars indicate standard deviations (n = 1).

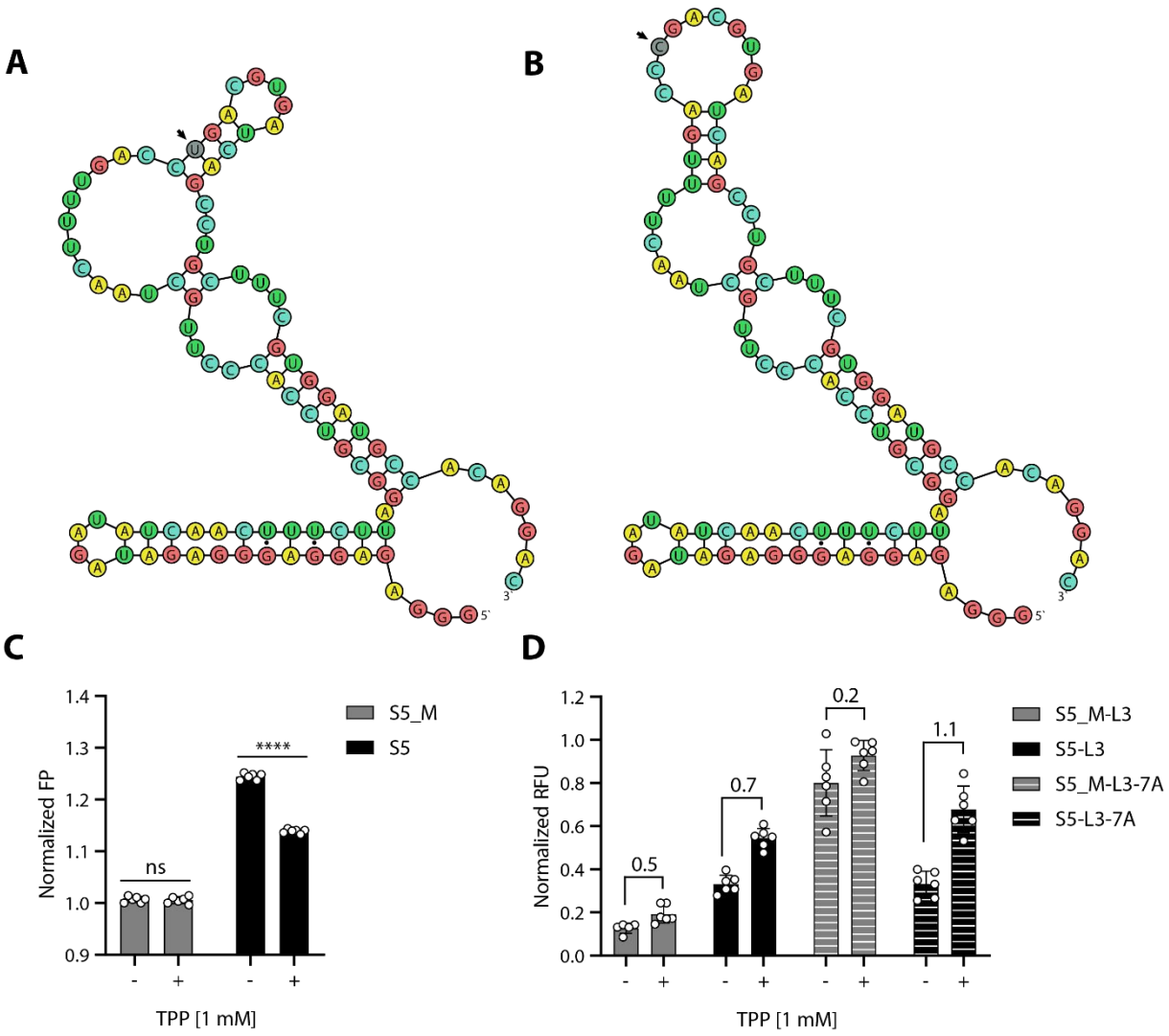

S6. Binding and sensing characterization of S5_M enriched sequence and S5 with a corrected point-mutation in the docking sequence. A) Predicted secondary structure of S5_M sequence. Arrow indicates a point mutation, which occurred in the docking sequence. **B)** Predicted secondary structure of S5 sequence with corrected mutation in the docking sequence indicated with an arrow. **C)** Binding of S5_M and S5 aptamer to TPP measured by fluorescence polarization assay. P-values were calculated using the unpaired t-test; ****: p<0.0001. Error bars indicate standard deviations (n = 3). **D)** Allosteric control of DFHBI-1T binding to the Broccoli with linker 3 (-L3) extension in the presence of TPP connected to S5_M and S5 aptamer with and without linker 7A. Turn-on values (TO) were calculated for each pair of F_0 and F_T, $TO=(F_T- F_0)/ F_0$ where TO is the turn-on, F_T is the fluorescence of sample with TPP and F_0 is the fluorescence without TPP. Error bars indicate standard deviations (n = 3).

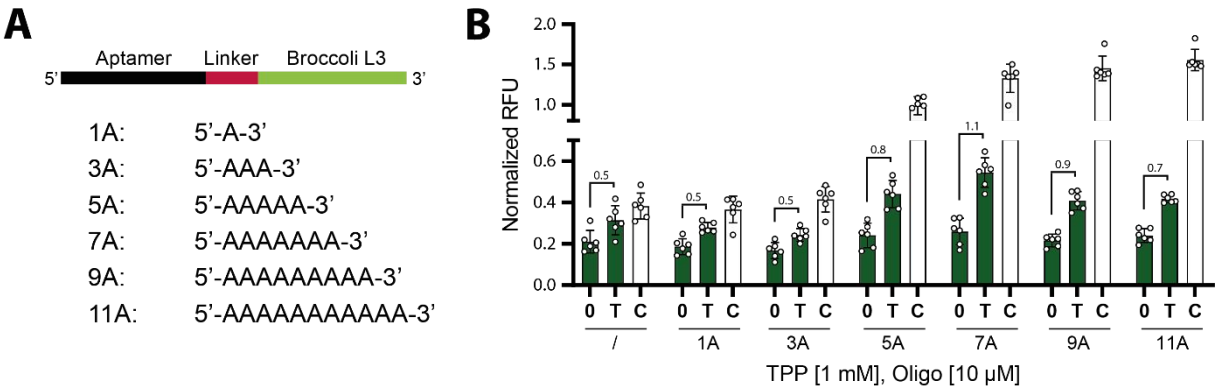

S7: Addition of poly(A) linkers between S1 aptamer sequence and Broccoli with linker 3 sequence extension. **A)** Scheme of different lengths of poly(A) linkers (1-11) inserted between the aptamer sequnece and Broccoli

extended with linker 3 (1A-11A). **B)** Allosteric control of DFHBI-1T binding to Broccoli extended with linker 3 and connected to S1 aptamer via different lenghts of poly(A) linkers upon addition of either 1 mM of Thiamine pyrophosphate (TPP) or 10 µM of complementary capture oligodeoxynucleotide (ODN). Addition of 7A linker increases the fluorescence signal in the presence of TPP the most, for turn-on value of 1.1. All values were normalized according to the Broccoli sample in the absence and presence of TPP and presence of capture ODN. Turn-on values (TO) were calculated for each pair of F_0 and F_T, TO=(F_T- F_0)/ F_0 where TO is the turn-on, F_T is the fluorescence of sample with TPP and F_0 is the fluorescence without TPP. Error bars indicate standard deviations (n = 3). 0: no TPP or capture ODN added, T: addition of TPP, C: addition of capture ODN.

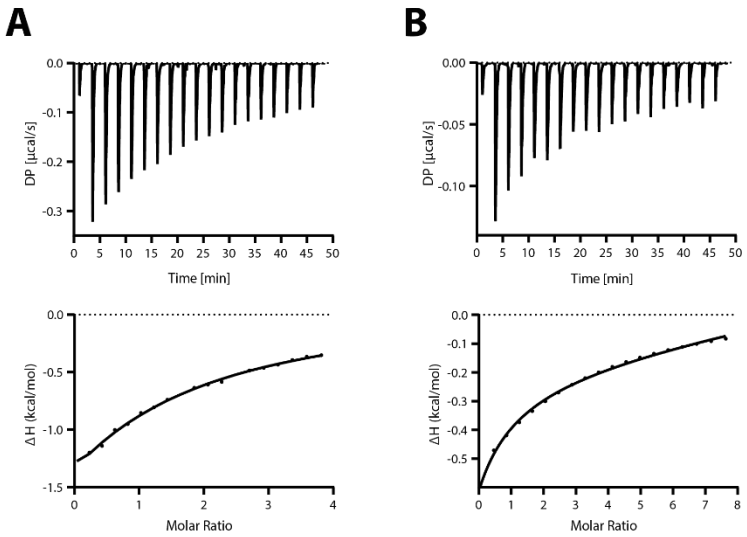

S8: Thermodynamic binding properties of aptamer S1 (A) and S5 (B) to TPP. Kd of binding is 479 ± 136 µM for S1 and 462 ± 94.8 µM for S5.

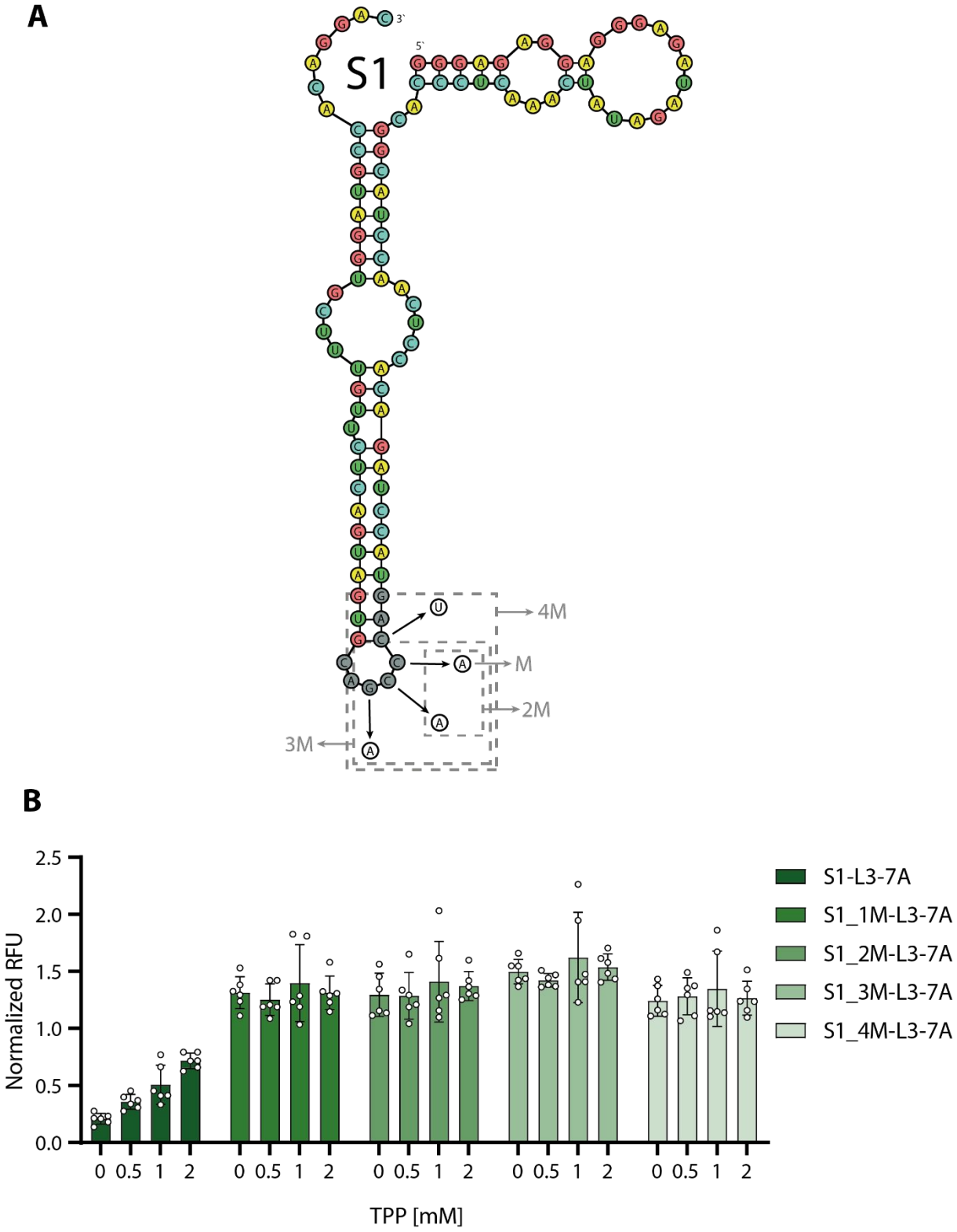

S9. S1 aptamer with different numbers of point-mutations. A) Predicted secondary structure of aptamer S1 with Broccoli-complementary part depicted in grey and 1M-4M point-mutations depicted in white. **B)** Concentration dependent sensing of sensor S1 with different number of point mutations (1M-4M) in the docking sequence. S1 aptamer and its point-mutants were connected to the Broccoli with extended linker 3 (-L3) via linker 7A (-7A). Fluorescence signal was normalized to the signal of Broccoli aptamer in the presence of corresponded concentration of TPP. Error bars indicate standard deviations (n = 3).

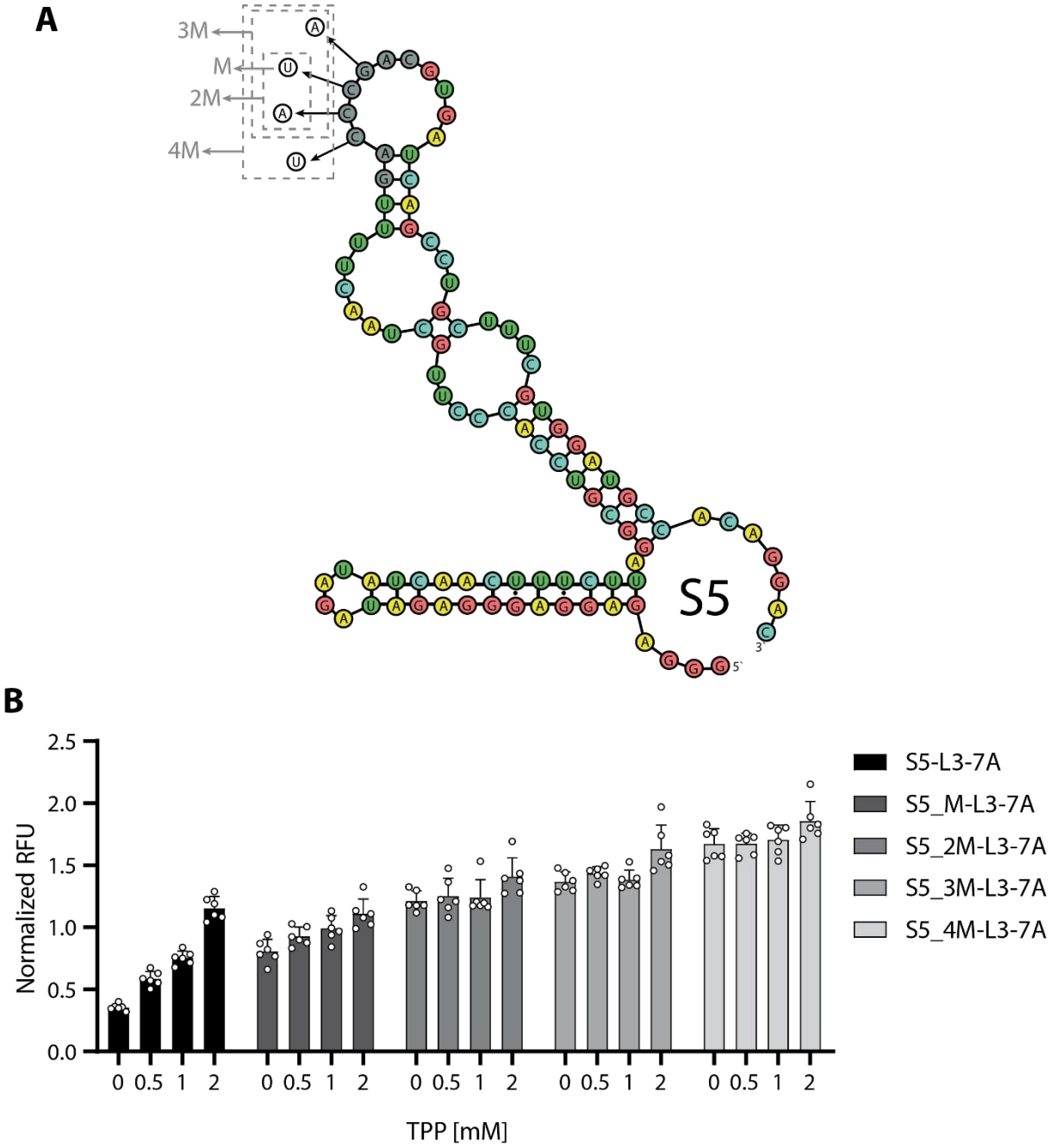

S10. S5 aptamer with different numbers of point-mutations. A) Predicted secondary structure of aptamer S5 with Broccoli-complementary part depicted in grey and M-4M point-mutations depicted in white. **B)** Concentration dependent sensing of sensor S5 with different number of point mutations (M-4M) in the docking sequence. S5 aptamer and its point-mutants were connected to the Broccoli with extended linker 3 (-L3) via linker 7A (-7A). Fluorescence signal was normalized to the signal of Broccoli aptamer in the presence of corresponded concentration of TPP. Error bars indicate standard deviations (n = 3).

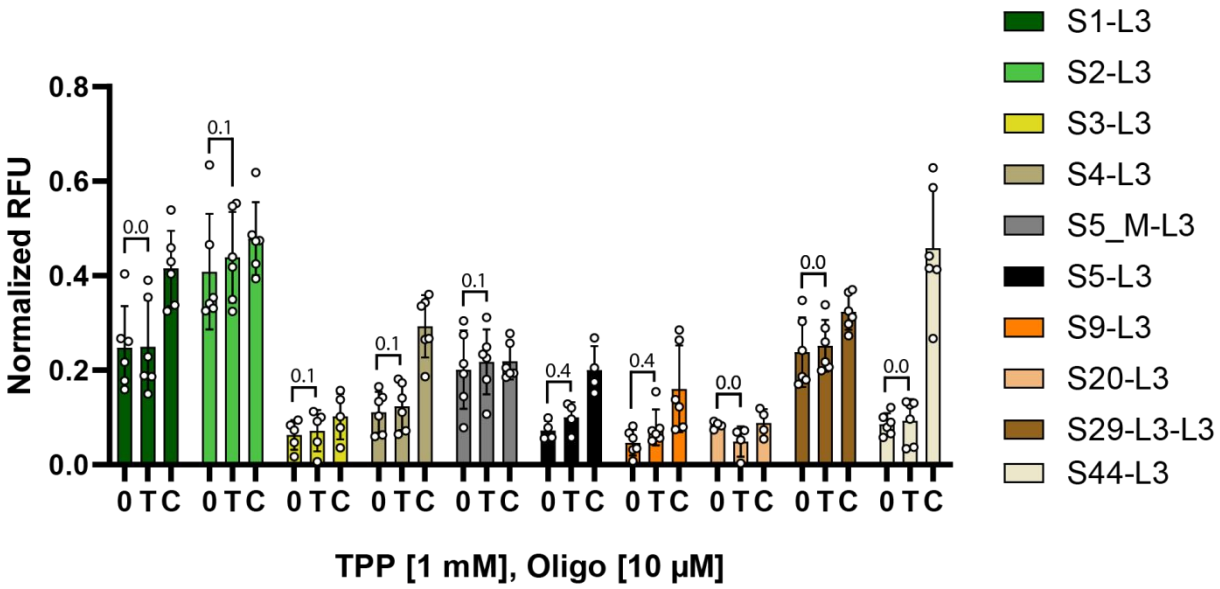

S11. Allosteric binding of OBI to Red broccoli in the presence of TPP or capture-oligodeoxynucleotide (ODN) in Red broccoli L3 constructs. All values were normalized according to the fluorescence signal of Red broccoli in the absence or presence of TPP or capture-ODN. Turn-on values (TO) were calculated for each pair of F_0 and F_T, $TO=(F_T- F_0)/ F_0$ where TO is the turn-on, F_T is the fluorescence of sample with TPP and F_0 is the fluorescence without TPP. Error bars indicate standard deviations (n = 3). S5_M-L3 has the C to U point mutant in the docking region (see Supp. Fig. 3G and 5A); S5-L3 is the corrected sequence having the original C in the respective docking sequence version).

Table S1. List of utilized sequences.

Sensor library 12	GGGAGAGGAGGGAGATAGATATCAA-N30-GGACCCGACCGT-N10-TTTCGTGGATGCCACAGGAC
Capture ODN 12	Biotin-C18-ACGGTCGGGTCC
Sensor library 10	GGGAGAGGAGGGAGATAGATATCAA-N30-TGACCCGACCGG-N10-TTTCGTGGATGCCACAGGAC
Capture ODN 10	Biotin-C18- CCGGTCGGGTCA
Sensor library 8	GGGAGAGGAGGGAGATAGATATCAA-N30-TGACCCGACGTG-N10-TTTCGTGGATGCCACAGGAC
Capture ODN 8	Biotin-C18- CACGTCGGGTCA
Sensor library 6	GGGAGAGGAGGGAGATAGATATCAA-N30-TGACCCGCAGTG-N10-TTTCGTGGATGCCACAGGAC
Capture ODN 6	Biotin-C18- CACTGCGGGTCA
Sensor library 4	GGGAGAGGAGGGAGATAGATATCAA-N30-TTGCCCGCAGTG-N10-TTTCGTGGATGCCACAGGAC
Capture ODN 4	Biotin-C18- CACTGCGGGCAA
Fwd primer + T7 promoter	AATTCTAATACGACTCACTATAGGGAGAGGAGGGAGATAGATATCAA
Rev primer	GTCCTGTGGCATCCACGAAA
Rev primer + rev Broccoli	GACGGAGCCCACACTCTACTCGACAGATACGAATATCTGGACCCGACCGTCTCCATCGTCCTGTGGCATCCACGAAA
Rev primer + rev Red Broccoli	GACGGAGCCCACACTCTACTCGACAGATACGAATATCTGGACCCGACCGTCTCCATCGTCCTGTGGCATCCACGAAA
S1	GGGAGAGGAGGGAGATAGATATCAAACTCCCACGGCATCCAACTCCACAGATCCATGACCCGACGTGATGACTCTTGTTTCGTGGATGCCACAGGAC
S1_1M	GGGAGAGGAGGGAGATAGATATCAAACTCCCACGGCATCCAACTCCACAGATCCATGACACGACGTGATGACTCTTGTTTCGTGGATGCCACAGGAC
S1_2M	GGGAGAGGAGGGAGATAGATATCAAACTCCCACGGCATCCAACTCCACAGATCCATGACAAGACGTGATGACTCTTGTTTCGTGGATGCCACAGGAC
S1_3M	GGGAGAGGAGGGAGATAGATATCAAACTCCCACGGCATCCAACTCCACAGATCCATGACAAAACGTGATGACTCTTGTTTCGTGGATGCCACAGGAC
S1_4M	GGGAGAGGAGGGAGATAGATATCAAACTCCCACGGCATCCAACTCCACAGATCCATGATAAAACGTGATGACTCTTGTTTCGTGGATGCCACAGGAC
S1-L3-7A (Broccoli)	GGGAGAGGAGGGAGATAGATATCAAACTCCCACGGCATCCAACTCCACAGATCCATGACCCGACGTGATGACTCTTGTTTCGTGGATGCCACAGGACAAAAAAAAGATGGAGACGGTCGGGTCCAGATATTCGTATCTGTCGAGTAGAGTGTGGGCTCCGTC
S5	GGGAGAGGAGGGAGATAGATATCAACTTTCTTAGGCGTCCACCCTTGCTAACTTTTGACCCGACGTGATCAGCCTGCTTTCGTGGATGCCACAGGAC
S5_M	GGGAGAGGAGGGAGATAGATATCAACTTTCTTAGGCGTCCACCCTTGCTAACTTTTGACCTGACGTGATCAGCCTGCTTTCGTGGATGCCACAGGAC
S5_2M	GGGAGAGGAGGGAGATAGATATCAACTTTCTTAGGCGTCCACCCTTGCTAACTTTTGACATGACGTGATCAGCCTGCTTTCGTGGATGCCACAGGAC

S5_3M	GGGAGAGGAGGGAGATAGATATCAACTTTCTTAGGCGTCCACCCTT GCTAACTTTTGACATAACGTGATCAGCCTGCTTTCGTGGATGCCACA GGAC
S4_4M	GGGAGAGGAGGGAGATAGATATCAACTTTCTTAGGCGTCCACCCTT GCTAACTTTTGATATAACGTGATCAGCCTGCTTTCGTGGATGCCACA GGAC
S5-L3-7A (Broccoli)	GGGAGAGGAGGGAGATAGATATCAACTTTCTTAGGCGTCCACCCTT GCTAACTTTTGACCCGACGTGATCAGCCTGCTTTCGTGGATGCCACA GGACAAAAAAAAGATGGAGACGGTCGGGTCCAGATATTCGTATCTGT CGAGTAGAGTGTGGGCTCCGTC
S2	GGGAGAGGAGGGAGATAGATATCAACCCTCTTACCAAGTGGCATTA CATGTCCCTGACCCGACGTGTTTACATGAGTTTCGTGGATGCCACAG GAC
S3	GGGAGAGGAGGGAGATAGATATCAACTCTTCGGGCGACATCCACTT TACGATTATTGACCCGACGTGCAATCACCTGTTTCGTGGATGCCACA GGAC
S4	GGGAGAGGAGGGAGATAGATATCAAGCTCGGGGCATCCAACTCTC GCAATCATGTTGACCCGACGTGTGTTACTGTCTTTCGTGGATGCCAC AGGAC
S9	GGGAGAGGAGGGAGATAGATATCAACCTTCCATCCACGAATCGCTA CCCCGCCAATGACCCGACGTGATTATTAGCCTTTCGTGGATGCCACA GGAC
S20	GGGAGAGGAGGGAGATAGATATCAACCTGACTCTAGGCATTCACG GACTCCCAGATGACCCGACGTGACTTCGATGATTTCGTGGATGCCA CAGGAC
S29	GGGAGAGGAGGGAGATAGATATCAACATCTGCTGTGACAAACACG ATATCTGTCCTGACCCGACGCGATCACCCCTCTTTCGTGGATGCCAC AGGAC
S44	GGGAGAGGAGGGAGATAGATATCAAACTCTTACAGCTGCATTCACG AGAACGCCCTGACCCGACGTGTACTTAACTGTTTCGTGGATGCCAC AGGAC
Broccoli	GGAGACGGTCGGGTCCAGATATTCGTATCTGTCGAGTAGAGTGTGG GCTCC
Red Broccoli	GGAGACGGTCGGGTCCAGTCCCAACGATGTTGGCTGTTGAGTAGTG TGTGGGCTCC

Materials

Thiamine pyrophosphate, thiamine, thiamine monophosphate and guanosine 5´-diphosphate (GDP) were purchased from Sigma-Aldrich, Germany. ATP was purchased from Genaxxon, Germany. DFHBI-1T and OBI were obtained from Bio-Techne, USA and Lucerna, USA, respectively.

Selection of TPP RNA sensor

Library and other utilized oligonucleotides were purchased as DNA from Ella biotech and are shown in Table S1. RNA library was prepared from large scale PCR with forward primer bearing T7 promotor and subsequent *in vitro* transcription with obtained dsDNA template. RNA was purified on a 10% PAGE gel. In the starting round, 1.5 nmol of RNA and 1.5 nmol of biotinylated oligodeoxynucleotides (ODN) were mixed in 100 µl selection buffer (PBS, 3 mM Mg^{2+} pH 7.4) and left to anneal by incubating it at 50°C for 15 min and slowly cooling down to 30°C for 45 min with gentle shaking. In the meantime, 2.5 mg of Dynabeads™ M-280 Streptavidin (ThermoFisher Scientific, USA) was washed 3-times with selection buffer on DynaMag™-2 Magnet rack (ThermoFisher Scientific, USA). Finally, the beads were resuspended in 50 µl selection buffer and mixed with RNA-ODN solution. The mixture was incubated for 30 min at 21°C with gentle shaking to allow RNA-ODN complexes to be coupled to the beads. Afterwards, the supernatant was discarded and beads were washed three-times with the selection buffer. Next, the buffer was removed and 1 mM TPP solution was added and incubated for another 15 min. Eluted RNA in the supernatant was removed and mixed with reverse transcription mix (M-MLV buffer (Promega), 0.5 µM biotinylated-reverse primer). The solution was heat up to 65°C for 5 min and cool down to RT to allow denaturation of RNA molecules. Next, 2 U/µl M-MLV was added and incubated for 15 min at 40°C. After reverse transcription, the biotinylated cDNA was coupled to 0.25 mg of Dynabeads™ M-280 Streptavidin to allow the purification of cDNA coding molecules of the TPP. Then, the beads were washed with selection buffer and fresh PCR solution (GoTag buffer, 1.5 mM Mg^{2+}, 1 µM reverse primer, 1 µM forward primer, 0.3 mM dNTPs, 5 U/µl Taq polymerase (Promega) was added to them. PCR was performed with the program: (1) 95°C 2 min, (2) 95°C 1 min, (3) 56°C 1 min, (4) 72°C 1 min, (5) 72°C 3 min, with repeated steps 2-4 for 5 cycles. After amplification, 10 µl of PCR product was transferred to the *in vitro* transcription mix (40 mM Tris pH 7.9, 5 mM DTT, 25 mM Mg^{2+}, 2.5 mM NTPs, 10 µM biotinylated capture ODN, T7-RNA polymerase (NEB)) and was incubated for 1.5 hour at 37°C. Captured RNA on the beads was then washed three-times with the selection buffer and was subjected to the next round of

selection starting with the elution with the TPP molecule. The selection pressure was increased during the selection by lowering the target concentration from 1 mM to 50 µM and by lowering the elution time from 15 min down to 5 min, and transcription time from 1.5 hour to 30 min.

Preparation of Broccoli and Red broccoli constructs

Broccoli and Red broccoli sequences were introduced to the library and monoclonal sequences during the PCR and subsequent *in vitro* transcription (IVT). Reverse complementary sequence of Broccoli and Red broccoli was connected with reverse primer as shown in Table S1. PCR was performed with the program: (1) 95°C 3 min, (2) 62°C 1 min, (3) 72°C 1 min, (4) 72°C 3 min, with repeated steps 2-4 for 9 cycles. After Ethanol precipitation, PCR product was utilized for IVT reaction and furthermore, the generated RNA was purified on 10 % Urea-PAGE gel.

DFHBI-1T and OBI fluorescence-based assay

Broccoli and Red broccoli constructs were prepared by *in vitro* transcription and were heat up to 80°C for 3 min before start of the assay. Next, 1 µM RNA, 10 µM DFHBI-1T (Bio-Techne, USA) or OBI (Lucerna, USA) and 1 mM of small molecule were incubated in PBS with 3 mM Mg^{2+} for 1 hour in ProxiPlate-384 Plus F, Black 384-shallow well Microplate (Perkin Elmer, USA). Afterwards, the fluorescence was measured by EnSpire Multimode Plate Reader (PerkinElmer, USA) at excitation light 462 nm and emission light 503 nm for Broccoli constructs and excitation light 541 nm and emission light 590 nm for Red broccoli constructs.

Fluorescence polarization assay

Cy3-labelled capture oligonucleotides (ODN) were purchased from Ella Biotech, Germany. Sequences of different capture ODNs are provided in Table S1. The assay was performed in a final volume of 50 µl (100 nM Cy3-ODN, 500 nM RNA, 1 mM small molecule) PBS with 3 mM Mg^{2+} and 0.05 % Tween 20. Firstly, RNA and small molecule were mixed together and incubated for 30 min at 21°C and 500 rpm. Secondly, Cy3 ODN was added and incubated for another 30 min at 21°C and 500 rpm. Finally, the solution was transferred to the Corning® 96 Well Half-Area Microplate (Sigma Aldrich, Germany) and was measured by Tecan Ultra Micro Plate Reader (Tecan, Switzerland) at excitation light 535 nm, and emission light 595 nm. The fluorescence polarization values were normalized according to the value of corresponded Cy3-ODN sample.

Next-generation sequencing

The starting library and the selection round pool 2 to 12 were used for Next generation sequencing (NGS). Pools were amplified with different primers synthetized by Ella Biotech. For the performance of 75 bp NGS run, the forward and reverse primer-binding sites were truncated by utilizing shorter 17 nt and 14 nt primers during the amplification step, respectively. Additionally, 6 nt long index sequence (inx) was included to the primers, which was specific for each selection round. A PCR reaction mix was prepared for each pool and for an additional No Template Control (NTC), using a proofreading *Pfu*-Polymerase (homemade). PCR product was purified with Nucleospin® Gel and PCR clean-up columns (Macherey Nagel, Germany) according to the manufacturer's instructions. 0.125 µg of each DNA was mixed together and used for the following step. Next, adapter needed for immobilization and processing of the sample on the Illumina instruments was ligated to the DNA sequences using TruSeq DNA PCR-Free Sample Preparation Kit LT (Illumina, USA). Ligation was done according to manufacturer instructions. The ligated products were afterwards separated on an agarose gel, cutting out only the longest sequence (app. 200 bp) with ligated adapters on both sides. The DNA was purified from the gel using Nucleospin® Gel and PCR clean-up columns, following manufacturer instructions. Finally, DNA was eluted with the resuspension buffer (TruSeq DNA PCR-Free Sample Preparation Kit LT) and was used for Illumina sequencing with NextSeq500 with High Output v2 chemistry. The NGS run was performed from forward and reverse strand and it covered either only full random region or the random region with additional 3 nt of the 3' forward primer-binding site, respectively. Analysis of sequencing data was completed on in-house NGS software (AptaNext), which requires at least 6 nucleotides for recognition of primer-binding site sequence. Since the program would not be able to recognize the ending of the reverse strand as the start of the forward primer-binding site, the further analysis was performed only on the isolated forward sequences.

ITC measurement

The RNA for affinity measurement was prepared by *in vitro* transcription. After ethanol precipitation the RNA was resuspended in the binding buffer and further washed several times with the same buffer on the 3K Amicon® Ultra 0.5 mL Centrifugal Filters (Merck, Germany). 2 mM of the TPP in the syringe was titrated to either 50 µM or 100 µM of the S1 and S5 aptamer in the sample cell, respectively, with first injection of 0.4 µl and subsequent 18 injections of 2 µl. The affinity was measured on MicroCalTM PEAQ-ITC (Malvern Panalytical, UK) with power of 10 µcal/sec and spacing time 180 sec.

ACKNOWLEDGMENTS

During my PhD journey, I met many wonderful people who have supported me throughout the years.

I extend my deepest gratitude to Prof. Dr. Günter Mayer for the engaging topic, the insightful discussions, and the support during my PhD.

I sincerely thank Prof. Dr. Michael Famulok, Jr. Prof. Dr. Elena S. Reckzeh, and Prof. Dr. Ulrich Ettinger for joining my committee.

A big thanks to the AK Mayer group: Franziska Pffeifer, Laura Lledo Bryant, Laia Civit, Christian Renzl, David Otte, Silvana Haßler, Julia Siegl, Milena Mund, Anna Jonczyk, Anna Weber, and Malte Rosenthal for the wonderful time and experience. Special thanks to Olga Plückthun, Laura Eiden, and Usman Akhtar for the daily 'Tee time'. A very special thanks to Tejal Patwari, Rezzan Fazlioglu, Mehrnaz Jahani, Mihn Naguyen, Moujab Choukeife, Ignazio Geraci, and Georg Pietruschka for all the 'after lab' fun activities, the amazing and memorable trips we've shared, and of course for all the scientific discussions and encouragement to finish this journey together!

Special thanks to the laboratory supporters: Stefan Breuers for supporting and teaching me with the SELEX robot, Nicole Krämer for preparing all enzymes and assisting with radioactive work, and Justina Stark for maintaining the lab. Thank you for sharing your experiences and helping with daily routines.

I especially want to thank everyone in the neighbouring groups of AK Famulok and AK Kath-Schorr for the productive discussions during our weekly aptamer meetings and the enjoyable 'after lab' activities.

Of course, I want to thank my family for their ongoing support. Although this journey took me far from you, you were always in my heart. Thank you very much.

Finally, I want to thank the most important person who supported me throughout my dissertation process, through all my mental ups and downs: Nima. Firstly, thank you for your emotional support, scientific discussions, and proofreading of my thesis. Thank you for helping me see the light at the end of the tunnel when I couldn't.

And last but not least, I want to thank Sony, Eli and Meshki for your fluffy support.